MÔNICA CARNEIRO ALVES SENNA

CAPACIDADE DE REGENERAÇÃO DA FLORESTA TROPICAL AMAZÔNICA SOB DEFICIÊNCIA NUTRICIONAL: RESULTADOS DE UM ESTUDO NUMÉRICO DA INTERAÇÃO BIOSFERA-ATMOSFERA

Tese apresentada à Universidade Federal de Viçosa, como parte das exigências do Programa de Pós-Graduação em Meteorologia Agrícola, para obtenção do título de *Doctor Scientiae*.

VIÇOSA
MINAS GERAIS – BRASIL
2008

Ficha catalográfica preparada pela Seção de Catalogação e Classificação da Biblioteca Central da UFV

T
S478c
2008

Senna, Mônica Carneiro Alves, 1981-
Capacidade de regeneração da floresta tropical amazônica sob deficiência nutricional: resultados de um estudo numérico da interação biosfera-atmosfera / Mônica Carneiro Alves Senna. – Viçosa, MG, 2008.
xi, 126f.: il. (algumas col.) ; 29cm.

Orientador: Marcos Heil Costa.
Tese (doutorado) - Universidade Federal de Viçosa.
Referências bibliográficas: f. 109-126.

1. Climatologia agrícola. 2. Amazônia - Clima - Modelos matemáticos. 3. Amazônia - Desmatamento. 4. Fertilidade do solo. I. Universidade Federal de Viçosa. II.Título.

CDD 22.ed. 630.2515

MÔNICA CARNEIRO ALVES SENNA

CAPACIDADE DE REGENERAÇÃO DA FLORESTA TROPICAL AMAZÔNICA SOB DEFICIÊNCIA NUTRICIONAL: RESULTADOS DE UM ESTUDO NUMÉRICO DA INTERAÇÃO BIOSFERA-ATMOSFERA

Tese apresentada à Universidade Federal de Viçosa, como parte das exigências do Programa de Pós-Graduação em Meteorologia Agrícola, para obtenção do título de *Doctor Scientiae*.

APROVADA: 22 de abril de 2008.

Prof. Luiz Cláudio Costa
(Co-Orientador)

Prof. Aristides Ribeiro

Pesq. Marcos Daisuke Oyama

Prof. José Maria Nogueira da Costa

Prof. Marcos Heil Costa
(Orientador)

O prêmio de uma boa ação é tê-la praticado.

Se aproveitares bem o dia de hoje, dependerás menos do de amanhã.

(Sêneca)

AGRADECIMENTOS

A Deus, pelo dom da vida, pela saúde, força, proteção, amor e sabedoria dadas no decorrer de toda a minha vida.

Ao meu marido, Thomaz Schröder Senna, pelo amor e carinho sempre presente em momentos de alegria ou dificuldade. Sem você tudo fica sem sentido. Te aminho muitão!

Aos meus pais, pelo apoio constante e pelos sacrifícios. Obrigada pela confiança depositada em mim.

Ao meu orientador, Professor Marcos Heil Costa, e aos co-orientadores, por todos os ensinamentos, atenção, incentivos e pelas valiosas sugestões dadas no decorrer deste trabalho.

À amiga Gabrielle, por toda ajuda nos scripts de NCL, pela amizade e por toda dedicação e capricho. É bom saber que posso contar com você!

Aos amigos de trabalho Varejão, pela disposição e boa vontade nos ensinamentos de NCL; Clever, pela ajuda constante no Illustrator; Luciana e Lucía, pelos mapas de precipitação e radiação solar; Francisca, pelas sugestões e companheirismo; Hewlley,

pelos gráficos de calibração do IBIS; Edson e Thomé, pelas conversas, lanchinhos e pelos risos; e a todos os outros do grupo de pesquisa pela boa convivência e descontração.

A todos os demais professores, colegas e funcionários do Departamento de Engenharia Agrícola e Ambiental da UFV, pelo apoio e amizade.

BIOGRAFIA

MÔNICA CARNEIRO ALVES SENNA, filha de Esperidião Alves Xavier Filho e Jacel Carneiro de Figueiredo Alves, nasceu em 08 de abril de 1981, na cidade de Cruzeiro do Sul – AC.

Em dezembro de 1997 concluiu o curso técnico em Meteorologia pelo Centro Federal de Educação Tecnológica Celso Suckow da Fonseca (CEFET-RJ).

De janeiro de 2000 a novembro de 2001 trabalhou como Técnica em Meteorologia na Fundação Instituto Geotécnica do Município do Rio de Janeiro (GEO-RIO).

Em março de 2002 concluiu o curso de graduação em Meteorologia pela Universidade Federal do Rio de Janeiro (UFRJ).

Em fevereiro de 2004 concluiu o curso de pós-graduação, em nível de Mestrado, em Meteorologia Agrícola na Universidade Federal de Viçosa (UFV).

Em fevereiro de 2004 iniciou o curso de pós-graduação, em nível de Doutorado, em Meteorologia Agrícola na Universidade Federal de Viçosa (UFV), dedicando-se ao estudo das interações atmosfera-biosfera.

RESUMO

SENNA, Mônica Carneiro Alves, D.Sc., Universidade Federal de Viçosa, abril de 2008. **Capacidade de regeneração da floresta tropical amazônica sob deficiência nutricional: resultados de um estudo numérico da interação biosfera-atmosfera.** Orientador: Marcos Heil Costa. Co-Orientadores: Carlos Afonso Nobre e Luiz Cláudio Costa.

Essa tese investiga como as retroalimentações do clima e da disponibilidade de nutrientes no solo interagem na regulação dos padrões de recrescimento da floresta tropical amazônica após um desmatamento de grande escala. Nesse estudo foi utilizado o modelo acoplado biosfera-atmosfera CCM3-IBIS. Inicialmente, o modelo foi validado através de observações de variáveis climáticas e de dinâmica e estrutura da vegetação amazônica. O clima da Amazônia (média anual e sazonalidade) é muito bem simulado tanto para a precipitação quanto para a radiação solar incidente. Os padrões de cobertura vegetal representam bem os padrões observados. A produção primária líquida e as taxas de respiração simuladas diferem em 5% e 16% das observações, respectivamente. O desempenho das variáveis simuladas que dependem da alocação de carbono, como a partição da produção primária líquida, o índice de área foliar e a biomassa, é alto em uma média regional, mas é baixa quando são considerados os padrões espaciais. Uma

melhor representação desses padrões espaciais depende da compreensão da variação espacial da alocação de carbono e sua dependência com fatores ambientais. Para avaliar a capacidade de recrescimento da floresta foram realizados dois experimentos. O primeiro experimento considera diferentes tipos de limitação nutricional e um hipotético desmatamento total. O segundo experimento considera o tipo de limitação nutricional mais realístico e diferentes cenários de desmatamento, com o intuito de encontrar um limite máximo de desmatamento que não causaria interferências prejudiciais na regeneração da floresta. Os resultados mostram que a redução da precipitação é proporcional à quantidade de desmatamento e é mais drástica quando mais do que 40% da extensão original da floresta é desmatada. Além disso, apenas a redução da precipitação simulada não é suficiente para impedir a regeneração da floresta secundária. Entretanto, quando a redução da precipitação é associada com uma deficiência nutricional do solo, um processo de savanização pode ocorrer sobre o norte do Mato Grosso, independente da extensão da área desmatada. Esses resultados são preocupantes, pois essa região tem as mais altas taxas de desmatamento da Amazônia. A baixa resiliência da floresta com deficiência nutricional indica que o norte do Mato Grosso deveria ser o alvo principal de iniciativas para a conservação.

ABSTRACT

SENNA, Mônica Carneiro Alves, D.Sc., Federal University of Viçosa, April 2008. **Amazon rainforest regrowth under nutrient stress: results from a biosphere-atmosphere interaction numerical study.** Adviser: Marcos Heil Costa. Co-Advisers: Carlos Afonso Nobre and Luiz Cláudio Costa.

This thesis investigates how the climate feedback and the nutrient feedback interact to regulate the patterns in the regrowth of the Amazon tropical forest after a large-scale deforestation. The study is performed using the fully coupled biosphere-atmosphere model CCM3-IBIS. Initially, the model was validated against observed climate and vegetation dynamics and structure variables. The Amazon climate (annual mean and seasonality) is extremely well simulated for both precipitation and incident solar radiation. Vegetation cover patterns reproduce well the observed patterns. The simulated net primary production and respiration rates are within 5% and 16% of observed data, respectively. The performance of simulated variables that depend on carbon allocation, like net primary production partitioning, leaf area index and biomass, although good on a regional mean, is low when spatial patterns are considered. A better representation of these spatial patterns depends on the understanding of the spatial variation in carbon allocation and its relationship to environmental factors. To evaluate

the rainforest regrowth two experiments were done. The first experiment considers different types of nutrient stress and a hypothetical full deforestation. The second experiment considers the most realistic type of nutrient stress and different deforestation scenarios, looking for a threshold of deforestation that could cause dangerous interference on the Amazon recovery. Results show that the reduction in rainfall is proportional to the amount of deforestation and is more drastic when the deforested area is higher than 40% of the original forest extent. In addition, this simulated precipitation reduction alone is not sufficient to prevent the rainforest regrowth. However, when the precipitation reduction is associated with a soil nutrient stress, a savannization process may start over northern Mato Grosso, no matter how much is deforested. This is concerning because this region has the highest clearing rates in Amazonia. The low resilience of the forest under nutrient stress indicates that northern Mato Grosso should be a major target for conservation initiatives.

CONTENTS

GENERAL INTRODUCTION

The Amazon tropical forest is the world's largest rainforest, an ecosystem that supports perhaps 30 percent of terrestrial species [*Godoy et al.*, 1999; *Prance et al.*, 2000; *Dirzo and Raven*, 2003], and plays a crucial role in the climate system, particularly as a driver of atmospheric circulation [*Zeng and Neelin*, 1999; *Costa and Foley*, 2000]. Recent studies have suggested that the Amazon may reduce in extension and lose biomass during the 21st century through a savannization process [*Magrin et al.*, 2007]. In addition, changes in the carbon balance of this region could have significant effects on the global carbon cycle and on the greenhouse effect [*Denman et al.*, 2007; *Bala et al.*, 2007].

Over the last few decades, high rates of deforestation have been occurring in the region [*Skole and Tucker*, 1993; *Nepstad et al.*, 1999; *INPE*, 2007]. The reasons for land-clearing in the Amazon are compelling: cheap land, low labor costs, booming demand for commodities driven by a surging China, and growing interest in biofuels. In less than a generation, these factors have helped Brazil become a large exporter of beef, cotton, soybean, and sugar, among other products. Amazon landowners have seen their

land values double every 4-5 years in areas that just a decade ago were rainforests. The market is driving deforestation [*Soares-Filho et al.*, 2006; *Nepstad et al.*, 2006].

This conversion of forests to agricultural land is more than just the loss of trees. The deforestation also affects species composition, productivity, and biomass along edges and in remaining fragments, and can influence the likelihood of fires [*Laurance et al.*, 1997; *Mesquita et al.*, 1999; *Cochrane et al.*, 1999; *Nepstad et al.*, 2001].

Early studies focused on climate change induced by deforestation [*Nobre et al.*, 1991; *Hahmann and Dickinson*, 1997; *Lean and Rowntree*, 1997; *Costa and Foley*, 2000], whereas coupled changes of climate and vegetation [*Levis et al.*, 2000; *Cox et al.*, 2004] are the current interest. The majority of biosphere-atmosphere studies in Amazonia investigate the sensitivity of climate to the full Amazon deforestation, which is not a realistic scenario. Two recent studies, however, evaluate the response of the Amazonian climate to the partial deforestation [*Costa et al.*, 2007; *Sampaio et al.*, 2007], concluding that the precipitation reduction in this region is more evident when deforestation exceeds 40-50% of the original forest cover.

As deforestation of tropical forests continues, one of the future hopes for these damaged ecosystems is the regeneration of secondary forests. Some areas that were once slash-and-burned for cattle ranching or subsistence agriculture have been abandoned, allowing scientists to study the possibility of recovery in the rainforest. Amazonian regrowth forests are an important reservoir of genetic diversity of forest species [*Vieira et al.*, 2003] and have a substantial role in sequestering carbon [*Zarin et al.*, 2001]. This secondary forest regrowth, however, may be limited by climate and nutrient availability.

Shukla et al. [1990] suggest that the reduction of precipitation caused by deforestation might prevent an eventual forest regrowth. In addition, the highly

weathered, nutrient impoverished and acidic soils of the Amazon are a challenge to plant growth. Further soil degradation and nutrient loss through intense land-use and frequent fires may result in reduced growth rates in successional species [*Davidson et al.*, 2004; *Zarin et al.*, 2005]. However, after decades of regrowth in a conservative nutrient cycling legacy, the secondary forest rebuilds nutrient stocks in advanced successional and mature stages [*Davidson et al.*, 2007] because most of the rainforest essential nutrients are locked up in the living vegetation, dead wood, and decaying leaves. As organic material decays, it is quickly recycled.

Although research shows the effects of changing precipitation and changing nutrient status on the forest regrowth, we still do not know how these factors interact to regulate the forest regrowth and if these interactions vary in different parts of Amazonia. Considering these issues, the objective of this thesis is to investigate these feedbacks in the Amazon region using the fully coupled climate-biosphere model CCM3-IBIS. This study is organized as follows: Chapter 1 investigates how well this fully coupled model can reproduce vegetation structure and dynamics in Amazonia, to the extent permitted by available data. Chapter 2 studies how the climate and nutrient feedbacks may affect the forest regrowth after a hypothetical full deforestation, considering two types of nutrient stress (fixed vs. dynamic). Chapter 3 investigates how the climate and nutrient feedbacks may alter the rainforest regrowth after different deforestation scenarios from *Soares-Filho et al.* [2006] and *Sampaio et al.* [2007], which assume that recent deforestation trends will continue in the next decades/centuries.

CHAPTER 1

CHALLENGES OF A COUPLED CLIMATE-BIOSPHERE MODEL TO REPRODUCE VEGETATION STRUCTURE AND DYNAMICS IN AMAZONIA

1.1. INTRODUCTION

Terrestrial biosphere and climate interact through several complex feedbacks. The global pattern of natural vegetation cover is governed by climate through precipitation, solar radiation, temperature and CO_2 concentration [*Prentice*, 2001; *Nemani et al.*, 2003; *Liu et al.*, 2006]. Changes in climate may alter competitive relationships among species, and thus may alter the structure and biogeography of ecosystems. On the other hand, changes in community composition and ecosystem structure may alter the fluxes of energy, water, momentum, CO_2, and other atmospheric gases, consequently affecting climate [*Pielke et al.*, 1998; *Bonan*, 2002; *Foley et al.*, 2003].

The interactive coupling of terrestrial ecosystems and climate has been examined by fully integrated dynamic global vegetation models within global climate models [*Betts et al.*, 1997; *Foley et al.*, 1998, 2000; *Bonan et al.*, 2003; *Krinner et al.*, 2005]. In these coupled models, vegetation growth and biogeography are influenced by temperature, precipitation, and other climate variables. In turn, vegetation height, leaf area, rooting depth, and other vegetation parameters influence albedo, radiative exchange, turbulent fluxes and hydrology, therefore influencing climate. These models

also incorporate processes such as mortality and competition among plant functional types [*Bonan*, 2002; *Moorcroft*, 2003].

Several coupled climate-biosphere models have been applied to problems of the global carbon cycle [*Cox et al.*, 2000; *Friedlingstein et al.*, 2001, 2006] and climate change [*Betts et al.*, 1997; *Brovkin et al.*, 1999; *Foley et al.*, 2000; *Liu et al.*, 2006; *Notaro et al.*, 2007]. The initial climate projections with a coupled ocean-vegetation-atmosphere general circulation model that consider carbon exchanges among the oceans, land, and atmosphere showed that the overall effect of carbon-climate interaction is a positive feedback, mostly due to the negative impacts of climate change on land carbon storage [*Cox et al.*, 2000; *Friedlingstein et al.*, 2001], but the magnitude of this feedback varied a lot between these studies. Results from the Coupled Climate-Carbon Cycle Model Intercomparison Project (C^4MIP) show a unanimous agreement among all the 11 models that the climate-carbon cycle feedback is positive [*Friedlingstein et al.*, 2006]. However, large disagreement remains on the magnitude of this feedback strength, as well as on the regional aspects of this feedback.

A major uncertainty in the carbon budget relates to changes in the carbon stocks of tropical forests. Old growth tropical forests contain large stores of live biomass, soil organic matter, and are very dynamic, accounting for a major fraction of global net primary production and global live biomass. Changes in the carbon balance of these regions could have significant effects on global CO_2 [*Denman et al.*, 2007; *Bala et al.*, 2007].

Of the tropical forest regions, the Amazon is of primary importance, not only because it contains more than half of the world's tropical rainforests, but also because recent studies, including the last Intergovernmental Panel on Climate Change (IPCC)

report, have suggested that it may reduce in extension and lose biomass during the 21st century [*Magrin et al.*, 2007] through a savannization process.

Despite such predictions, the models involved have not been fully validated against the available field and remote sensing measurements that characterize the vegetation dynamics of the region. In this study, we investigate how well a fully coupled atmosphere-biosphere model can reproduce vegetation structure and dynamics in Amazonia. Evaluating and improving the representation of the vegetation structure, dynamics and carbon cycle of Amazonia in coupled atmosphere-biosphere models will increase our ability to understand the impacts of land-use changes on the global carbon cycle and to perform reliable projections of future climate changes.

The accurate representation of the coupled climate-biosphere dynamics requires the accurate representation of climate, net primary production, and its partition among the several carbon pool components. We focus the climate analysis on precipitation (P) and incident solar radiation (S_{in}), because they are the most important climate variables for Amazon vegetation dynamics, and we validate the resulting land cover and other variables related to vegetation dynamics and structure.

1.2. MATERIALS AND METHODS

1.2.1. Model Description

In this study we use the coupled climate-biosphere model CCM3-IBIS, which is virtually the same core model of the LLNL (Lawrence Livermore National Laboratory) model used in the C^4MIP project, except for our own tuning for the rainforest (described below). The atmospheric component of the coupled model is the NCAR Community Climate Model (CCM3) version 3.6.16 [*Kiehl et al.*, 1998]. CCM3 is an atmospheric general circulation model with spectral representation of the horizontal fields. It simulates the large-scale physics (radiative transfer, hydrologic cycle, cloud development, thermodynamics) and dynamics of the atmosphere. In this study, we operate the model at a spectral resolution of T42 (~2.81º X 2.81º latitude/longitude grid), 18 vertical levels, and a 15-min time step. The oceans are represented by monthly averaged fixed sea-surface temperatures of the 1990s that serve as boundary conditions for the atmosphere.

CCM3 is coupled to the Integrated Biosphere Simulator (IBIS) version 2.6.4 [*Foley et al.*, 1996; *Kucharik et al.*, 2000]. IBIS is a comprehensive model of terrestrial biospheric processes that represents the physical, physiological, and ecological

processes occurring in vegetation and soils. IBIS simulates land surface processes, plant phenology and vegetation dynamics, and represents vegetation as two layers (trees and grasses). In IBIS a grid cell can contain one or more plant functional types (PFTs) that together comprise a vegetation type. Land surface physics and canopy physiology are calculated at the same time step used by CCM3. The plant phenology algorithm has a daily time step and the vegetation dynamics is solved with an annual time step. IBIS is a 0-dimensional model that operates on each CCM3 land surface grid point. When dynamic vegetation component is enabled, vegetation structure and biogeography change in response to climate. A detailed description of the model follows, as relevant to the validation.

IBIS represents vegetation dynamics using very simple competition rules. The relative abundance of 12 PFTs in each grid cell changes in time according to their ability to photosynthesize and use water. Thus the model can mechanistically simulate the competition between different plant forms. The competition between plant types of the same basic form is driven by differences in the annual carbon balance resulting from differences in phenology, leaf form, and photosynthetic pathway.

IBIS calculates roots maintenance respiration (R_{root}) as a function of the carbon contained in root biomass and the soil temperature in the rooting zone. The efflux of carbon from the soil, including the litter decomposition ($R_{soil+litter}$), is the sum of R_{root} and carbon that is respired by the microbial biomass ($R_{heterotrophic}$) during its oxidation of the soil organic matter. $R_{heterotrophic}$ depends on soil moisture and temperature, and on the amount of available substrate.

Total net primary production (NPP_{total}) is calculated integrating primary production through the year discounting maintenance respiration and the carbon lost due to growth respiration. NPP_{total} is allocated in three carbon pools: leaves (C_l), wood (C_w),

and roots (C_r). Changes in the carbon pool i (C_i) are described by the differential equation

$$\frac{\partial C_i}{\partial t} = a_i . NPP_{total} - \frac{C_i}{\tau_i} - \delta . C_i \quad (1)$$

where a_i represents the carbon allocation coefficient of leaves (a_l), wood (a_w), and roots (a_r); τ_i describes the residence time of carbon in leaves (τ_l), wood (τ_w), and roots (τ_r). In IBIS, a_i and τ_i are assumed to be fixed in space and time within a given PFT. δ is a generic parameter for disturbances, such as fires, herbivory, etc., which is set to zero in this simulation.

NPP_{total} is divided into belowground and aboveground net primary production (NPP_{bg} and NPP_{ag}, respectively). Aboveground wood net primary production (NPP_{agw}) is the rate at which carbon is fixed into aboveground woody biomass structures, like trunks, stems and branches. NPP_{agw} is calculated by multiplying NPP_{total} by a_w (Equation (1)).

In IBIS, the changes in leaf display and physiological activity are triggered by climatic events, when there are one or more unfavorable seasons. Drought deciduous plants (e.g. tropical deciduous trees) are assumed to respond to changes in net canopy carbon budget. The leaf area index (LAI) of each PFT is obtained by dividing leaves carbon (C_l) by specific leaf area. In this study, the specific leaf area for both tropical evergreen and tropical deciduous trees are set to 17 m^2 kg-C^{-1} [*Figueira et al.*, 2002].

IBIS represents transient changes in biomass directly proportional to the carbon allocation coefficient – a_l, a_w, and a_r – and inversely proportional to the residence time (from loss of biomass through mortality and tissue turnover) – τ_l, τ_w, and τ_r – of each biomass compartment (Equation (1)). Total biomass is divided into belowground (BGLB) and aboveground live biomass (AGLB). AGLB is the sum of C_l and C_w.

1.2.2. Model Calibration

The data used for model calibration were collected at four micrometeorological sites in areas of primary forest of the Large Scale Biosphere-Atmosphere Experiment in Amazonia (LBA) (Figure 1.1): Jaru (10.8º S; 61.9º W), Manaus (2.6º S; 60.2º W), Tapajós km 67 (2.9º S; 55.0º W), and Tapajós km 83 (3.1º S; 54.9º W) [*Imbuzeiro*, 2005; *Yanagi*, 2006]. We calibrated an offline version of the model, and the optimized parameters were then transferred to the coupled model. The model is initially optimized for net radiation exchange (Rn), then for mass and energy fluxes – latent heat flux (LE), sensible heat flux (H), net ecosystem exchange (NEE). The calibration process involves a reasonably large number of simulations selecting, in each one of them, values for specific model parameters. The optimized model parameters and their optimized value are leaf reflectance in visible and near infrared bands (ρ_{vis}, ρ_{nir}), orientation of the upper canopy leaves (χ_u), coefficient that relates canopy conductance with net photosynthesis (m), maximum capacity of the Rubisco enzyme at 15°C (V_{max}), heat capacity of the stems (C_s), and a parameter related to the vertical distribution of the root system (β_2). In each simulation, the results of the model output are compared against observed data, seeking to minimize the root mean square error (RMSE) while keeping an unbiased mean.

1.2.3. Simulation Setup and Validation Data

Delire et al. [2002, 2003] investigated the basic global climate and carbon cycle simulated by this coupled model and showed that CCM3-IBIS can be used to explore geographic and temporal variations in the global carbon cycle. In this study, we focus on the Amazon climate and carbon cycle.

To investigate how well CCM3-IBIS can reproduce vegetation dynamics in Amazonia, we conduct a simulation for a period of 50 years: the last 20 years are averaged to analyze the results, while the first 30 years are left for the model to approach an equilibrium state, specifically with respect to soil moisture and carbon pools. The land cover is initialized with modern natural vegetation [*Ramankutty and Foley*, 1999] and the dynamic vegetation component is enabled. During the simulation, CO_2 concentration was kept constant at 380 ppmv. The initialization values for the rainforest C pools are 0.38, 10.83, and 0.19 kg-C m^{-2} for C_l, C_w, and C_r, respectively. Carbon allocation coefficients for the rainforest are 0.4, 0.4, and 0.2 for a_l, a_w, and a_r, and carbon residence times are 1.01, 25, and 1 year for τ_l, τ_w, and τ_r, respectively.

To minimize initialization period, we have initialized the rainforest carbon pools with values very close to the equilibrium state, obtained from previous runs. We have also verified that live C pools were in equilibrium after 30 years in different points of Amazonia.

We should note here that, since the climate dynamics and the vegetation structure and dynamics are fully interdependent, a correct representation of both is required. Otherwise, an error in the simulated climate may introduce and error in the vegetation cover, which may feedback again on climate.

The climate produced by CCM3 is validated against precipitation (P) and incident solar radiation (S_{in}) data. P and S_{in} are the two variables most relevant to vegetation dynamics in the Amazon. We also validate the following vegetation dynamics variables: heterotrophic respiration ($R_{heterotrophic}$), root respiration (R_{root}), soil and litter respiration ($R_{soil+litter}$), net primary production (NPP_{total}), aboveground net primary production (NPP_{ag}), and aboveground wood net primary production (NPP_{agw}). The validated vegetation structure variables are leaf area index (LAI), and aboveground live biomass (AGLB). The next paragraphs describe each validation dataset.

Simulated precipitation is compared against eight different precipitation databases, including three climatological surface rain gauge datasets – CRU (Climatic Research Unit - *New et al.* [1999]), *Legates and Willmott* [1990], and *Leemans and Cramer* [1990]; three that blend remote sensing data with surface rain gauges – CMAP (CPC Merged Analysis of Precipitation - *Xie and Arkin* [1997]), GPCP (Global Precipitation Climatology Project - *Huffman et al.* [1997]), and TRMM (Tropical Rainfall Measuring Mission - *Kummerow et al.* [1998]); and two reanalysis datasets – NCEP/NCAR [*Kalnay et al.*, 1996] and ERA-40 [*Uppala et al.*, 2005]. All available data in the time series are used to describe the precipitation climatology. The use of a large number of precipitation datasets is important because regional precipitation estimates in Amazonia are considerably different among themselves [*Costa and Foley*, 1998].

Simulated incident solar radiation at surface is compared against GOES data as processed by the algorithm GL1.2 [*Ceballos et al.*, 2004]. This algorithm uses reflectance in visible channel from GOES 8 for assessing solar flux in two different broadband intervals (visible and near-infrared), where physical characteristics of radiative transfer is processed. Ultraviolet fluxes enter mainly as a second-order (but not

negligible) term. The GL1.2 algorithm includes cloud cover assessments, water vapor, carbon dioxide, and ozone absorption. However, it does not include the presence of aerosols. The series used are from 1997 to 2006.

Land cover is compared against the SAGE (Center for Sustainability and the Global Environment) potential vegetation dataset, described in *Ramankutty and Foley* [1999]. The potential vegetation map is intended to represent the vegetation that would exist in a location without human intervention.

$R_{heterotrophic}$, R_{root}, $R_{soil+litter}$, NPP_{total} and NPP_{ag} are compared against data from *Malhi et al*. [submitted], who carefully synthesized results on the carbon stocks, nutrient stocks and particularly the internal carbon allocation in forests in three sites: Manaus (2.6º S; 60.2º W), Tapajós (2.9º S; 55.0º W), and Caxiuanã (1.8º S; 51.5º W) (Figure 1.1).

NPP_{agw} is compared against a large dataset from *Malhi et al.* [2004]. These data were collected at old-growth humid forests with no evidence of major human-induced disturbance for at least a century. The plots are spread through Brazil, Bolivia, Peru, Ecuador, Colombia, Venezuela, Guyana, Suriname, and French Guiana, with a good coverage of Amazonia.

LAI is compared against in situ measurements of ABRACOS (Anglo-Brazilian Amazonian Climate Observation Study) and LBA forest sites, and remote sensing estimates from the MODIS MOD-15 product. The data from ABRACOS are annual mean values of Ji-Paraná (10.1º S; 61.9º W), Manaus (3.0º S; 60.0º W), and Marabá (5.8º S; 49.2º W) sites (Figure 1.1). Various methods were used to measure and estimate LAI and there was overall consistency in the estimates for each site [*Roberts et al.*, 1996]. The data from LBA are monthly mean values of Tapajós site (2.9º S; 55.0º W) [unpublished data from *M. H. Costa*]. The estimates from the MOD-15 product are

monthly values of Tapajós site from December 2003 to November 2004. We use the collection 4 LAI dataset at 1 km spatial resolution.

AGLB is compared against two different datasets. The first one is a spatially extensive dataset from *Malhi et al.* [2006], presenting the AGLB of undisturbed old-growth Amazonian forests plots. The plots are spread through Brazil, Bolivia, Peru, Ecuador, Colombia, Venezuela, Guyana, Suriname, and French Guiana. The second one, from *Saatchi et al.* [2007], combines a large number of AGLB plots and remote sensing data for the entire Amazon tropical forest.

1.3. RESULTS

1.3.1. Model Calibration

The model parameters that minimized Rn, H, LE and NEE are $\rho_{vis} = 0.062$, $\rho_{nir} = 0.280$, $\chi_u = 0.86$, $m = 8$, $V_{max} = 120$ μmol m^{-2} s^{-1}, $C_s = 5.27 \times 10^4$ J m^{-2} K^{-1}, and $\beta_2 = 0.997$ [*Imbuzeiro*, 2005, *Yanagi*, 2006]. Table 1.1 shows the mean relative error (e) and the root mean square error (RMSE) of simulated H, LE, and NEE before and after calibration, for the Tapajós km 83 and km 67, Manaus and Jaru sites. The values of e and RMSE in general decreased when the parameters were calibrated. Figure 1.2 shows selected charts of the dispersion, cumulative and temporal patterns of H, LE and NEE for the four sites after calibration. The new set of IBIS parameters produces good results for hourly variability (Figure 1.2g) and for cumulative pattern along the year (Figure 1.2a, 1.2c and 1.2e) for H, LE and NEE, although the dispersion may vary from site to site (Figure 1.2b, 1.2d, 1.2f and 1.2h).

1.3.2. Precipitation

Table 1.2 shows the annual mean P for the Amazon tropical forest region simulated and calculated from eight different P databases. Annual mean P estimates vary considerably from 4.98 to 6.70 mm/day. The CCM3-IBIS estimate (6.20 mm/day) is in the middle of the P dataset range and is within 5% of the ERA-40, Leemans and Cramer, Legates and Willmott and TRMM datasets. The greater difference is 24.5% for the CRU dataset.

Figure 1.3 presents the monthly variation of Amazon tropical forest P simulated by CCM3-IBIS and according to the eight datasets. Simulated P amplitude is within the amplitude of the datasets, and the seasonality is well simulated too, although it is advanced in time by one month.

Figure 1.4 illustrates the spatial pattern of annual mean P for South America simulated and for three selected datasets (Legates and Willmott, Leemans and Cramer, and TRMM), and the difference between them. CCM3-IBIS (Figure 1.4a) simulates the main features of South America climate: high P near the equator, with a maximum near the Brazil-Colombia border, a dry region in Northeast Brazil, the South Atlantic Convergence Zone (SACZ), the Atacama desert dry climate, a dry region in Pampas, and a P maximum in southern Chile.

Figures 1.4c, 1.4e, and 1.4g illustrate areas where CCM3-IBIS overestimates (positive values) or underestimates (negative values) P according to Legates and Willmott (Figure 1.4b), Leemans and Cramer (Figure 1.4d), and TRMM (Figure 1.4f) datasets, respectively. In central Amazonia CCM3-IBIS overestimates P according to Legates and Willmott, and Leemans and Cramer, but not according to TRMM. Due to the convective nature of P in this region and to the very low density of gauges, it is

possible that the products Legates and Willmott, and Leemans and Cramer do not capture spatial patterns of P properly, while the TRMM product should overcome this limitation. CCM3-IBIS underestimates P over the Guyanas, Amapá and the Marajó Island in Brazil, and over the Peru-Ecuador border, according to these datasets.

1.3.3. Incident Solar Radiation

The annual mean S_{in} for the Amazon tropical forest region simulated by CCM3-IBIS is 227 W/m^2, and calculated from GOES GL1.2 is 214 W/m^2, with a difference of 6.1%. Figure 1.5 presents the monthly variation of Amazon tropical forest S_{in} simulated and according to the GOES GL1.2 dataset. The simulated amplitude and seasonality are similar to GOES GL1.2 estimate. The greater differences are in February and March, but simulated S_{in} is inside the GOES GL1.2 confidence interval (shaded area) for all months.

Figure 1.6 illustrates the spatial pattern of annual mean S_{in} for South America simulated (Figure 1.6a), for GOES GL1.2 dataset (Figure 1.6b), and the difference between them (Figure 1.6c). In the major part of the continent, the values are between 200-250 W/m^2. CCM3-IBIS represents very well S_{in} over most of the continent, although overestimating S_{in} in western Amazonia, with a maximum over the Andes and southern Bolivia (Figure 1.6c). There are a few points where the model underestimates S_{in} over the Atlantic Ocean, Brazil, Suriname, and Colombia. Over most of Amazon tropical forest region, though, there is a good agreement between CCM3-IBIS and the GOES GL1.2 estimates.

1.3.4. Land Cover

Figure 1.7 shows the land cover distribution simulated (Figure 1.7a) and from the SAGE potential vegetation dataset (Figure 1.7b). Despite the low spatial resolution, CCM3-IBIS successfully reproduces tropical evergreen forest in the Amazon region. Nonetheless, simulated land cover differs from potential vegetation in some areas. Over Roraima in Brazil, CCM3-IBIS simulates grassland where the vegetation should be savanna; over northern Venezuela, eastern Colombia, and southeast Amazonia, the simulated land cover is tropical deciduous forest while the potential vegetation map shows the existence of savanna. This is an artifact of the simulation setup because disturbances are turned off in this simulation. Savanna ecosystems are characterized by the co-occurrence of trees and grasses, and are strongly influenced by disturbances like fire. According to Lund-Rizzini hypothesis, a savanna is created by the frequent burning of a tropical deciduous forest [*Lund*, 1843; *Rizzini*, 1979]. This occurs because frequent fires reduce the woody vegetation cover and favor the grassland expansion. Several fire-protected savanna experiments in South America [*Coutinho*, 1982, 1990; *San-José and Fariñas*, 1991; *Hoffmann*, 1996; *Henriques and Hay*, 2002], Africa [*Brookman-Amissah et al.*, 1980; *Trollope*, 1982] and Australia [*Gill et al.*, 1981, *Lacey et al.*, 1982] resulted in an increase in tree density and species richness, particularly of fire-sensitive species, evolving towards a tropical deciduous forest community. Theory suggests that such shifts may be attributed to alternate stable states of savanna/tropical deciduous forest [*Miranda et al.*, 2002; *Scheffer et al.*, 2005; *Lapola*, 2007]. A modeling sensitivity study by *Botta and Foley* [2002] confirmed these results. They conducted simulations of land cover for Amazonia and Central Brazil with uniform disturbance

rates, finding that frequent disturbances favor grasses over trees, causing large increases in the geographic extent of savanna in southern and eastern Amazonia.

Despite the general agreement of the major biome distribution, there are a few regions (a total of three T42 cells) where the simulated land cover is in error. Over eastern Venezuela and Amapá, the simulated land cover are open shrubland and tropical deciduous forest, respectively. But the potential vegetation in these areas is tropical evergreen forest. This misrepresentation is due to precipitation underestimation in these areas (Figure 1.4). The simulated land cover in the Andes is not realistic because the sharp elevation gradient of this region introduces heterogeneity in climate and in vegetation distribution [*Botta and Foley*, 2002], which is difficult to reproduce in a T42 grid.

1.3.5. Respiration

Table 1.3 presents the $R_{heterotrophic}$, R_{root}, and $R_{soil+litter}$ simulated by CCM3-IBIS and observed by *Malhi et al.* [submitted] for the Manaus, Tapajós, and Caxiuanã sites, and an average over the three sites. The simulated $R_{heterotrophic}$ is 1.10, 1.02, and 0.81 kg-C m^{-2} y^{-1} for Manaus, Tapajós, and Caxiuanã, respectively. CCM3-IBIS underestimates $R_{heterotrophic}$ by 14% for Caxiuanã and 32% for Tapajós and overestimates it by 15% for Manaus. The simulated R_{root} for Manaus (0.56 kg-C m^{-2} y^{-1}) is equal to the observed value, but the simulated R_{root} for Tapajós (0.49 kg-C m^{-2} y^{-1}) is overestimated by 32%, and for Caxiuanã (0.38 kg-C m^{-2} y^{-1}) is underestimated by 49%. The simulated $R_{soil+litter}$ is overestimated by 9% for Manaus and is underestimated by 18% and 29% for Tapajós and Caxiuanã, respectively.

Although there are large errors in respiration rates at individual sites, an average over the sites shows an attenuation of these errors. The average simulated respiration rates are within 15% of the average observed data. A majority of these errors are due to simplistic representations of $R_{heterotrophic}$ and R_{root} and their dependence on soil temperature and moisture. Factors such as soil profiles of O_2 and CO_2, soil pH, the type of microbial fauna, and the presence of heavy metals, all not parameterized in IBIS, may affect CO_2 production. Moreover, the oversimplification of fine root dynamics can also contribute to errors in annual estimates of soil CO_2 flux [*Kucharik et al.*, 2000].

1.3.6. Net Primary Production and Partition

Table 1.4 shows the NPP_{total}, NPP_{ag}, and the fraction NPP_{ag}/NPP_{total} simulated by CCM3-IBIS and observed by *Malhi et al.* [submitted] for Manaus, Tapajós, Caxiuanã, and an average over the three sites. The simulated NPP_{total} is overestimated by 22% for Manaus (1.23 kg-C m^{-2} y^{-1}) and is underestimated by 19% for Tapajós (1.16 kg-C m^{-2} y^{-1}) and by 9% for Caxiuanã (0.91 kg-C m^{-2} y^{-1}). The simulated NPP_{ag} is 0.98, 0.92, and 0.73 kg-C m^{-2} y^{-1} for Manaus, Tapajós, and Caxiuanã, respectively. The simulated NPP_{ag} is in very good agreement with Caxiuanã observation, but CCM3-IBIS overestimates NPP_{ag} by 34% in Manaus and underestimates it by 19% in Tapajós.

The simulated pattern of NPP_{total} and NPP_{ag} is similar to the simulated pattern of respiration rates (Table 1.3), with higher values in Manaus and lower values in Caxiuanã. The partition of simulated NPP_{total} to NPP_{ag} is fixed at 80% (a_w+a_l). However, observed values show a partition of 72% in Manaus and Caxiuanã, and 79% in Tapajós. CCM3-IBIS underestimates NPP_{total} and NPP_{ag} in Tapajós, but one should note that the observed values are significant higher at Tapajós than the other two sites. There is a

conjecture that the Tapajós site has experienced recent major disturbance, and the reminiscent individuals may be disproportionately allocating carbon to wood production [*Malhi et al.*, submitted]. This kind of event is not taken into account in this simulation.

An average over the three sites shows an excellent agreement between the simulated and observed NPP_{total} and NPP_{ag}. Average simulated NPP_{total} and NPP_{ag} are within 5% and 2% of the observed data, respectively.

1.3.7. Spatial Patterns of NPP Partition to Wood

Although simulated climate and average NPP patterns are positively evaluated, a quick analysis of the remaining variables analyzed (NPP_{agw}, LAI and AGLB) shows important discrepancies. These variables depend on the carbon allocation and residence time (hereafter CART) coefficients. Realizing the limitation of the a and τ coefficients used in the initial simulation, we run a sensitivity analysis with additional five simulations, in which the only changes are in the coefficients a and τ, according to Table 1.5. In these simulations, climate and NPP are nearly the same, the only changes are the size of the carbon pools.

In the analyses below (NPP_{agw}, LAI and AGLB), because of the large number of points involved, we present two kinds of analyses for all six simulations of the sensitivity study. First, we present basic statistics like the mean error (ε) (Equation (2)), mean relative error (e) (Equation (3)), and the mean absolute error (MAE) (Equation (4)). Second, we attempt to investigate whether the spatial distribution of the error is caused by errors in the simulated climate variables. To do so, we evaluate the correlation coefficient between the error in NPP_{agw}, LAI or AGLB and the error in S_{in} or P (Tables 1.6, 1.8, 1.9, and 1.10).

$$\varepsilon = \frac{1}{n}\sum (S_i - O_i) \tag{2}$$

$$e = \frac{1}{n}\sum \frac{(S_i - O_i)}{O_i} \tag{3}$$

$$MAE = \frac{1}{n}\sum \left|S_i - O_i\right| \tag{4}$$

where S_i and O_i represent the simulated and observed values, respectively.

Table 1.6 presents the simulated NPP_{agw} averaged over the 21 T42 cells that have observed data by *Malhi et al.* [2004] for the six simulations of the sensitivity study. The simulation a4t25 has the best estimate (0.35 kg-C m^{-2} y^{-1}) compared to the mean observed value of 0.30 kg-C m^{-2} y^{-1}, with the lowest values of ε, e, and MAE (0.05 kg-C m^{-2} y^{-1}, 15.5%, and 0.10 kg-C m^{-2} y^{-1}, respectively). When wood allocation coefficient and residence time increase, the mean simulated NPP_{agw} increases and so does ε, e, and MAE. For the best simulation (a4t25), the correlation coefficients between NPP_{agw} error and S_{in} error (-0.04), and between NPP_{agw} error and P error according to Leemans and Cramer (0.10), Legates and Willmott (0.20) and TRMM (-0.09) P datasets, show that the spatial distribution of the NPP_{agw} error is not correlated to errors in the simulated S_{in} and P. From these analyses, our interpretation is that the errors in the spatial variability of NPP_{agw} are not caused by errors in the spatial simulations of climate, suggesting that the carbon allocation itself may vary spatially.

This becomes more clear if we analyze the 21 T42 grid cells individually. Table 1.7 shows NPP_{agw} simulated by CCM3-IBIS for the best simulation (a4t25) and observed for each cell. The mean simulated NPP_{agw} over these cells is overestimated by 16%, although NPP_{agw} errors calculated at individual sites may be as high as 147% in Colombia. *Malhi et al.* [2004] suggest a positive relationship between NPP_{agw} and soil fertility, concluding that the large spatial variation in NPP_{agw} may be explained by a

shifting balance in carbon allocation between respiration, wood carbon, and fine root production from site to site. Results from *Litton et al.* [2007] also indicate that the use of carbon allocation schemes that vary spatially may provide a more realistic picture of forest carbon cycling.

CCM3-IBIS assumes that carbon allocation to wood is spatially constant. If the *Malhi et al.* [2004] and *Litton et al.* [2007] conclusions are correct, then the spatial variation in allocation and its relation to environmental variables need to be explicitly modeled. Representing this process in a model is a challenge, as we still lack the knowledge of the mechanisms that drive it.

1.3.8. Leaf Area Index

Table 1.8 shows the simulated and observed annual mean LAI for Ji-Paraná, Manaus, Marabá, and Tapajós. The LAI MODIS estimate is for Tapajós site only. The a4t25 simulation has the best LAI estimate for all sites, with 7.58, 9.01, 6.91, and 8.93 $m^2\ m^{-2}$ for Ji-Paraná, Manaus, Marabá, and Tapajós respectively. This simulation also has the lowest ε (2.81 $m^2\ m^{-2}$), e (53.1 %), and MAE (2.81 $m^2\ m^{-2}$). However, the overestimation of LAI is very large in all cases, indicating excessive allocation of carbon to leaves in the model. A cross-analysis of Table 1.4 and 1.8 for the sites of Manaus and Tapajós indicates that the carbon allocation to leaves indeed vary spatially. While Tapajós observed NPP_{total} is about 43% higher than in Manaus (1.44 vs. 1.01 kg-C $m^{-2}\ y^{-1}$), Tapajós LAI is actually 17% lower than Manaus LAI (5.07 vs. 6.10 $m^2\ m^{-2}$). Although this is another evidence that allocation to leaves vary spatially, we should also consider interannual variations, as these measurements were taken in different periods.

Figure 1.8 illustrates the monthly mean LAI simulated by six CCM3-IBIS sensitivity simulations, estimated by MODIS, and observed by *M. H. Costa* [unpublished data] for Tapajós site. This is apparently the only available ground-based monthly measurements of LAI in Amazonia. All simulations overestimate the observed LAI in all months. The a4t25 simulation has the closest estimate. The MODIS estimate is inside the confidence interval of the observed data only in the dry season (May to August), a period with the high use of the main algorithm. At other months, MODIS overestimates LAI because the estimates are contaminated by cloudiness and obtained via the less reliable secondary algorithm.

1.3.9. Aboveground Live Biomass

Table 1.9 presents the simulated AGLB averaged over the 37 T42 cells of observed data by *Malhi et al.* [2006], for the six CCM3-IBIS sensitivity simulations. The AGLB closest estimate is from a5t40 simulation (16.19 kg-C m^{-2}), with the lowest ε (0.99 kg-C m^{-2}) and e (6.5%). The a4t50 simulation has the lowest MAE (2.84 kg-C m^{-2}), with a close estimate too (14.02 kg-C m^{-2}). When a_w and τ_w increase, the simulated mean AGLB increases reaching 17.86 kg-C m^{-2} in a5t50 simulation. For the best simulation (a5t40), the correlation between AGLB error and S_{in} error is zero. The correlation coefficients between AGLB error and P error according to Leemans and Cramer (0.34), Legates and Willmott (0.29) and TRMM (0.32) P datasets, show a weak connection between these errors. So, errors in AGLB are not caused by errors in climate variables.

Table 1.10 shows the simulated AGLB averaged over the 64 T42 cells of aggregated data from *Saatchi et al.* [2007]. The cells with high levels of deforestation

were excluded from the analysis. Initially, we should note that Saatchi's et al. average estimate of biomass (11.2 kg-C m^{-2}) is significantly lower than Malhi's et al. estimate (15.2 kg-C m^{-2}). This may be due to errors introduced by the Saatchi et al. algorithm, or to the sampling by Malhi et al. The simulation a4t25 has the best estimate (9.87 kg-C m^{-2}) with the lowest ε, e, and MAE (-1.35 kg-C m^{-2}, -11.7%, and 3.03 kg-C m^{-2}, respectively). Simulations with higher a_w and τ_w overestimate AGLB. For the best simulation, the small correlation coefficients between AGLB error and S_{in} error (-0.04), and between AGLB error and P error according to Leemans and Cramer (0.17), Legates and Willmott (0.21) and TRMM (0.26) P datasets, indicate again that the spatial distribution of the AGLB error is not climate driven, leaving us with the hypothesis that carbon allocation varies spatially.

Figure 1.9 illustrates the spatial pattern of AGLB for the Amazon region simulated by six CCM3-IBIS sensitivity simulations, AGLB aggregated from *Saatchi et al.* [2007], and the difference between them. Simulated AGLB (Figures 1.9b, 1.9c, 1.9d, 1.9h, 1.9i, and 1.9j) is higher in central Amazonia, Colombia, and in some parts of Bolivia and Peru. Lower AGLB is simulated over southeast Amazonia. CCM3-IBIS underestimates AGLB over eastern Venezuela and Amapá in Brazil, because in these regions the precipitation is underestimated too (Figure 1.4). In eastern Venezuela, the land cover simulated is not even forest (Figure 1.7), which explains the very low simulated AGLB.

Figure 1.9e illustrates areas where the best simulation (a4t25) overestimates (positive values) or underestimates (negative values) AGLB according to *Saatchi et al.* [2007] (Figure 1.9a). In southeast Amazonia CCM3-IBIS overestimates AGLB because this area is deforested and these simulations do not take anthropogenic land use into account. Some regions in Peru, Ecuador, Colombia, and Manaus in Brazil are

overestimated too. In western Amazonia – parts of Acre, Amazonas, Peru, and Colombia – CCM3-IBIS underestimates AGLB.

In a5t40 and a5t50 simulations, the simulated AGLB is greater than 17 kg-C m^{-2} over most of Amazon region (Figures 1.9i and 1.9j). Although the use of these parameters represent well the high biomass values found by Saatchi et al. at the Brazil-Peru border, the differences between these simulations and the aggregated map from *Saatchi et al.* [2007] (Figures 1.9l and 1.9m) show that in almost all Amazonia AGLB is overestimated.

Observed AGLB has a significant spatial variability, which may be related to climate conditions and soil fertility, leading to maximum biomass in wet regions with low wood productivities and infertile soils (central Amazonia and the Guyana coast), and lower biomass in dynamic western Amazonia, and the dry southern and northern Amazon region [*Malhi et al.*, 2006; *Saatchi et al.*, 2007]. For example, wood residence time is 67 years in central Amazonia, compared to 44 years in western Amazonia [*Malhi et al.*, 2004]. Since spatial variations in climate are well represented in these simulations, this leaves spatial variations in CART, possibly driven by soil fertility, as the major reason why spatial patterns of AGLB were not well represented. In order to have better estimates of the magnitude and the spatial variability of AGLB in the future, the CART and their relation to environmental variables need to be better understood and explicitly modeled.

1.4. DISCUSSION AND CONCLUSIONS

The accurate representation of the coupled climate-biosphere dynamics requires the accurate representation of climate (in particular P and S_{in}, the most relevant climate variables to vegetation dynamics in the Amazon), NPP, and its partition among the several carbon pools components.

Most variables that do not depend on carbon allocation are simulated within 10% of the estimates: average P is within 5% of four P estimates, average S_{in} is within 7% of observations, average NPP_{total} is within 5% and average NPP_{ag} is within 2% of observations. Respiration rates and NPP_{agw} are within 15% and 16% of the observations, respectively. Considering only the default run (a4t25), simulated AGLB is within 12% of *Saatchi et al.* [2007] estimates, but underestimates *Malhi et al.* [2006] AGLB by 37%. In both cases, simulated AGLB is underestimated, and LAI is overestimated, which motivated us to run a sensitivity study, in which higher values of AGLB are obtained using elevated wood CART parameters.

Although some of these biases could be easily fixed by adjusting a few model parameters, a larger issue remains, which is the spatial variability of some parameters, in particular the CART. For example, adjusting the carbon allocation to leaves may

remove the average LAI bias, but would produce a higher LAI at Tapajós than at Manaus, while the inverse is observed.

We conclude that the correct simulation of seasonal and spatial patterns of climate, land cover and NPP does not warrant an accurate representation of the spatial patterns of vegetation structure and dynamics in Amazonia. Spatial patterns of CART parameters are needed. To obtain them, there are two possibilities.

The first one is to input the available spatial parameter data [*Malhi et al.*, 2004; *Phillips et al.*, 2004] into the model. Although this will certainly improve the spatial performance of the model in Amazonia, we still have no clue about the spatial variability of these parameters in other tropical forest regions of the world. In addition, the turnover rates (inverse of the residence time) have been increasing in the last 30 years in Amazonia [*Phillips et al.*, 2004], suggesting that this simple parameterization may not be representative, for example, in a higher CO_2 climate.

The second one is to parameterize the known CART coefficients to environmental variables – the best candidate is soil fertility, according to the data provided by *Phillips et al.* [2004] – which creates an additional problem: there are no global maps of soil fertility, again restricting the application to Amazonia.

On the other hand, the temporal and spatial change of the CART parameters may be an important adaptative mechanism of the tropical rainforest under climate change. For example, if the climate becomes drier and there is a trend towards savannization, plants may respond by allocating more carbon to roots, or forest composition may change favoring deep root trees instead of tall trees. Moreover, this may happen only in southern and eastern Amazonia, regions that are in principle more prone to vegetation change.

Concluding, this specific coupled climate-biosphere model represents well most average climate, vegetation structure and dynamics variables in Amazonia – all within 20% of error (with the exception of LAI). Despite this, there are important spatial differences in the vegetation variables, regardless of good spatial representations of climate.

Although the current performance is probably sufficient for global experiments that rely on the region-wide carbon balance, such as C^4MIP, the vegetation structure and dynamics regional performance still needs improvement. This is a challenging research topic, as there are few studies that measured all components to allow estimation of partitioning coefficients [*Litton et al.*, 2007]. We also must understand better the mechanisms that drive them.

Understanding spatial variation in carbon allocation and its relation to climate and CO_2 is a central part of improving the representation of the Amazon spatial patterns. With a coupled climate-biosphere model that represents well the Amazon structure and dynamics, we may perform reliable projections of future climate change for this region, identifying vulnerable areas of potential ecological disruption.

Table 1.1. The mean percentual relative error (e (%)) and the root mean square error (RMSE) of simulated sensible heat (H), latent heat (LE), and net ecosystem exchange (NEE) before and after calibration, for the four sites. The units refer to RMSE only. From *Imbuzeiro* [2005].

	Calibration	Error	**H** ($W\ m^{-2}$)	**LE** ($W\ m^{-2}$)	**NEE** ($kg\text{-}C\ ha^{-1}\ hr^{-1}$)
Tapajós km 83	Before	e (%)	53	-22	33
		RMSE	61.93	118.96	4.41
	After	e (%)	7	6	42
		RMSE	45.84	98.58	4.02
Tapajós km 67	Before	e (%)	14	7	-99
		RMSE	30.60	52.43	5.70
	After	e (%)	11	11	-1
		RMSE	33.07	52.43	1.13
Manaus	Before	e (%)	0	4	-216
		RMSE	58.70	87.87	6.60
	After	e (%)	-4	8	37
		RMSE	45.40	79.34	4.20
Jaru	Before	e (%)	-6	-42	-39
		RMSE	81.51	117.20	4.24
	After	e (%)	-4	-6	-6
		RMSE	64.67	100.70	4.58

Table 1.2. Annual mean precipitation for the Amazon tropical forest region, from different sources. The mean percentual relative difference (e (%)) is calculated using each dataset as reference. Dataset values from *Pinto* [2007].

Precipitation dataset	**Precipitation (mm/day)**	**e (%)**
CRU	4.98	24.5
GPCP	5.36	15.7
CMAP	5.45	13.8
ERA-40	5.91	4.9
Leemans and Cramer [1990]	5.95	4.2
CCM3-IBIS	6.20	-
Legates and Willmott [1990]	6.20	0.0
TRMM	6.39	-3.0
NCEP/NCAR	6.70	-7.5

Table 1.3. Respiration rates (kg-C m^{-2} y^{-1}) simulated by CCM3-IBIS and observed by *Malhi et al.* [submitted] for Manaus, Tapajós, Caxiuanã, and an average of the three sites. e (%) is the mean percentual relative error.

	Manaus			**Tapajós**			**Caxiuanã**			**Sites Average**		
	Sim.	**Obs.**	**e (%)**	**Sim.**	**Obs.**	**e (%)**	**Sim.**	**Obs.**	**e (%)**	**Sim.**	**Obs.**	**e (%)**
$R_{heterotrophic}$	1.10	0.96	14.6	1.02	1.49	-31.5	0.81	0.94	-13.8	0.98	1.13	-13.6
R_{root}	0.56	0.56	0.0	0.49	0.37	32.4	0.38	0.74	-48.6	0.48	0.56	-14.4
$R_{soil+litter}$	1.66	1.52	9.2	1.52	1.86	-18.3	1.19	1.68	-29.2	1.46	1.69	-13.6

Table 1.4. Total and aboveground net primary production (NPP_{total} and NPP_{ag}, respectively) in kg-C m^{-2} y^{-1} and the fraction NPP_{ag}/NPP_{total} simulated by CCM3-IBIS and observed by *Malhi et al.* [submitted] for Manaus, Tapajós, Caxiuanã, and an average of the three sites. e (%) is the mean percentual relative error.

	Manaus			**Tapajós**			**Caxiuanã**			**Sites Average**		
	Sim.	**Obs.**	**e (%)**	**Sim.**	**Obs.**	**e (%)**	**Sim.**	**Obs.**	**e (%)**	**Sim.**	**Obs.**	**e (%)**
NPP_{total}	1.23	1.01	21.8	1.16	1.44	-19.4	0.91	1.00	-9.0	1.10	1.15	-4.3
NPP_{ag}	0.98	0.73	34.2	0.92	1.14	-19.3	0.73	0.72	1.4	0.88	0.86	1.5
NPP_{ag}/NPP_{total}	0.80	0.72	11.1	0.80	0.79	1.3	0.80	0.72	11.1	0.80	0.75	6.7

Table 1.5. Summary of the CCM3-IBIS simulations used in this study. The simulation a4t25 was the first, and it is described in materials and methods section. The differences among the six simulations are the coefficients a_w, a_l, a_r, and τ_w (Equation (1)).

Simulations	$\mathbf{a_w}$	$\mathbf{a_l}$	$\mathbf{a_r}$	$\boldsymbol{\tau_w}$ (years)
a4t25	0.4	0.4	0.2	25
a4t40	0.4	0.4	0.2	40
a4t50	0.4	0.4	0.2	50
a5t25	0.5	0.4	0.1	25
a5t40	0.5	0.4	0.1	40
a5t50	0.5	0.4	0.1	50

Table 1.6. Simulated and observed mean NPP_{agw} (kg-C m^{-2} y^{-1}) over the cells from *Malhi et al.* [2004]. The mean error (ε), mean percentual relative error (e (%)), mean absolute error (MAE), and the correlation coefficient between NPP_{agw} error and GOES GL 1.2 S_{in} error ($\rho(\varepsilon_{NPPagw}, \varepsilon_{Sin})$); NPP_{agw} error and Leemans and Cramer P error ($\rho(\varepsilon_{NPPagw}, \varepsilon_{PLC})$); NPP_{agw} error and Legates and Willmott P error ($\rho(\varepsilon_{NPPagw}, \varepsilon_{PLW})$); and NPP_{agw} error and TRMM P error ($\rho(\varepsilon_{NPPagw}, \varepsilon_{PTRMM})$), are shown for each simulation.

Simulations	**NPP_{agw}**	**ε**	**e (%)**	**MAE**	**$\rho(\varepsilon_{NPPagw}, \varepsilon_{Sin})$**	**$\rho(\varepsilon_{NPPagw}, \varepsilon_{PLC})$**	**$\rho(\varepsilon_{NPPagw}, \varepsilon_{PLW})$**	**$\rho(\varepsilon_{NPPagw}, \varepsilon_{PTRMM})$**
a4t25	0.35	0.05	15.5	0.10	-0.04	0.10	0.20	-0.09
a4t40	0.36	0.06	19.4	0.10	-0.07	0.11	0.23	-0.07
a4t50	0.36	0.06	20.0	0.10	-0.05	0.10	0.23	-0.07
a5t25	0.44	0.14	46.7	0.16	-0.14	0.07	0.20	-0.05
a5t40	0.44	0.14	47.0	0.16	-0.11	0.07	0.20	-0.08
a5t50	0.44	0.14	47.6	0.16	-0.10	0.05	0.19	-0.08
Observation	0.30							

Table 1.7. Observed and simulated NPP_{agw}, and the mean percentual relative error (e (%)). The simulation used was a4t25, which has the best NPP_{agw} estimate.

Lat. (deg.)	Long. (deg.)	Country	Observed NPP_{agw}	Simulated NPP_{agw}	e (%)
-4.19	-73.13	Peru	0.36	0.38	4.6
-1.40	-75.94	Ecuador	0.37	0.39	5.2
-1.40	-59.06	Brazil	0.23	0.42	86.7
-1.40	-73.13	Colombia	0.17	0.42	147.0
-9.98	-50.63	Brazil	0.28	0.33	18.9
-1.40	-50.63	Brazil	0.23	0.29	25.7
4.19	-56.25	Suriname	0.28	0.38	32.8
-15.35	-61.88	Bolivia	0.31	0.25	-18.2
9.77	-73.13	Venezuela	0.35	0.36	3.3
-12.56	-70.31	Peru	0.33	0.44	31.0
1.40	-75.94	Ecuador	0.52	0.45	-12.6
-1.40	-61.88	Brazil	0.21	0.39	86.1
-1.40	-78.75	Ecuador	0.41	0.20	-50.2
-1.40	-53.44	Brazil	0.25	0.19	-23.2
-18.14	-39.38	Brazil	0.31	0.18	-41.7
-1.40	-47.81	Brazil	0.25	0.36	41.5
-12.56	-73.13	Peru	0.34	0.28	-16.1
4.19	-53.44	French Guiana	0.27	0.39	46.1
-9.98	-73.13	Peru	0.36	0.38	6.0
1.40	-67.50	Venezuela	0.19	0.39	103.9
-1.40	-56.25	Brazil	0.26	0.37	42.1
Mean:			**0.30**	**0.35**	**15.5**

Table 1.8. Annual mean leaf area index (m^2 m^{-2}) simulated and observed for Ji-Paraná, Manaus, Marabá, and Tapajós. The LAI MODIS estimate is for Tapajós only. The mean error (ε), mean percentual relative error (e (%)), and mean absolute error (MAE) for each simulation.

Simulations	**Ji-Paraná**	**Manaus**	**Marabá**	**Tapajós**	**ε**	**e (%)**	**MAE**
a4t25	7.58	9.01	6.91	8.93	2.81	53.1	2.81
a4t40	7.72	9.08	7.06	9.08	2.94	55.5	2.94
a4t50	7.88	9.11	7.19	9.13	3.03	57.3	3.03
a5t25	8.51	9.80	7.73	9.75	3.65	69.0	3.65
a5t40	8.43	9.95	7.87	9.94	3.75	70.9	3.75
a5t50	8.56	9.91	7.71	10.06	3.77	71.1	3.77
Observation	4.63	6.10	5.38	5.07			
MODIS				5.49			

Table 1.9. Simulated and observed mean AGLB (kg-C m^{-2}) over the cells from *Malhi et al.* [2006]. The mean error (ε), mean percentual relative error (e (%)), mean absolute error (MAE), and the correlation coefficient between AGLB error and GOES GL 1.2 Sin error ($\rho(\varepsilon_{AGLB}, \varepsilon_{Sin})$); AGLB error and Leemans and Cramer P error ($\rho(\varepsilon_{AGLB}, \varepsilon_{PLC})$); AGLB error and Legates and Willmott P error ($\rho(\varepsilon_{AGLB}, \varepsilon_{PLW})$); and AGLB error and TRMM P error ($\rho(\varepsilon_{AGLB}, \varepsilon_{PTRMM})$), are shown for each simulation.

Simulations	**AGLB**	**ε**	**e (%)**	**MAE**	**$\rho(\varepsilon_{AGLB}, \varepsilon_{Sin})$**	**$\rho(\varepsilon_{AGLB}, \varepsilon_{PLC})$**	**$\rho(\varepsilon_{AGLB}, \varepsilon_{PLW})$**	**$\rho(\varepsilon_{AGLB}, \varepsilon_{PTRMM})$**
a4t25	9.55	-5.65	-37.2	5.67	0.20	0.51	0.51	0.44
a4t40	12.54	-2.66	-17.5	3.26	0.07	0.42	0.40	0.40
a4t50	14.02	-1.19	-7.8	2.84	0.03	0.39	0.34	0.37
a5t25	12.38	-2.82	-18.5	3.35	0.11	0.44	0.42	0.40
a5t40	16.19	0.99	6.5	3.56	0.00	0.34	0.29	0.32
a5t50	17.86	2.66	17.5	4.92	-0.03	0.31	0.27	0.31
Observation	15.20							

Table 1.10. Simulated and observed mean AGLB (kg-C m^{-2}) over the rainforest cells aggregated from *Saatchi et al.* [2007]. The mean error (ε), mean percentual relative error (e (%)), mean absolute error (MAE), and the correlation coefficient between AGLB error and GOES GL 1.2 Sin error ($\rho(\varepsilon_{AGLB}, \varepsilon_{Sin})$); AGLB error and Leemans and Cramer P error ($\rho(\varepsilon_{AGLB}, \varepsilon_{PLC})$); AGLB error and Legates and Willmott P error ($\rho(\varepsilon_{AGLB}, \varepsilon_{PLW})$); and AGLB error and TRMM P error ($\rho(\varepsilon_{AGLB}, \varepsilon_{PTRMM})$), are shown for each simulation.

Simulations	**AGLB**	**ε**	**e (%)**	**MAE**	**$\rho(\varepsilon_{AGLB}, \varepsilon_{Sin})$**	**$\rho(\varepsilon_{AGLB}, \varepsilon_{PLC})$**	**$\rho(\varepsilon_{AGLB}, \varepsilon_{PLW})$**	**$\rho(\varepsilon_{AGLB}, \varepsilon_{PTRMM})$**
a4t25	9.87	-1.35	-11.7	3.03	-0.04	0.17	0.21	0.26
a4t40	13.20	2.08	18.1	3.50	-0.10	0.20	0.24	0.32
a4t50	14.82	3.75	32.6	4.33	-0.10	0.20	0.24	0.32
a5t25	12.97	1.85	16.1	3.31	-0.08	0.20	0.25	0.31
a5t40	17.17	6.18	53.6	6.33	-0.13	0.21	0.26	0.34
a5t50	19.06	8.13	70.5	8.19	-0.15	0.22	0.27	0.35
Observation	11.18							

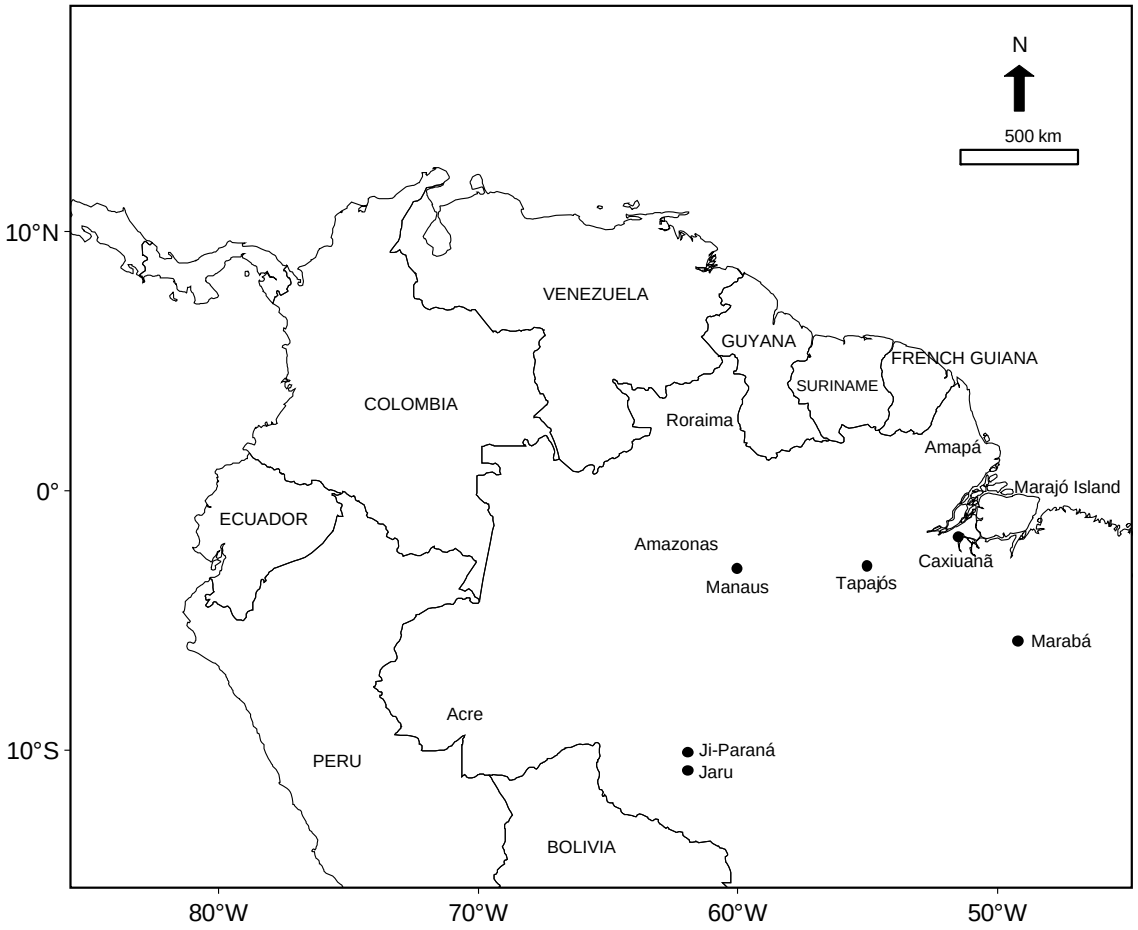

Figure 1.1. Orientation map.

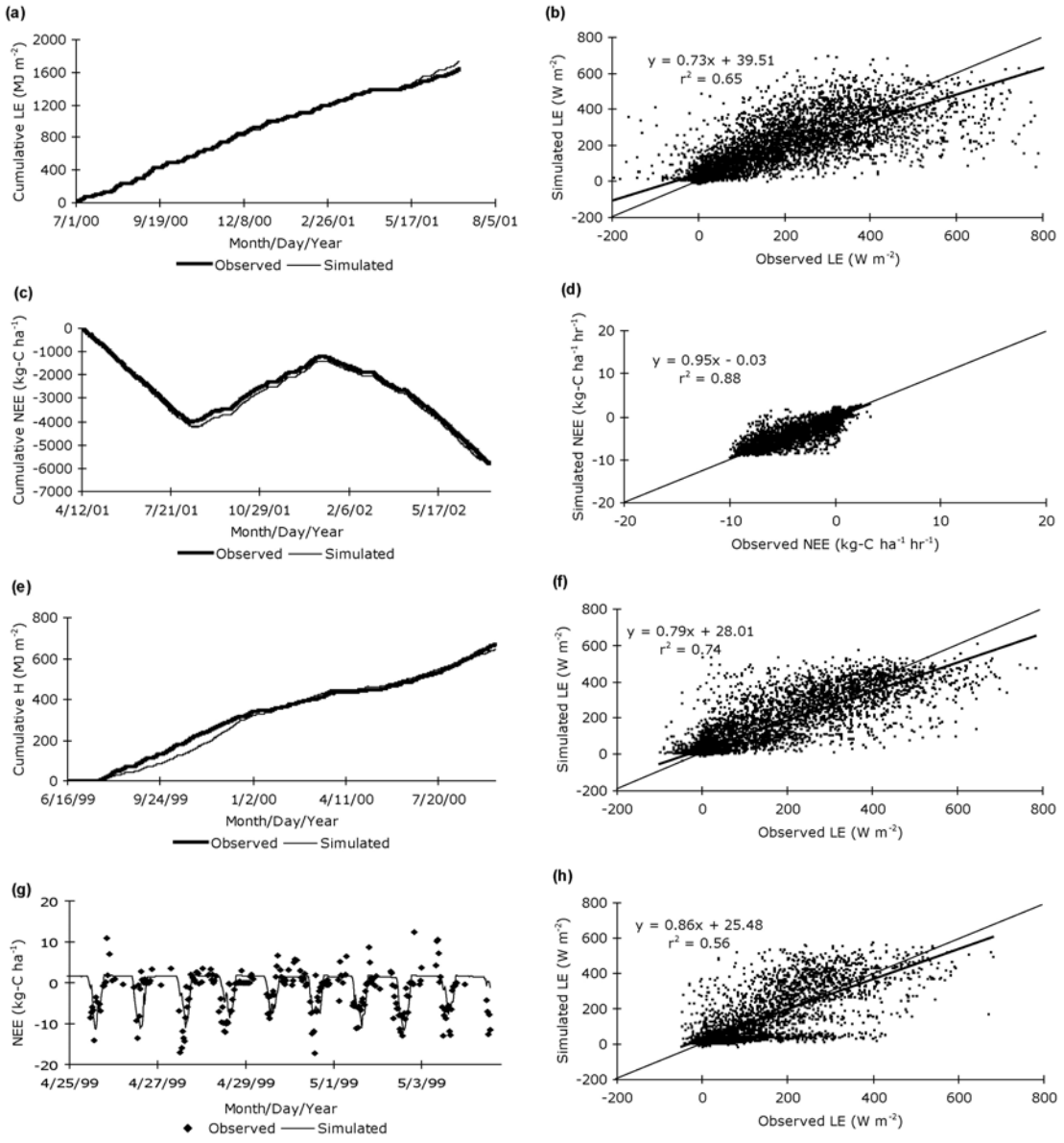

Figure 1.2. Dispersion, cumulative and temporal patterns of sensible heat (H), latent heat (LE), and net ecosystem exchange (NEE) for (a) and (b) Tapajós km 83, (c) and (d) Tapajós km 67, (e) and (f) Manaus and (g) and (h) Jaru sites, after calibration [*Imbuzeiro*, 2005].

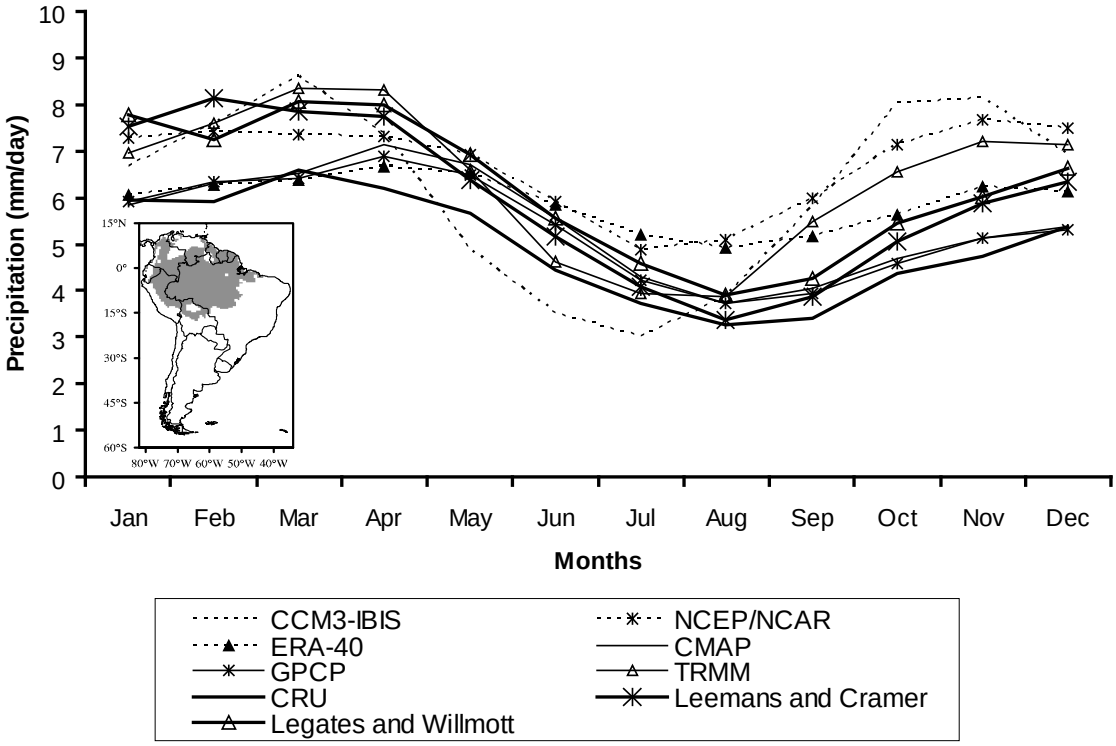

Figure 1.3. Monthly variation of precipitation for the Amazon tropical forest region (inset). Dataset values from *Pinto* [2007].

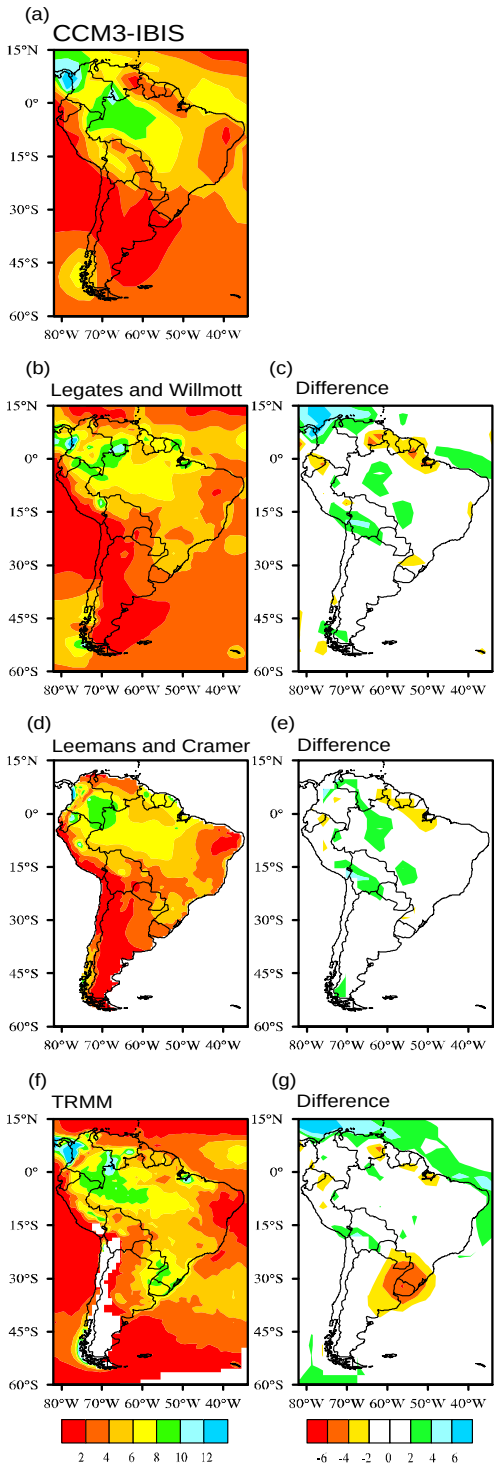

Figure 1.4. Annual mean precipitation climatology for South America (mm/day) (a) simulated by CCM3-IBIS, and for (b) Legates and Willmott, (d) Leemans and Cramer, and (f) TRMM datasets. (c), (e) and (g) The difference is calculated by CCM3-IBIS minus Legates and Willmott, Leemans and Cramer and TRMM datasets, respectively. Dataset values from *Pinto* [2007].

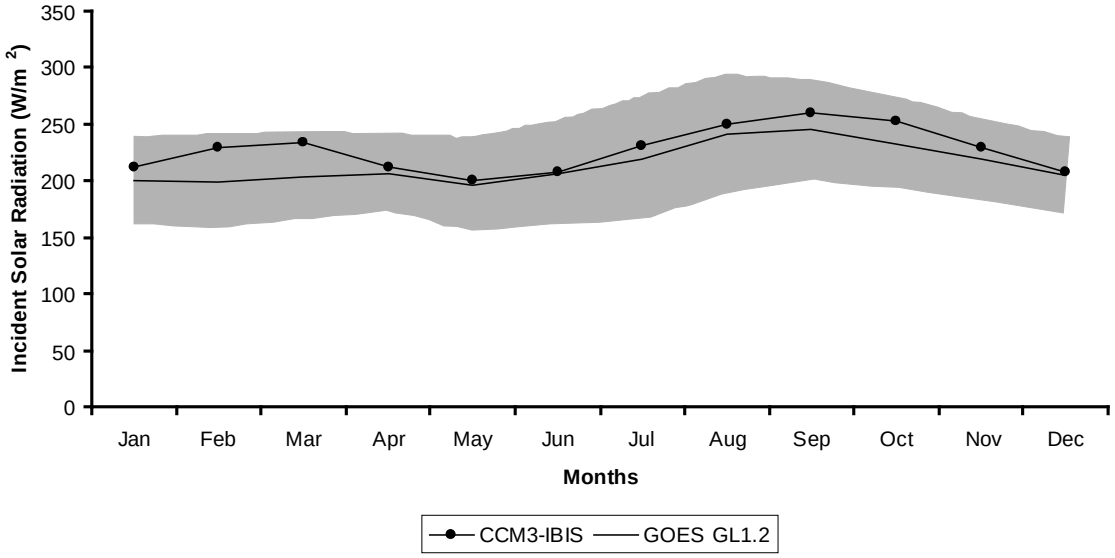

Figure 1.5. Monthly variation of incident solar radiation for the Amazon tropical forest region. The shaded area indicates the confidence interval for the GOES GL1.2 mean, at 95% level of confidence. GOES GL1.2 values from *Pinto* [2007].

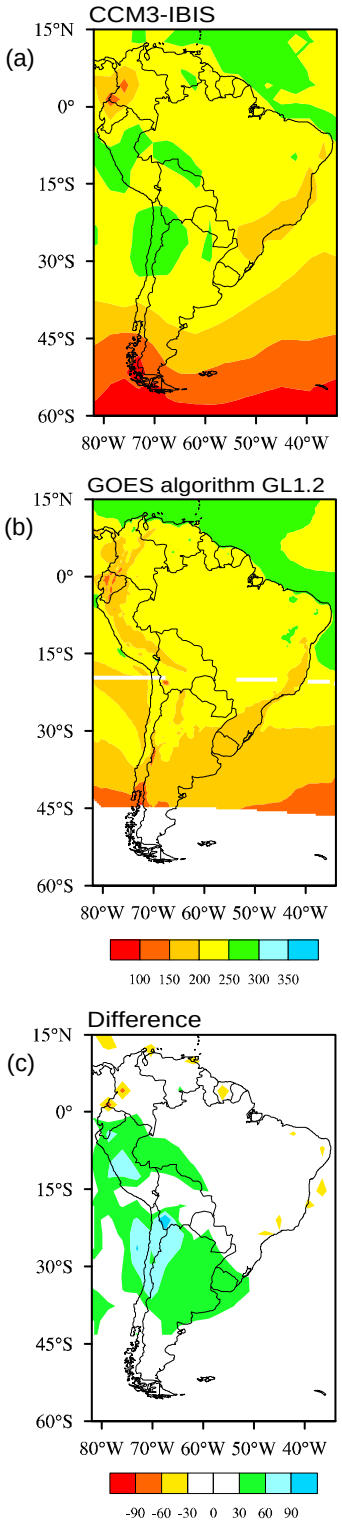

Figure 1.6. Annual mean incident solar radiation climatology for South America (W/m^2) (a) simulated by CCM3-IBIS, and for the (b) GOES algorithm GL1.2 dataset. (c) The difference is calculated by CCM3-IBIS minus GOES GL1.2 dataset. Dataset values from *Pinto* [2007].

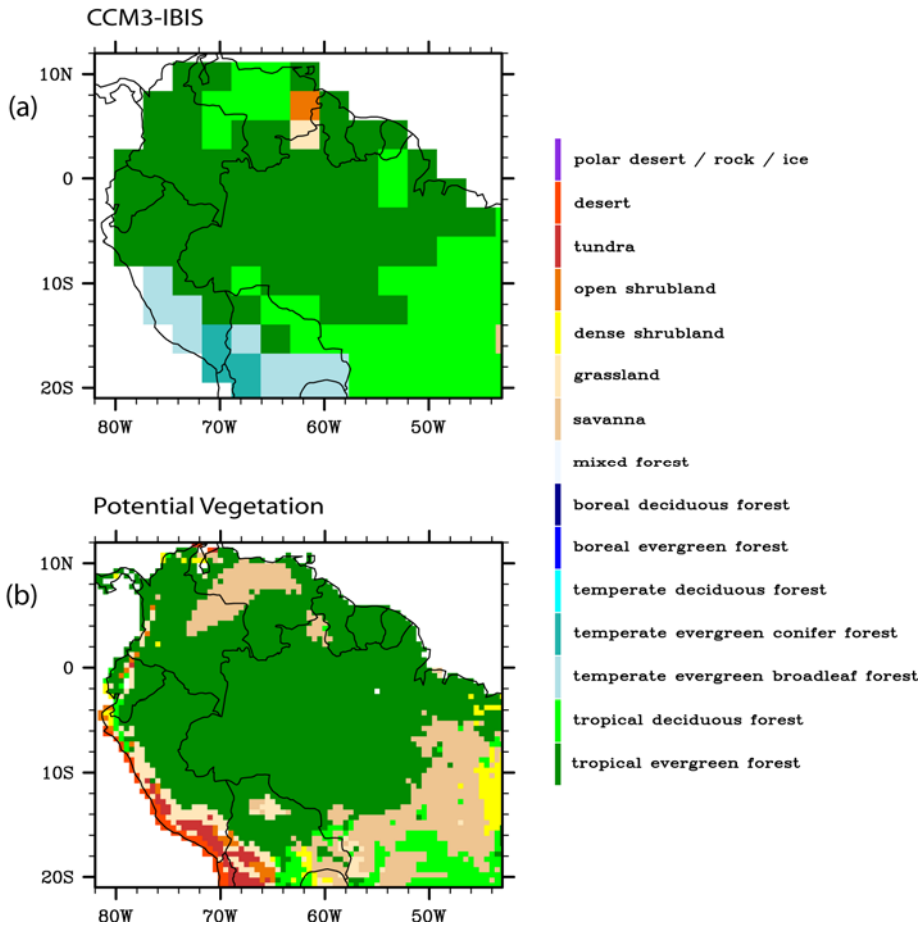

Figure 1.7. Land cover distribution (a) simulated by CCM3-IBIS and (b) from SAGE potential vegetation dataset.

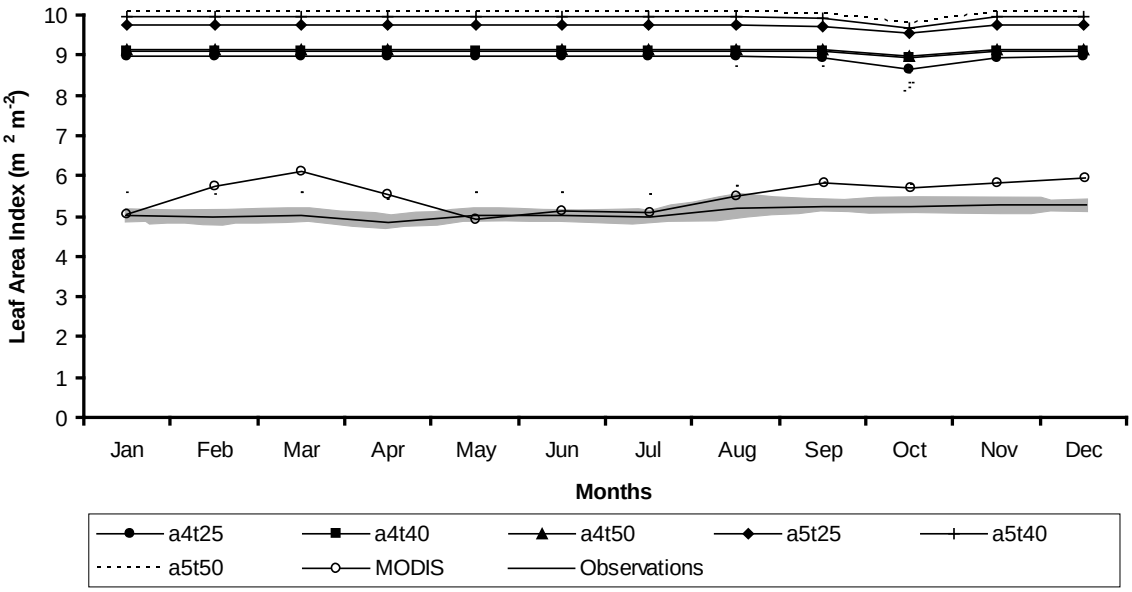

Figure 1.8. Monthly mean leaf area index for Tapajós site observed and obtained by six CCM3-IBIS sensitivity simulations. The shaded area indicates the confidence interval for the observed mean, at 95% level of confidence. The MODIS values for this pixel are also shown.

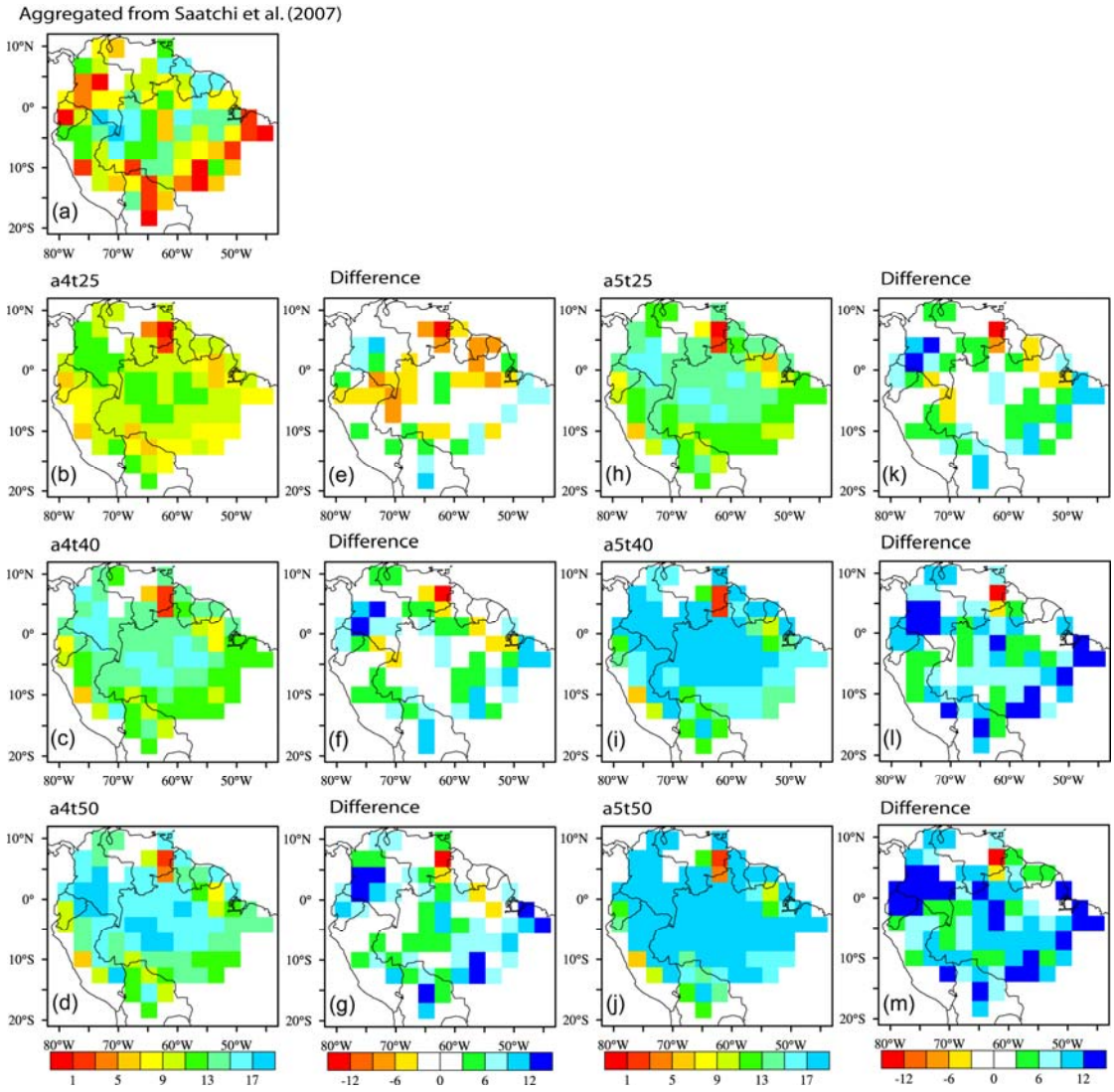

Figure 1.9. Aboveground live biomass distribution (kg-C m^{-2}) (a) aggregated from *Saatchi et al.* [2007] and from CCM3-IBIS simulations: (b) a4t25, (c) a4t40, (d) a4t50, (h) a5t25, (i) a5t40, and (j) a5t50. The differences (e), (f), (g), (k), (l), and (m) are calculated by a4t25, a4t40, a4t50, a5t25, a5t40, and a5t50 minus aggregated data from *Saatchi et al.* [2007], respectively.

CHAPTER 2

REGROWTH OF THE AMAZON FOREST UNDER DIFFERENT TYPES OF NUTRIENT STRESS FOR A LARGE-SCALE DEFORESTATION

2.1. INTRODUCTION

The Amazon tropical forest is one of the world's most important ecosystems, with a vital role for the world biodiversity [*Godoy et al.*, 1999; *Prance et al.*, 2000; *Dirzo and Raven*, 2003] and for the global carbon cycle [*Clark et al.*, 2003; *Clark*, 2004]. Large areas of the Amazon forest have been deforested in recent decades by cattle ranchers, with an increasing role being played by soybeans [*Skole and Tucker*, 1993; *Nepstad et al.*, 1999, 2006; *Laurance et al.*, 2001; *INPE*, 2007]. Deforestation degrades environmental services such as maintenance of biodiversity, water cycling and carbon stocks [*Foley et al.*, 2007]. The rainforest future may be dependent on at least three positive feedbacks associated with the deforestation.

The first feedback suggests that the reduction of precipitation after a large-scale deforestation might prevent an eventual forest regrowth [*Shukla et al.*, 1990]. The Amazon helps to fuel the Hadley and Walker circulations in the tropical atmosphere. Several climate modeling experiments indicate that as deforestation increases, the subsequent reductions in evapotranspiration and atmospheric heating may weaken moisture recycling and deep convection over the Amazon, thus lowering precipitation

[*Shukla et al.*, 1990; *Nobre et al.*, 1991; *Costa and Foley*, 2000; *Costa et al.*, 2007; *Sampaio et al.*, 2007].

The second feedback is related to the use of fire for land-clearing and for slash-and-burn agriculture, which is widespread in the Amazon [*Nepstad et al.*, 2001; *Zarin et al.*, 2005]. Fires used in the establishment of cattle pasture or crops and in their management, often spread beyond the intended boundaries, increasing the susceptibility of forests to recurrent burning by killing trees, thereby allowing sunlight to penetrate the forest canopy, and increasing the fuel load on the forest floor [*Nepstad et al.*, 1999, 2001].

The third feedback is related to the effects of frequent burning on soil fertility and future forest productivity. Soil nutrients are considerably lost to the atmosphere after repeated fire events, including N and S losses by volatilization and P, K, Ca, and Mg losses by ash transport. Nutrients in the remaining ash might be lost by leaching to surface and groundwater [*Kauffman et al.*, 1993; *Mackensen et al.*, 1996; *Sampaio et al.*, 2003]. In fertilization studies [*Gehring et al.*, 1999; *Davidson et al.*, 2004, *Silva et al.*, 2006], the secondary forest responded to application of P and N, indicating that soil nutrient limitation may reduce the vegetation regrowth and the biomass accumulation rate. In addition, rates of secondary forest regrowth in Amazonia have been inversely correlated with the number of fires, and the biomass accumulation rate decreases 47% in areas with a history of frequent fires [*Zarin et al.*, 2005]. These studies indicate that nutrient limitation is a main factor in reducing the rate of forest regrowth. Nutrient stress also varies with forest age because the secondary forest regrowth increases the accumulation of total ecosystem N [*Davidson et al.*, 2007]. So, while the forest maturation has the capacity to rebuild nutrient stocks, improving the environment for

the forest regrowth, the reduction of forest regrowth rate makes this nutritional recuperation difficult.

Despite the evidence on the effects of changing precipitation, fire frequency, and nutrient status, we still do not know how these controls may interact to regulate the secondary forest regrowth and how these interactions may vary in different parts of Amazonia. Here, we investigate how the climate feedback and the nutrient feedback may affect the Amazon rainforest regrowth after a hypothetical full deforestation (the fire feedback is not included in this study). To address this question, we use the fully coupled climate-biosphere model CCM3-IBIS with different initial land cover conditions and different types of nutrient stress.

2.2. MATERIALS AND METHODS

2.2.1. Model Description

In this study, we use the National Center for Atmospheric Research (NCAR) Community Climate Model version 3 (CCM3) [*Kiehl et al.*, 1998] coupled with an updated version of the Integrated Biosphere Simulator (IBIS) [*Foley et al.*, 1996; *Kucharik et al.*, 2000]. We refer to this coupled model as CCM3-IBIS [*Delire et al.*, 2002]. This is virtually the same core of the Lawrence Livermore National Laboratory (LLNL) model used in the Intergovernmental Panel on Climate Change (IPCC) AR4 simulations and in the Coupled Climate-Carbon Cycle Model Intercomparison Project (C^4MIP project), except for our own tuning for the rainforest [see chapter 1]. CCM3-IBIS can reproduce the bi-directional interactions between vegetation and climate, being indispensable for the study of biome distribution, ecosystem function, and climate feedbacks in the context of both global climate change and land use change [*Foley et al.*, 2000].

CCM3 is an atmospheric general circulation model with spectral representation of the horizontal fields. It simulates the large-scale physics (radiative transfer, hydrologic cycle, cloud development, thermodynamics) and dynamics of the

atmosphere. Here, we operate the model at a spectral resolution of T42 (~2.81º X 2.81º latitude/longitude grid), 18 vertical levels, and a 15-min time step. The oceans are represented by monthly averaged fixed sea-surface temperatures of the 1990s that serve as boundary conditions for the atmosphere.

IBIS is a comprehensive model of terrestrial biospheric processes that represents the physical, physiological, and ecological processes occurring in vegetation and soils. IBIS simulates land surface processes, plant phenology and vegetation dynamics, and represents vegetation as two layers (trees and grasses). In IBIS a grid cell can contain one or more plant functional types that together comprise a vegetation type. Land surface physics and canopy physiology are calculated at the same time step used by CCM3. The plant phenology algorithm has a daily time step and the vegetation dynamics is solved with an annual time step. IBIS operates on the same T42 spatial grid as the CCM3, and with dynamic vegetation component enabled, so vegetation structure and biogeography change in response to climate. Although the spatial resolution is relatively coarse, the explicit links between vegetation and climate represent a considerable step forward.

To date, IBIS does not contain a complete N cycle. Although soil N transformations are tracked in the soil biogeochemistry module reported in *Kucharik et al.* [2000], there are no soil N controls on vegetation productivity. So, we penalize the NPP of the regrowth forest directly, assuming that the nutrient limitation is caused by frequent fires before the beginning of the experiment. In this experiment, we consider two types of nutrient stress, dynamic and fixed. For a dynamic nutrient stress, the NPP is reduced according to an empirical relation that reflects a NPP decrease of 50% for trees biomass equal to zero, and no NPP decrease when the trees biomass reaches 10 kg-C m^{-2} or more (typical values of a mature forest). This assumption reproduces the

capacity of the secondary forest to rebuild nutrient stocks in mature stages [*Davidson et al.*, 2007]. For a fixed nutrient stress, the forest NPP is 47% of the unlimited case, following the results for a young forest in Paragominas (eastern Amazonia) found by *Davidson et al.* [2004], and the results for sites with a history of frequent fires found by *Zarin et al.* [2005].

CCM3-IBIS was calibrated against Large Scale Biosphere-Atmosphere Experiment in Amazonia (LBA) tower results, and extensively validated against spatial fields of incident solar radiation, precipitation, land cover patterns, heterotrophic and root respiration, total NPP, aboveground NPP, wood NPP, leaf area index, and aboveground live biomass. The Amazon climate (annual mean and seasonality) is very well simulated for both incident solar radiation and precipitation. Average incident solar radiation and precipitation are within 7% and 5% of the observations, respectively. Average total NPP is within 5% and average aboveground NPP is within 2% of observations. Respiration rates and wood NPP are within 15% and 16% of the observations, respectively. Simulated aboveground live biomass is within 12% of *Saatchi et al.* [2007] estimates. For more details, see chapter 1.

2.2.2. Experiment Design

The numerical experiment is designed to investigate the biosphere-atmosphere interaction of the Amazon rainforest regrowth under nutrient stress. The CO_2 concentration was kept constant at 380 ppmv. The experiment evaluated different initial conditions (forest/pastureland) and different types of nutrient stress (dynamic/fixed). It is divided in four 50-year long simulations, with three ensembles each:

- F: initial condition forest and no nutrient limitation (control run);

- P: initial condition pasture and no nutrient limitation;
- PND: initial condition pasture and with a dynamic nutrient limitation;
- PNF: initial condition pasture and with a fixed nutrient limitation.

2.3. RESULTS

2.3.1. Land Cover Patterns

The simulated land cover chronosequence with different initial conditions and different types of nutrient stress is illustrated in Figure 2.1. In the F simulation the Amazon tropical evergreen forest remains stable through the 50 years of the experiment, except for a small part in southeast Amazonia that becomes tropical deciduous forest, regionally called cerradão. Vegetation in few pixels in the Brazil-Venezuela border and in northeast Amazonia is misrepresented due to precipitation underestimation in these areas. In the P simulation the secondary forest regrows rapidly in all deforested area and the land cover patterns are quite similar to the F simulation after 50 years, although the biomass of this secondary forest is much smaller than the primary forest one [more details in Section 2.3.4]. In the PND case the forest regrowth is incomplete and is delayed by 20-30 years in much of the region. In contrast, the secondary forest is unable to regrow in most of the region in the PNF simulation. Analyzing the four simulations, three distinct regions are evident. In region 1, over Colombia and northwestern Amazonas state in Brazil, the secondary forest regrows in all simulations. In region 2, central Amazonia above 10º S (central-southern Amazonas state), after 50 years of

simulation, an evergreen rainforest regrows in the P simulation, the PND deforested region becomes a tropical deciduous forest and the PNF land cover changes from grassland to savanna (regionally called cerrado strictu sensu). And in region 3, southern Amazonia below 10º S (northern Mato Grosso state), after 50 years, the PND and PNF land cover becomes a savanna and a dense shrubland (regionally called campo sujo), respectively. Even with a more realistic nutrient stress [*Davidson et al.*, 2007] in the PND simulation, there is no regeneration of the forest over region 3. Below, we analyze the major variables that describe the climate-vegetation interaction in these three regions. Over each region, the mean values of these variables are calculated considering six grouped grid cells under the respective numbers shown in Figure 2.1.

2.3.2. Precipitation

The region 1 annual mean precipitation (Figure 2.2a) is very similar for all simulations; there are only few differences among them in the first years, when the deforested cases (P, PND, and PNF) have a smaller precipitation. The mean simulated precipitation for the 50 years is 8.8, 8.6, 8.8, and 8.3 mm day^{-1} for F, P, PND, and PNF, respectively. This means that precipitation in this region is nearly independent of the land cover. Over region 2 (Figure 2.2b), the annual mean precipitation of F simulation remains high, with an average of 8.4 mm day^{-1} through the 50 years. The precipitation of P case is slightly lower in the first 10 years, and then reaches the magnitude of F precipitation, with an average of 8.2 mm day^{-1} through the 50 years. The precipitation in the PND and PNF cases is significantly lower. In PND, the precipitation increases slowly through the years and after 40 years it reaches the F precipitation. This happens because only after 30-40 years the recovery of the secondary forest over region 2 is

more noticeable (Figure 2.1), and the mean simulated precipitation for the 50 years is 6.9 mm day^{-1}. In PNF, the average for all simulated period is 6.4 mm day^{-1} and the precipitation never reaches the F climate. In all four cases in region 2, precipitation is clearly dependent on the land cover. Over region 3 (Figure 2.2c), the precipitation also shows a clear dependence on the land cover, but its magnitude is lower than in the former regions. The F mean precipitation is 7.3 mm day^{-1} and the P is 7.1 mm day^{-1} through the 50 years. P precipitation is a little lower during the first 5-10 years because the forest is recovering. In the PND case, the 50-yr mean precipitation is 6.1 mm day^{-1}. In the PNF case, the 50-yr mean precipitation is 5.6 mm day^{-1}, the lowest value because in this region the grassland only grows to become a dense shrubland.

2.3.3. Net Primary Production (NPP)

Over region 1 (Figure 2.3a), the NPP of F simulation varies around 1.3 kg-C m^{-2} y^{-1}. The P case shows an initial period of intense growth, corresponding to the initial fast recovery of the secondary forest, with NPP reaching 2.0 kg-C m^{-2} y^{-1}, then decreasing and following the F NPP. The NPP of PND simulation increases until it reaches the magnitude of F simulation after 30 years, and its mean value is 1.0 kg-C m^{-2} y^{-1} through the 50 years. The PNF NPP never reaches high levels, with an average of 0.7 kg-C m^{-2} y^{-1} for the whole period. The region 2 NPP (Figure 2.3b) is very close to the region 1 NPP for the F and P simulations, both with a 50-yr mean value of 1.3 kg-C m^{-2} y^{-1}. The PND NPP increases but during the simulation span does not reach the F and P NPP levels, with a 50-yr mean value of 0.7 kg-C m^{-2} y^{-1}. In the PNF simulation, the NPP increases slightly through the years, with a 50-yr average of 0.5 kg-C m^{-2} y^{-1}. Over region 3 (Figure 2.3c), the F and P NPP remain together, although the average value is

1.0 kg-C m^{-2} y^{-1} through the entire period, lower than in the former regions, but still enough to build and maintain a rainforest. The PND and PNF NPP are significantly lower, with a 50-yr mean value of 0.3 kg-C m^{-2} y^{-1}, insufficient for a rainforest. A remarkable difference between regions 2 and 3 (southern Amazonas to northern Mato Grosso) is that while PND NPP increases with time in region 2, it remains constant at a low level in region 3.

2.3.4. Trees Biomass

For simplification, trees biomass was uniformly initialized at 11.2 kg-C m^{-2} in all forest areas in the F simulation, and zero in P, PND and PNF simulations. The simulated trees biomass over region 1 (Figure 2.4a) for F case is nearly constant through the 50 years, with a mean value of 11.1 kg-C m^{-2}. Trees biomass increases with time in all deforested cases over region 1, and at the end of the simulated period the P, PND, and PNF trees biomass are 10.3, 8.8, and 3.8 kg-C m^{-2}, respectively. Over region 2 (Figure 2.4b), the trees biomass behavior is similar to region 1, but the magnitudes are lower in the nutrient-limited cases. The trees biomass for the last simulated year are 10.8, 9.8, 5.5, and 1.8 kg-C m^{-2} for F, P, PND, and PNF, respectively. Over region 3 (Figure 2.4c), the F case trees biomass decreases with time, seeking a new equilibrium at 9.0 kg-C m^{-2}. This occurs because in this region the land cover adjusts from an initialization of 100% evergreen rainforest to a mix of tropical evergreen forest and tropical deciduous forest, which is a more realistic representation of the current forest and its biomass than the uniform initialization (Figure 2.1). The trees biomass for P case increases through the 50 years of the experiment, reaching 7.9 kg-C m^{-2}. In the PND and PNF simulations, the trees biomass increase is very small. PND reaches 1.2 kg-C m^{-2}

and PNF reaches 0.4 kg-C m^{-2} because in these simulations the secondary forest is unable to regrow. A contrast of the simulations in region 3 demonstrates how important the nutrient deficit could be for the regrowth of the secondary forest. In regions 1 and 2, the nutrient deficit just delays the forest regrowth, but the region 3 secondary forest does not regrow under nutrient stress, at least during the 50 years of this experiment.

2.3.5. Trees Leaf Area Index (LAI_{trees})

Over region 1 (Figure 2.5a), the F simulation LAI_{trees} is around 9.0 m^2 m^{-2}.¶ The P LAI_{trees} is similar to the F case after approximately 7 years. The PND LAI_{trees} reaches the F level after about 30 years. However, the PNF LAI_{trees} increases in the first 20 years and then it stabilizes at 3.5 m^2 m^{-2}. Over region 2 (Figure 2.5b) the F and P cases have the same LAI_{trees} characteristics after 8 years, with an average value of 8.5 m^2 m^{-2} through the last 40 years. The PND LAI_{trees} increases through the duration of the experiment, reaching a maximum value of 6.6 m^2 m^{-2}. The LAI_{trees} of the PNF simulation remains very small, reaching only 1.8 m^2 m^{-2}. Over region 3 (Figure 2.5c), the F LAI_{trees} is around 7.0 m^2 m^{-2}, and the P simulation LAI_{trees} is similar to F simulation after about 12 years. The PND LAI_{trees} is very small, with a final value of 1.6 m^2 m^{-2}, but is still attempting to increase. The PNF LAI_{trees} is stable and nearly zero. Again, the effect of nutrient limitation becomes clear on the secondary forest regrowth. The LAI_{trees} recovers more slowly over regions 1 and 2 in the PND and PNF simulations. Over region 3, the LAI_{trees} is inexpressive under nutrient constraints, indicating that the secondary forest can not regenerate.

¶Although this seems to be a very high LAI, there are no LAI measurements in this region, and remote sensing usually saturates at LAI over 5.

2.4. DISCUSSION AND CONCLUSIONS

This study describes the climate and soil nutrient feedbacks involved in the recovery of the Amazon rainforest after a hypothetical large-scale deforestation. The secondary forest regrows faster in the deforested simulation without nutrient stress and its recovery occurs in all regions. Under nutritional limitation, different regions in the Amazon may respond differently, allowing the regrowth of the secondary forest back to a primary forest or leading to a savannization, as suggested by some studies [*Nobre et al.*, 1991; *Oyama and Nobre*, 2003; *Hutyra et al.*, 2005].

Considering the most realistic scenario PND, which takes into account the secondary forest capability to rebuild nutrient stocks as it matures [*Davidson et al.*, 2007], after a hypothetical full-scale Amazon deforestation, an evergreen rainforest would regrow only over region 1, a mixed forest develops in region 2, and a process of savannization starts over region 3 (southern Amazonia). Although the full deforestation is useful to understand the extreme consequences of climate and nutrient feedbacks in regulating the forest regrowth, it is also important to investigate the response of these feedbacks to the partial deforestation. The partial deforestation results will be focused in chapter 3.

The PND simulation is the most realistic scenario, as long as we do not consider that disturbances like fire can occur in the region. If this model represented the fire disturbance probably these results would be more pessimistic in regions like the arc of deforestation; they would be more similar to those from the PNF simulation. Fire volatilizes significant stocks of ecosystem N [*Kauffman et al.*, 1995], preventing the secondary forest recovery and decreasing trees biomass [*Botta and Foley*, 2002; *Delire et al.*, 2003]. Once burnt, the forest becomes more vulnerable to further burns because fire-induced tree death allows more sunlight to reach the forest interior, drying dead leaves and branches on the forest floor [*Nepstad et al.*, 1999, 2001]. Besides, forests growing on nutrient-poor soils often develop thick roots above the mineral soil [*Kauffman et al.*, 1988], and may be particularly vulnerable to fire-induced tree mortality since a substantial portion of the root system can be killed.

The land cover shift in the P, PND, and PNF scenarios would release around 7, 34, and 51 Pg-C, respectively, including the initial deforestation emissions and the carbon sequestration during the 50 years of the experiment. Carbon emissions expected for each simulation were estimated by assuming that 85% of the carbon contained in deforested trees is released to the atmosphere [*Soares-Filho et al.*, 2006], and the entire Amazonia is considered. This large-scale degradation could speed the global warming, leading to a global climatic disruption [*Cox et al.*, 2000, 2004].

We conclude that the simulated precipitation reduction caused by deforestation is not sufficient to prevent the secondary forest regrowth, as we can see in P simulation in all regions. However, when it is associated with a soil nutrient stress, the secondary forest may not regrow in southern Amazonia where the precipitation rates are lower than in central and western Amazonia. In regions where the secondary forest regrows, the precipitation rates resume the normal values. *Sampaio* [2008] found a possible

second biome-climate equilibrium state, which is favorable to the savanna maintenance over the eastern Amazonia even in a scenario with no nutrient stress. More research is needed to clarify this disagreement.

Furthermore, the vegetation dynamics and structure variables show how the ecosystem changes through time. Over northwestern Amazonia, the final land cover is the same in all simulations, but the NPP of PNF case is lower than in the other simulations because of the fixed nutrient limitation. Simulated NPP falls within the limits of the observations for the biomes found in the three considered regions for all simulated scenarios [*Zaks et al.*, 2007]. Under nutrient stress, both trees biomass and LAI_{trees} recover slowly over northwestern and central Amazonia. However, the recovery of the forest, measured by these variables, is practically null over southern Amazonia, at least on the timescale of 50 years.

The simulated biosphere-atmosphere interactions indicate that the precipitation reduction caused by deforestation combined with soil nutrient limitations may prevent the regrowth of the rainforest in the Amazon region south of 10º S (northern Mato Grosso State). This is concerning, because this region has the highest clearing rates in Amazonia, not only for pasture conversion but also for cropland expansion [*Morton et al.*, 2006]. Fire is the dominant land-clearing and pasture maintenance method throughout this region, and is practiced by most farmers and ranchers [*Nepstad et al.*, 2001; *Zarin et al.*, 2005]. The low resilience of the forest under nutrient stress indicates that northern Mato Grosso should be a major target for conservation initiatives.

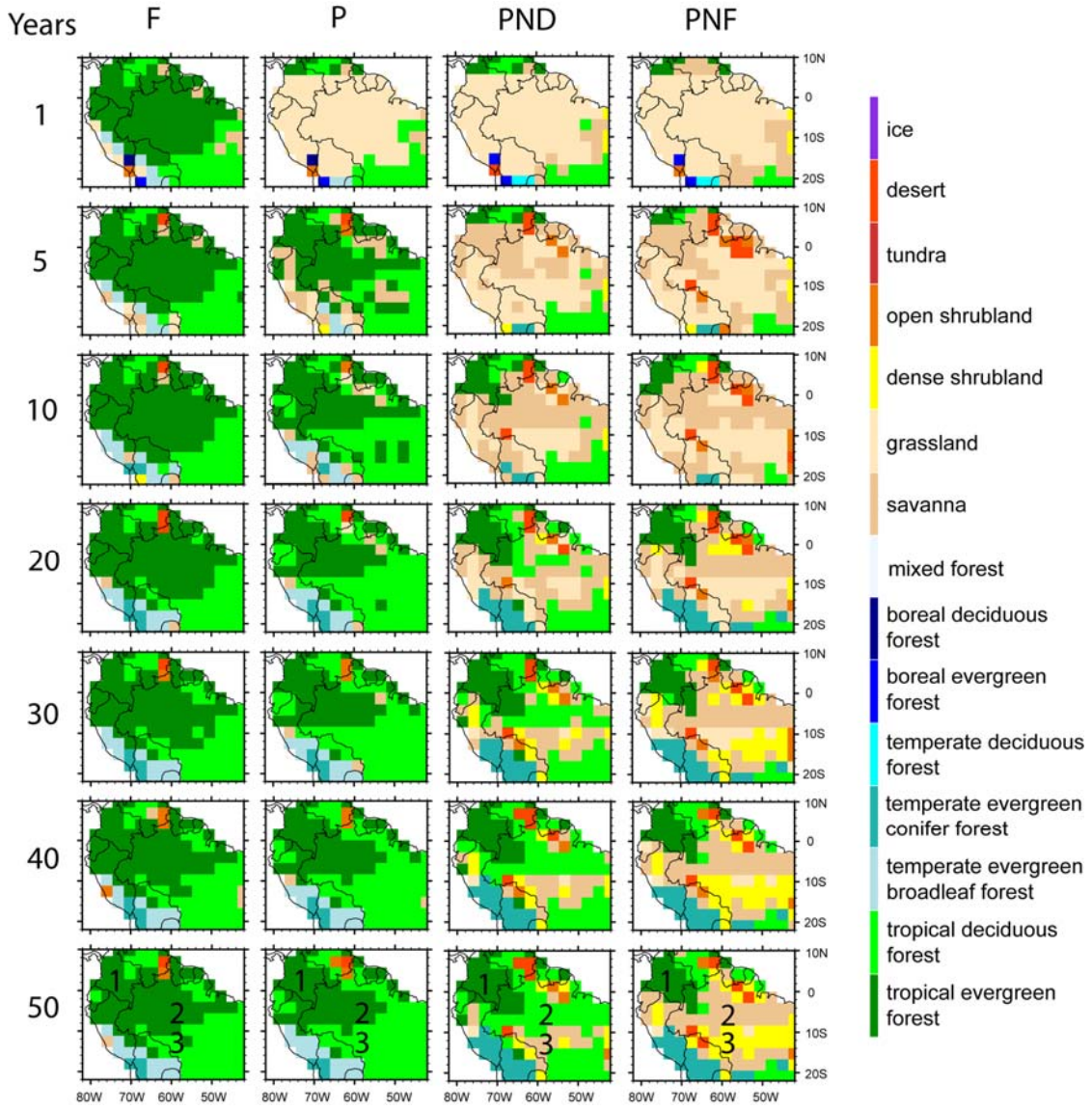

Figure 2.1. The simulated land cover chronosequence. The numbers 1, 2, and 3 represent the regions over Colombia and northwestern Amazonas state in Brazil, over central Amazonia above 10º S, and over southern Amazonia below 10º S (northern Mato Grosso State), respectively. These regions were chosen because of the distinct simulated land cover after 50 years.

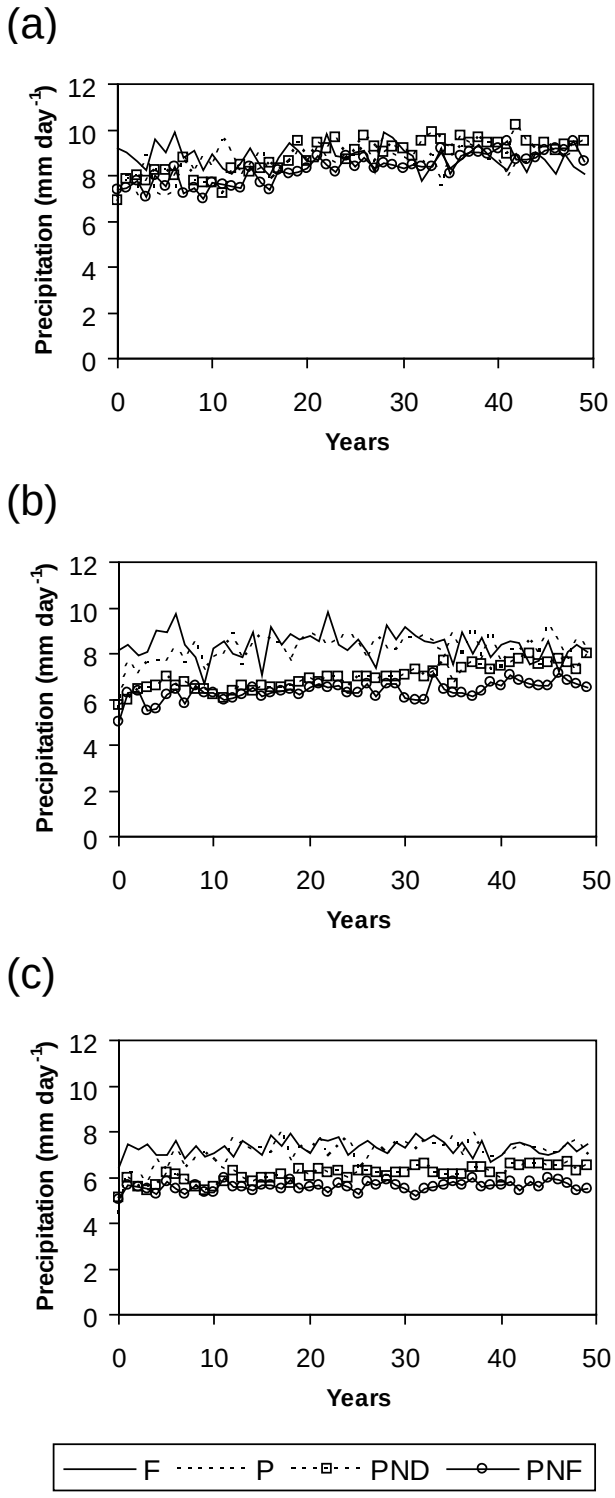

Figure 2.2. The simulated annual mean precipitation for (a) region 1 - Colombia and northwestern Amazonas state, (b) region 2 - central Amazonia above 10º S, and (c) region 3 - northern Mato Grosso State.

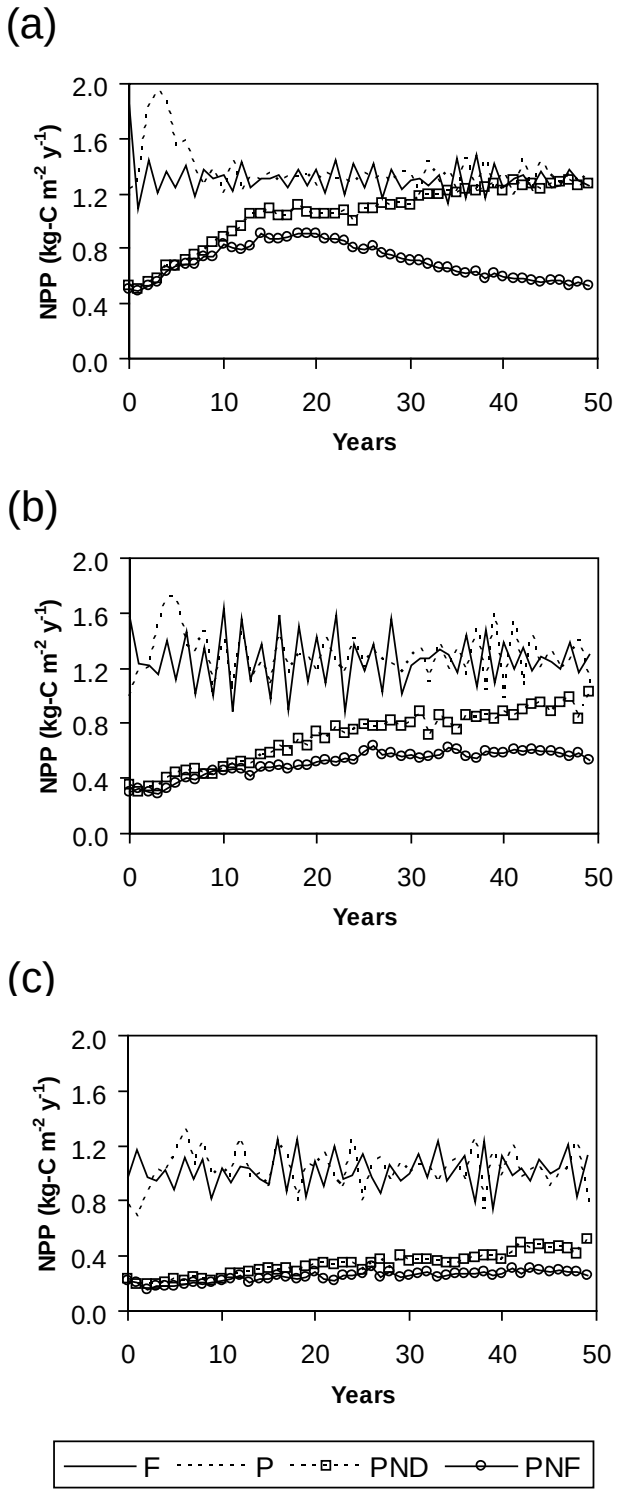

Figure 2.3. The simulated annual mean net primary production for (a) region 1 - Colombia and northwestern Amazonas state, (b) region 2 - central Amazonia above 10º S, and (c) region 3 - northern Mato Grosso State.

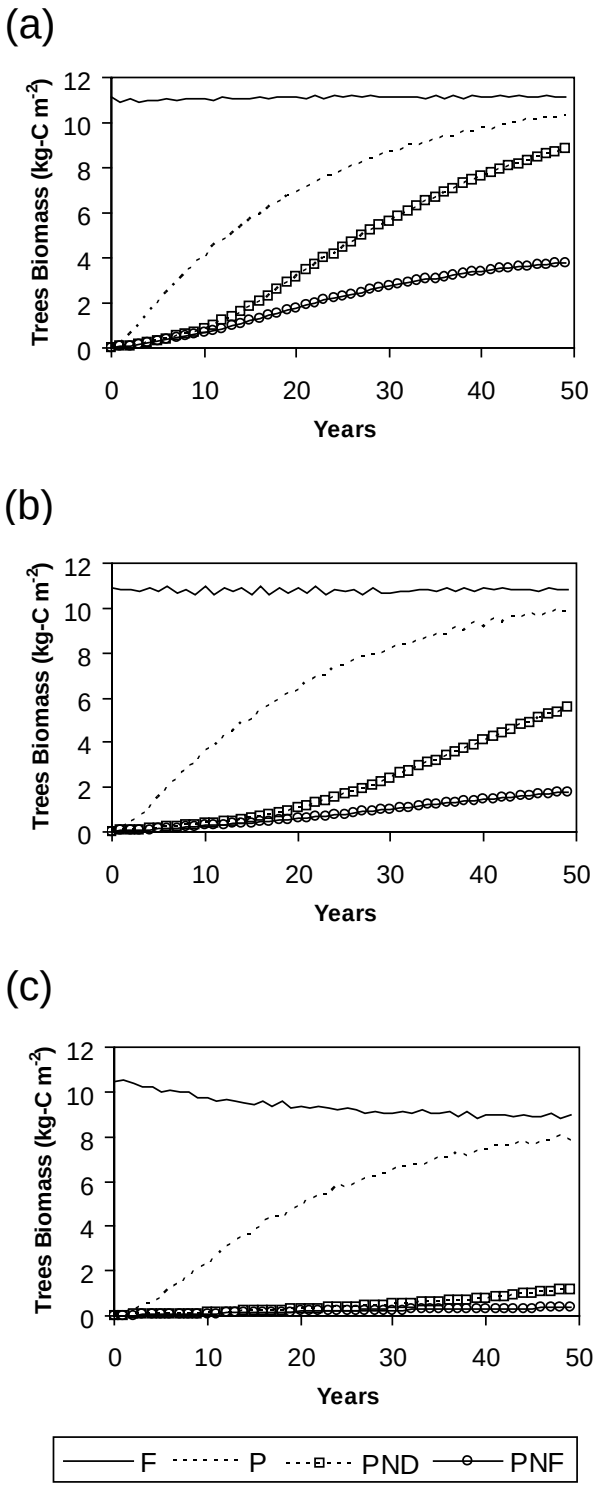

Figure 2.4. The simulated annual mean trees biomass for (a) region 1 - Colombia and northwestern Amazonas state, (b) region 2 - central Amazonia above 10º S, and (c) region 3 - northern Mato Grosso State.

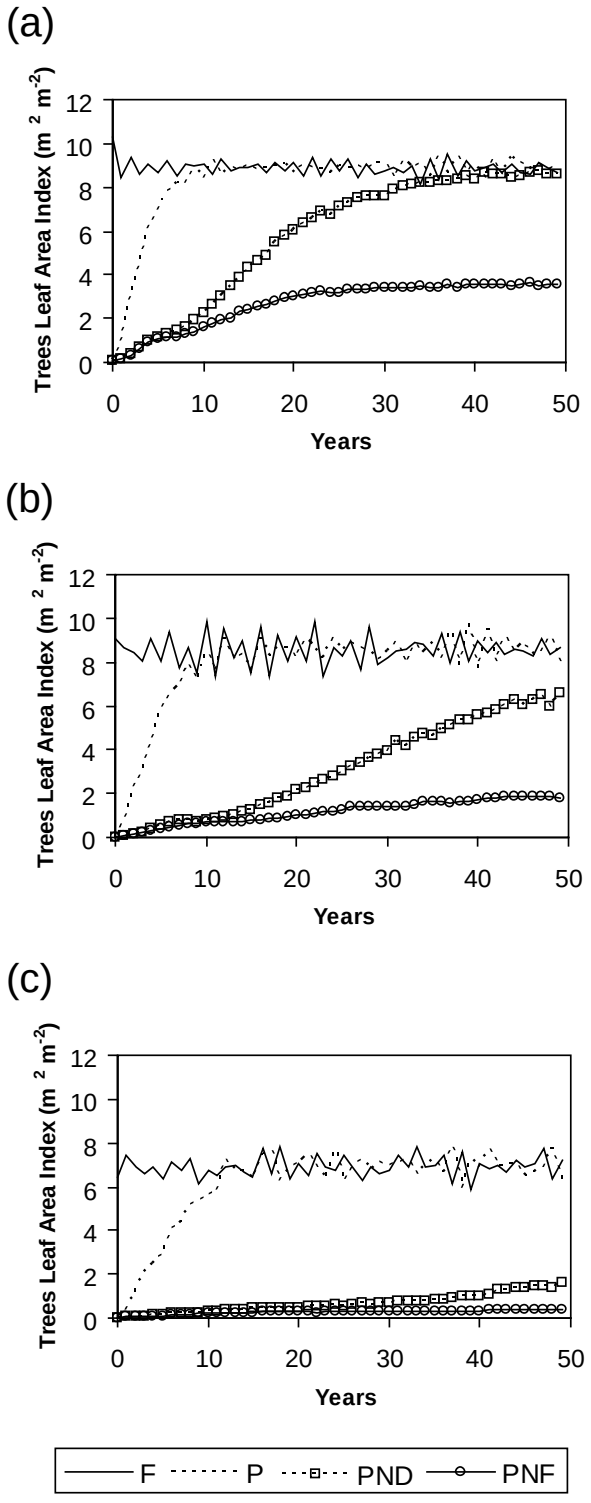

Figure 2.5. The simulated annual mean trees leaf area index for (a) region 1 - Colombia and northwestern Amazonas state, (b) region 2 - central Amazonia above 10º S, and (c) region 3 - northern Mato Grosso State.

CHAPTER 3

REGROWTH OF THE AMAZON FOREST UNDER NUTRIENT STRESS FOR SEVERAL DEFORESTATION SCENARIOS

3.1. INTRODUCTION

The Amazon forest has one of the greatest biological diversity on the planet [*Dirzo and Raven*, 2003] and is intimately connected to the world's climate [*Malhi et al.*, 2008]. Changes in climate may alter competitive relationships among species, and thus may alter the Amazonian vegetation cover, especially if it leads to significant reductions in precipitation in this region. On the other hand, changes in forest structure and composition may alter surface properties such as albedo, roughness, stomatal physiology, leaf area index, rooting depth, and nutrient availability, thus altering surface energy fluxes, the hydrologic cycle, and biogeochemical cycles, consequently affecting climate [*Pielke et al.*, 1998; *Bonan*, 2002; *Foley et al.*, 2003; *Betts et al.*, 2008].

Large areas of forest in Amazonia have been replaced by pasture, and more recently by soybean cropland. By 2003, the forest area had been reduced to 5.3 million km^2, 85% of the original area [*Soares-Filho et al.*, 2006]. In the future, rates of deforestation are likely to increase as more roads are built through the region's core and as international demand for tropical timber, soybeans, beef, and biofuels continues to grow [*Laurance at al.*, 2001; *Carvalho et al.*, 2002; *Soares-Filho et al.*, 2006].

Several studies have shown that the loss of forest may lead to a reduction in evapotranspiration and rainfall [*Shukla et al.*, 1990; *Nobre et al.*, 1991; *Costa and Foley*, 2000; *Silva Dias et al.*, 2002]. The evapotranspiration decrease is basically a consequence of three factors: the increased albedo reduces the net radiation at the surface; the reduced surface roughness decreases atmospheric turbulence, weakening vertical motions; and the reduced root depth leaves less soil moisture available to plants. Besides, the reduction in the net surface radiation cools the upper atmosphere over the deforested area, inducing a thermally driven circulation that results in subsidence [*Eltahir*, 1996]. These changes in the water and surface energy balance may cause a reduction in rainfall. According to *Shukla et al.* [1990], this reduction in precipitation might prevent an eventual forest regrowth on abandoned pastures, leading to a positive feedback in the region. Two recent climate modeling studies [*Costa et al.*, 2007; *Sampaio et al.*, 2007] evaluate the effect of a gradual deforestation on precipitation changes, and conclude that the precipitation reduction in Amazonia is more evident when deforestation exceeds 50% of the original forest cover.

In addition, another positive feedback related to the effects of frequent burning on soil fertility is supported by recent studies of secondary forest regrowth in the Amazon. Fire has been used extensively by farmers and ranchers to clear land and maintain pastures [*Nepstad et al.*, 2001; *Cochrane*, 2003]. Frequent fires volatilizes significant stocks of N [*Kauffman et al.*, 1995], provoking a co-limitation of this nutrient in forests recovering from repeated fire [*Davidson et al.*, 2004, 2007]. Nutrients in the remaining ash might be lost by ash transport, and leaching to surface and groundwater [*Kauffman et al.*, 1993; *Mackensen et al.*, 1996; *Sampaio et al.*, 2003]. *Zarin et al.* [2005] showed that forests with a history of five or more fires accumulate biomass at an average rate lower than 50% of forests that burned only once, and are

more susceptible to further burning. This is because slower growth results in delayed canopy closure, increasing light penetration and drying of fuels, elevating forest flammability [*Nepstad et al.*, 1999, 2001]. In fertilization studies [*Gehring et al.*, 1999; *Davidson et al.*, 2004, *Silva et al.*, 2006], the secondary vegetation responds significantly to additional nutrients by increasing biomass production, indicating that soil nutrient limitation might reduce the vegetation regrowth and the biomass accumulation rate. Moreover, young successional forests growing under nutrient stress exhibit conservative N-cycling properties, which persists for decades until N gradually reaccumulates in advanced successional stages and in mature forests [*Davidson et al.*, 2007].

In chapter 2, we evaluate the climate and nutrient feedbacks after a hypothetical full Amazon deforestation, which is not realistic for at least the first half of the 21st century. For the next decades, it is important to understand the response of these feedbacks to a gradual deforestation. Considering different deforestation scenarios, we may specify whether there is a threshold for the rainforest recovery and how it may vary in distinct regions of the Amazonia.

Here we investigate how the climate feedback and the nutrient feedback may affect the Amazon rainforest regrowth after different deforestation scenarios. To address this question, we use the fully coupled climate-biosphere model CCM3-IBIS that includes a forest productivity penalization due to soil nutrient stress. The model is forced by different initial land cover conditions that emulate possible scenarios of Amazon deforestation in the next decades/centuries.

3.2. MATERIALS AND METHODS

3.2.1. Model Description

In this study, we use the National Center for Atmospheric Research (NCAR) Community Climate Model version 3 (CCM3) [*Kiehl et al.*, 1998] coupled with an updated version of the Integrated Biosphere Simulator (IBIS) [*Foley et al.*, 1996; *Kucharik et al.*, 2000]. We refer to this coupled model as CCM3-IBIS. This is virtually the same core of the Lawrence Livermore National Laboratory (LLNL) model used in the Intergovernmental Panel on Climate Change (IPCC) AR4 simulations and in the Coupled Climate-Carbon Cycle Model Intercomparison Project (C^4MIP project), except for our own tuning for the rainforest [see chapter 1]. *Delire et al.* [2002, 2003] investigated the basic global climate and carbon cycle simulated by this coupled model and showed that CCM3-IBIS can be used to explore geographic and temporal variations in the global carbon cycle. In this study, we focus on the Amazon climate, nutrient stress and rainforest recovery.

CCM3 is an atmospheric general circulation model with spectral representation of the horizontal fields. It simulates the large-scale physics (radiative transfer, hydrologic cycle, cloud development, thermodynamics) and dynamics of the

atmosphere. Here, we operate the model at a spectral resolution of T42 (~2.81º X 2.81º latitude/longitude grid), 18 vertical levels, and a 15-min time step. The oceans are represented by monthly averaged fixed sea-surface temperatures of the 1990s that serve as boundary conditions for the atmosphere.

IBIS is a comprehensive model of terrestrial biospheric processes that represents the physical, physiological, and ecological processes occurring in vegetation and soils. IBIS simulates land surface processes, plant phenology and vegetation dynamics, and represents vegetation as two layers (trees and grasses). In IBIS a grid cell can contain one or more plant functional types that together comprise a vegetation type. Land surface physics and canopy physiology are calculated at the same time step used by CCM3. The plant phenology algorithm has a daily time step and the vegetation dynamics is solved with an annual time step. IBIS operates on the same T42 spatial grid as the CCM3, and with dynamic vegetation component enabled, so vegetation structure and biogeography change in response to climate.

To date, IBIS does not contain a complete N cycle. Although soil N transformations are tracked in the soil biogeochemistry module reported in *Kucharik et al.* [2000], there are no soil N controls on vegetation productivity. So, we penalize the NPP of the regrowth forest directly, assuming that the nutrient limitation is caused by frequent fires before the beginning of the experiment. The NPP is reduced according to an empirical relation that reflects a NPP decrease of 50% for trees biomass equal to zero, and no NPP decrease when the trees biomass reaches 10 kg-C m^{-2} or more (typical values of a mature forest). This assumption reproduces the capacity of the secondary forest to rebuild nutrient stocks in mature stages found by *Davidson et al.* [2007] for eastern Amazonia.

CCM3-IBIS was calibrated against Large Scale Biosphere-Atmosphere Experiment in Amazonia (LBA) tower results [*Imbuzeiro*, 2005], and extensively validated against spatial fields of incident solar radiation, precipitation, land cover patterns, heterotrophic and root respiration, total net primary production (NPP), aboveground NPP, wood NPP, leaf area index, and aboveground live biomass. The Amazon climate (annual mean and seasonality) is very well simulated for both incident solar radiation and precipitation. Average incident solar radiation and precipitation are within 7% and 5% of the observations, respectively. Average total NPP is within 5% and average aboveground NPP is within 2% of observations. Respiration rates and wood NPP are within 15% and 16% of the observations, respectively. Simulated aboveground live biomass is within 12% of *Saatchi et al.* [2007] estimates. For more details, see chapter 1.

3.2.2. Experiment Design

To examine the climate and soil nutrient feedbacks involved in the recovery of the Amazon rainforest, we conduct a set of simulations for a period of 50 years, with three ensembles each. In all simulations, CO_2 concentration was kept constant at 380 ppmv. The experiment evaluated different initial conditions and nutrient constraints, described below:

- F: control run, initial condition forest and no nutrient limitation.
- P100: initial condition pasture, full deforestation, and no nutrient limitation.
- PND20: initial condition pasture, ~20% of deforested area, and with nutrient limitation.

- PND40: initial condition pasture, ~40% of deforested area, and with nutrient limitation.
- PND60: initial condition pasture, ~60% of deforested area, and with nutrient limitation.
- PND80: initial condition pasture, ~80% of deforested area, and with nutrient limitation.
- PND100: initial condition pasture, full deforestation, and with nutrient limitation.

The land cover change scenarios with deforested areas smaller than 40% are from *Soares-Filho et al.* [2006], and greater than 40% are from *Sampaio et al.* [2007]. Both are "business-as-usual" scenarios, which assume that recent deforestation trends will continue; highways currently scheduled for paving will be paved; compliance with legislation requiring forest reserves on private land will remain low; and new protected areas will not be created. These scenarios do not consider forest impoverishment through logging and fire, nor do they consider the potential for forest substitution by savanna due to global warming.

3.2.3. Validation Data

Simulated aboveground biomass is compared against forest regrowth stands observations compiled by *Zarin et al.* [2005] for Manaus (2.0º S; 59.5º W), DAS (SUFRAMA agricultural district) (2.5º S; 60.5º W), Janauaca (3.0º S; 60.0º W), Paragominas (2.5º S; 47.5º W), Zona Bragantina (1.5º S; 47.5º W), Pedra (1.5º S; 48.5º W), and Tome-Açu (2.0º S; 48.0º W) sites (Figure 3.1).

3.3. RESULTS

3.3.1. Comparison Against Observations of Forest Regrowth

We use forest regrowth aboveground biomass data compiled by *Zarin et al.* [2005] to determine whether CCM3-IBIS can simulate this biomass accumulation. The Paragominas / Zona Bragantina / Pedra / Tome-Açu sites, hereafter eastern sites, are inside the same grid cell of CCM3-IBIS, thus they are together in Figure 3.2a. Aboveground biomass at Manaus, DAS, and Janauaca sites are shown in Figures 3.2b, 3.2c, and 3.2d, respectively.

At the eastern sites, the model captures most part of the observed aboveground biomass with the nutrient-limited simulations. Some observed points are exactly on the PND curves, which overlap. The P100 simulation, with higher biomass values, captures part of the observed data as well. At Manaus, DAS, and Janauaca sites, all PND simulations underestimate the observed biomass. The P100 simulation captures the aboveground biomass in these sites, except for Manaus where P100 tends to underestimate observed data for secondary forests older than 15-yr.

Approximately 2/3 of the observed points fit the nutrient-limited growth pattern at the eastern sites, while the remainder points do not seem to be nutrient-limited to

regrow. The other sites in central Amazonia do not seem to have nutrient constraints affecting the secondary forest recovery. Our interpretation is that some regrowth sites display nutrient-limited regrowth rates, while others do not. Given the scarcity of field measurements, the causes of such differences are still unclear.

3.3.2. Amazon Precipitation Patterns

Figure 3.3 shows the simulated annual mean precipitation averaged over the entire Amazon region. The chart presents a 3-year moving average to smooth out short-term fluctuations, thus highlighting longer-term trends associated with the rainforest regrowth. The Amazon precipitation is highly dependent on the deforested area. The control case (F) has a mean precipitation of 6.2 mm day^{-1} for the entire period. The precipitation of the P100 simulation increases fast in the first 15 years and then follows the control case precipitation, with an average of 6.0 mm day^{-1} through the 50 years. PND20 and PND40 precipitation have a similar behavior, increasing with time and reaching the control case after 40 years. The 50-yr mean precipitation is 5.8 mm day^{-1} for both PND20 and PND40. PND60, PND80, and PND100 are quite similar too, reaching the PND20 and PND40 precipitation after 25 years and the control case precipitation after 40 years. The mean precipitation for the entire period is 5.6 mm day^{-1} for PND60, PND80, and PND100. The simulated mean Amazon precipitation decreases with the increase of deforestation, and the reduction is more drastic when the deforested area is equal or exceeds 60% of the original forest extent. However, as the secondary forest regrows, the precipitation levels go back to normal after several decades.

3.3.3. Large-Scale Regrowth Patterns

The initial land cover scenarios and the simulated land cover chronosequence of each simulation are shown in Figure 3.4. In the F simulation the Amazon tropical evergreen forest remains stable through the 50 years, except for a small part in southeast Amazonia that becomes tropical deciduous forest, regionally called cerradão. This occurs because the land cover adjusts from an initialization of 100% evergreen rainforest to a mix of tropical evergreen forest and cerradão, which is a more realistic representation of the current forest than the uniform initialization. Vegetation in few pixels in the Brazil-Venezuela border and in northeast Amazonia is misrepresented due to precipitation underestimation in these areas [see chapter 1]. In the P100 simulation the secondary forest regrows rapidly in all deforested area and the land cover patterns are very similar to the F simulation after 50 years, although the biomass of this secondary forest is much smaller than the primary forest one.

In the PND20 simulation the secondary forest regrows in great part of the Amazon. This recovery is more evident mainly after 30 years, when the eastern Amazonia forest recovers. The southern Amazonia is the only region that the forest did not regrow, and the land cover shifts from grassland to savanna. In the PND40, PND60, PND80, and PND100 simulations the forest regrowth is very similar to the PND20 simulation, although in a slower way. In these cases the recovery is more evident after 40 years. In the PND60, PND80, and PND100 simulations, the area of tropical evergreen forest replaced by tropical deciduous forest after 50 years is greater than in the PND20 and PND40 simulations. In all PND simulations, a savannization process starts over southern Amazonia, no matter the deforested area extent.

3.3.4. Regrowth Analysis at Selected Regions

We select three regions to a more detailed analysis. In the region 1, at the eastern sites, observed data show that the rainforest regrowth might be nutrient-limited. In this region the simulated land cover becomes a tropical deciduous forest 50 years after abandonment. In the region 2, at the Manaus site, observations show that the secondary forest does not seem to be nutrient-limited. After 50 years of regrowth, this region has the same land cover simulated in region 1. In both cases, an extrapolation indicates that vegetation would continue to grow until it becomes a primary rainforest, which should take several centuries. The region 3, at southern Amazonia below 10º S (northern Mato Grosso state), was chosen because of the savannization process that begins when we deforest this region considering the nutrient stress.

Below we analyze important variables that describe the climate-vegetation interactions in these three regions. The mean values plotted on Figures 3.5, 3.6 and 3.7 are obtained using a 3-year moving average.

• **Region 1 – Eastern Sites:** The simulated annual mean precipitation for eastern sites (Figure 3.5a) is very similar for all simulations, with an average of about 4.5 mm day^{-1} through the 50 years. This means that precipitation in this region is nearly independent of the land cover. The simulated annual mean net primary production (NPP) (Figure 3.5b) of F and P100 simulations remains stable with a 50-yr mean value of 1.1 kg-C m^{-2} y^{-1}. NPP increases with time in all PND cases, as the rainforest regrows and the nutrient cycling resumes, and reaches the F and P100 NPP after 40 years. Their mean NPP through the 50 years is 0.8 kg-C m^{-2} y^{-1}. The high levels reached by NPP indicate that

this forest will continue to accumulate biomass, evolving to a mature primary forest again in a matter of centuries.

• **Region 2 – Manaus Site:** At Manaus, the simulated annual mean precipitation (Figure 3.6a) of F simulation remains high, with an average of 7.9 mm day^{-1} through the entire period. The precipitation of P100 case is lower in the first 15 years, and then reaches the magnitude of F precipitation, with a 50-yr mean value of 7.1 mm day^{-1}. The precipitation of PND simulations increases through the years but is significantly lower. The average for all simulated period is 6.2, 6.0, 4.9, 5.2, and 5.4 mm day^{-1} for PND20, PND40, PND60, PND80, and PND100, respectively. In this region, precipitation is clearly dependent on the land cover and on the rate of deforestation, with a higher precipitation reduction in the 60% deforested area scenario. The F NPP varies around 1.3 kg-C m^{-2} y^{-1} (Figure 3.6b). The P100 NPP shows an initial period of intense growth, corresponding to the initial fast recovery of the secondary forest, then decreasing and following the F NPP, with a 50-yr mean value of 1.3 kg-C m^{-2} y^{-1}. NPP increases with time in all PND simulations, but it does not reach the magnitude of F NPP in 50 years. The average through the entire period is 0.8, 0.8, 0.5, 0.6, and 0.6 kg-C m^{-2} y^{-1} for PND20, PND40, PND60, PND80, and PND100, respectively.

• **Region 3 – Northern Mato Grosso:** Over northern Mato Grosso, the precipitation also shows a clear dependence on the land cover (Figure 3.7a). The F mean precipitation is 6.9 mm day^{-1} and the P100 is 6.8 mm day^{-1} through the 50 years. The P100 precipitation increases during the first 10 years because of the rainforest fast recovery in this non-limited soil nutrient simulation. The precipitation is significantly lower in the nutrient-limited simulations. The precipitation of the PND simulations is close and

almost constant with time. The 50-yr mean value is 5.3, 5.2, 5.4, 5.5, and 5.6 mm day^{-1} for PND20, PND40, PND60, PND80, and PND100, respectively. This means that precipitation in this region is not dependent on the rate of deforestation, just on the land cover underneath. The simulated annual mean NPP (Figure 3.7b) shows a drastic reduction for the simulations with nutrient limitation. While F and P100 NPP have a 50-yr mean value of 1.0 kg-C m^{-2} y^{-1}, the PND cases NPP have a 50-yr mean value of 0.3 kg-C m^{-2} y^{-1}. This low NPP is not enough to build and maintain a rainforest. An important difference between this region and the others is that in regions 1 and 2 the NPP of nutrient-limited simulations increases with time, while in region 3, it is almost constant and very low, indicating that the rainforest can not regrow, at least on the timescale of 50 years.

Why the nutrient-stressed simulations have a different behavior than the non-limited ones in Mato Grosso, and behave similarly elsewhere? In other words, why the nutrient limitation, in combination with rainfall decrease, prevents the regrowth of the rainforest in northern Mato Grosso, but not elsewhere?

The answer is in the duration of the dry season (Figure 3.8). This region has a well-defined dry season and when it is deforested and nutrient-limited, the dry season increases from four months (May-August) to five months (May-September). Moreover, there are large differences in precipitation magnitude in the transition from the dry to the rainy season. In October for example, the PND simulations precipitation is approximately 1.0 mm day^{-1}, while F precipitation is 8.0 mm day^{-1} in the first ten years of simulation (Figure 3.8a). In the last ten years (Figure 3.8b), the October PND precipitation is 3.0 mm day^{-1} while F precipitation remains about 8.0 mm day^{-1}. This suggests that the synergistic effects of climate and nutrient feedbacks after deforestation may lead to a savannization, as suggested by previous studies [*Nobre et al.*, 1991;

Oyama and Nobre, 2003; *Hutyra et al.*, 2005]. This savannization is mainly caused by a longer dry season, although this process only starts in the presence of soil nutrient limitations.

3.4. DISCUSSION AND CONCLUSIONS

The goal of this study is to describe the biogeochemical and the climate feedbacks involved in the Amazon rainforest regrowth after different deforestation scenarios. At eastern sites, the secondary forest regrowth indicates that there are biogeochemical interactions due to soil nutrient limitations affecting this regrowth (Figure 3.2a). The nutrient-limited simulations reproduce well this biomass accumulation. However, the regrowth of the rainforest at Manaus, DAS, and Janauaca do not seem to be nutrient-limited (Figures 3.2b, 3.2c and 3.2d). In these sites the forest recovery is more similar to the simulation with no nutrient stress, and the nutrient-limited simulations underestimate the biomass accumulation at these sites. A remarkable difference between eastern sites and the other sites is that the soil texture classification of the former is sandy (except for Paragominas), while the latter is non-sandy [*Zarin et al.*, 2005]. *Laurance et al.* [1999] found a strong negative correlation between soil sand content and the biomass of Amazonian old-growth forests. This might be one of the possible reasons for the existence of biogeochemical feedbacks in some regions after deforestation, but not in others. Unfortunately, *Zarin et al.* [2005]

did not measure soil physical and chemical properties, neither foliar nutrient concentration.

Considering the entire Amazonia, the effects of deforestation on precipitation are proportional to the amount of deforestation (Figure 3.3). The simulations with nutrient stress show a lower precipitation because of the slower forest recovery. The reduction in the 50-yr mean precipitation is about 3% for P100 simulation, 6% for PND20 case, 7% for PND40, and 10% for PND60, PND80, and PND100. *Sampaio et al.* [2007] found a precipitation reduction over eastern Amazonia proportional to the increase of deforested area, and *Costa et al.* [2007] found a decrease in precipitation for high levels of deforestation. In both studies, the land cover is fixed, while here it changes in response to climate. Thus, the Amazon precipitation magnitude of deforested scenarios reaches the control case magnitude as the rainforest regrows.

The simulated precipitation reduction caused by deforestation alone (non-limiting soil nutrients) is not sufficient to prevent the rainforest regrowth (Figures 3.4-3.7). This is noticeable in P100 simulation, where the rainforest regrows faster and in all regions. However, when the precipitation reduction is associated with a soil nutrient stress, different regions in the Amazon may respond differently. Over eastern sites and Manaus, a mix of tropical evergreen forest and cerradão regrows. Over northern Mato Grosso, the rainforest does not recover on the timescale of 50 years, no matter how much is deforested, and a process of savannization starts. In this region, a large precipitation reduction in the transition from the dry to the rainy season and an increase in the dry season duration (Figure 3.8) are favorable to the savanna maintenance on nutrient-limited simulations. In the presence of nutrient limitations, this new drier ecosystem might be a second biome-climate equilibrium state because it has a higher albedo and a lower evapotranspiration, and thus inhibit precipitation [*Oyama and*

Nobre, 2003]. However, this state may not be in stable equilibrium because any change in the precipitation or nutrient deposition may remove the system from this state of equilibrium.

The land cover shift simulated here would release to the atmosphere around 7, 13, 19, 26, 29, and 34 Pg-C for P100, PND20, PND40, PND60, PND80, and PND100, respectively, including the initial deforestation emissions and the carbon sequestration during the 50 years of the experiment. Carbon emissions expected for each simulation were estimated by assuming that 85% of the carbon contained in deforested trees is released to the atmosphere [*Soares-Filho et al.*, 2006], and the entire Amazonia is considered. The deforestation can itself be a driver of climate change and a positive feedback on externally forced climate change [*Malhi et al.*, 2008].

The different deforestation scenarios, with a gradual replacement of rainforest by pastures, can give us a threshold of deforestation that could cause dangerous interference on the Amazon rainforest. When we consider soil nutrient limitations interacting with climate feedbacks on these scenarios, the rainforest might not regrow in northern Mato Grosso, even with a small deforested area. We should note here that the PND20 deforestation scenario, which assumes 20% of deforestation, is very similar to the current level of deforestation (17%).

Finally, the growing world demand for soybeans, biofuel, and meat are increasing the profitability of agriculture and livestock in northern Mato Grosso [*Nepstad et al.*, 2006], that already has the highest clearing rates in Amazonia [*Morton et al.*, 2006]. Besides, the most common land-use practices in this region depend upon fire as a management tool [*Nepstad et al.*, 1999, 2001; *Alencar et al.*, 2006], decreasing its soil fertility. The biogeochemical and climate feedbacks simulated here indicate that

northern Mato Grosso should be a major target for conservation initiatives, preventing the impacts of this land cover shift on the global carbon cycle and on climate change.

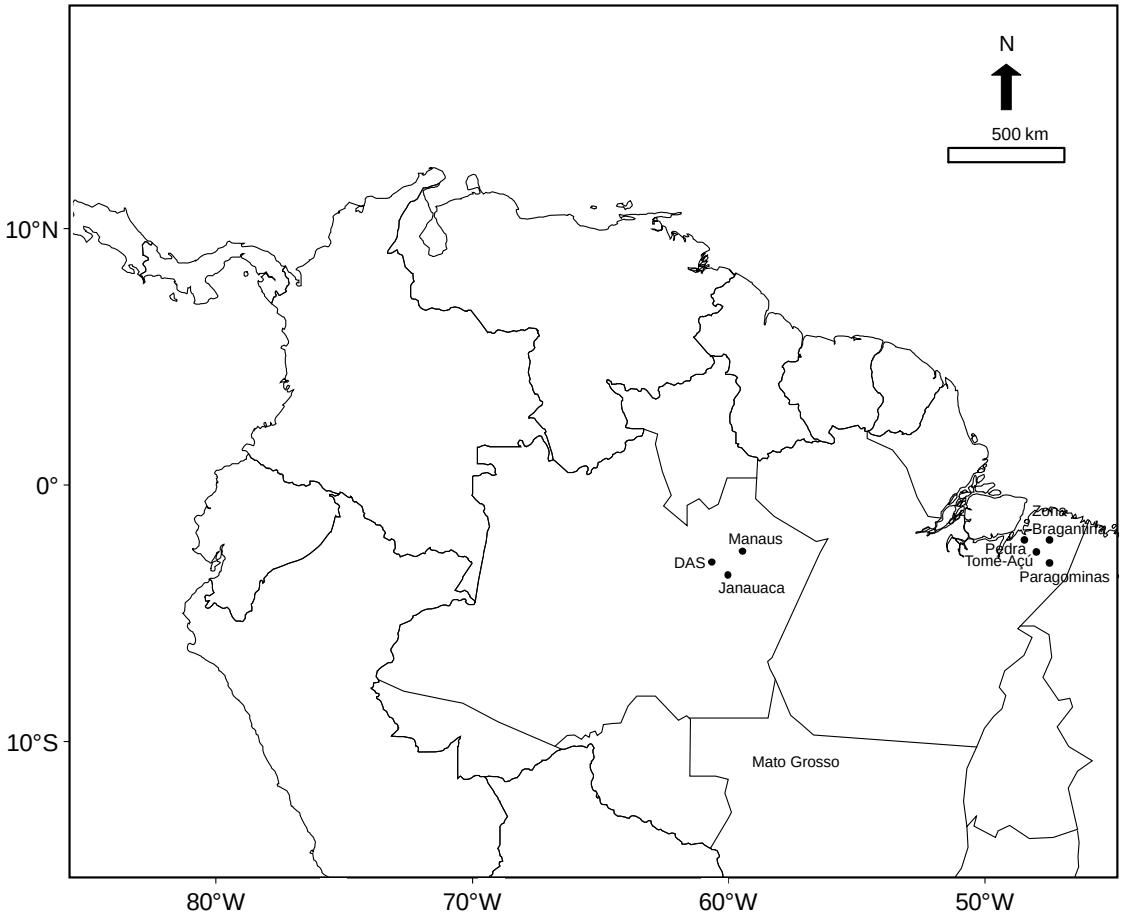

Figure 3.1. Orientation map.

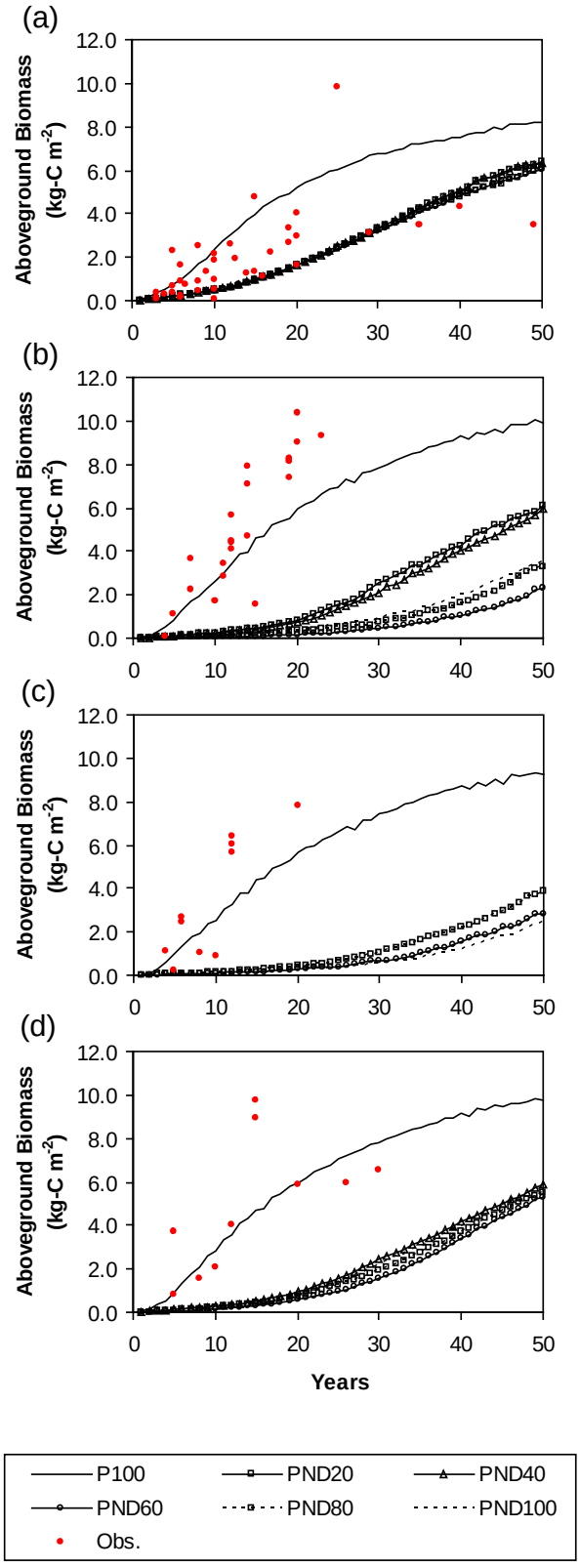

Figure 3.2. Forest regrowth aboveground biomass accumulation observed (red points) and simulated by CCM3-IBIS (curves) at (a) Paragominas / Zona Bragantina / Pedra / Tome-Açu, (b) Manaus, (c) DAS and (d) Janauaca sites.

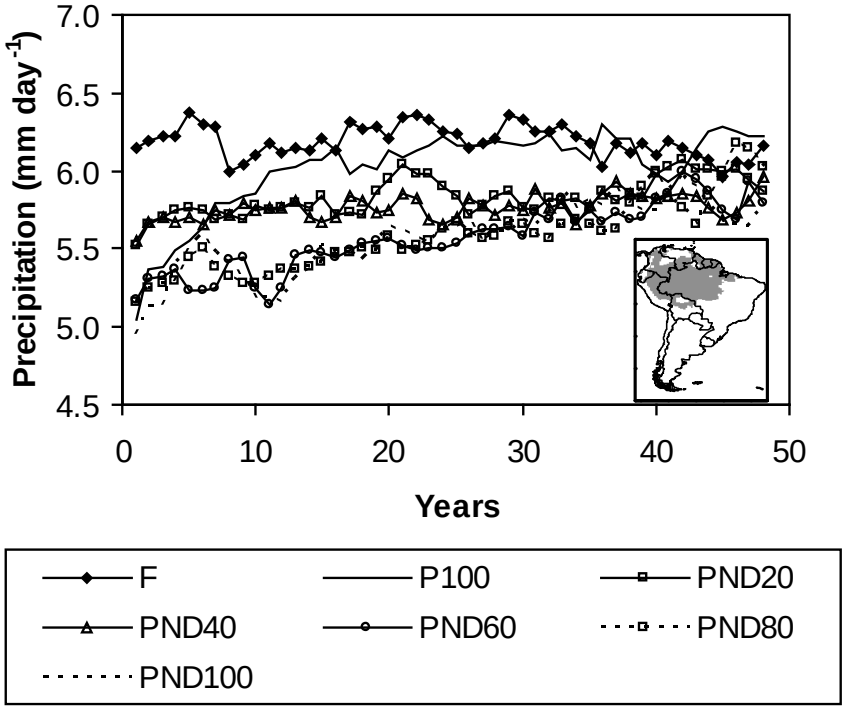

Figure 3.3. The simulated annual mean precipitation obtained using a 3-year moving average for the Amazon tropical forest region (inset).

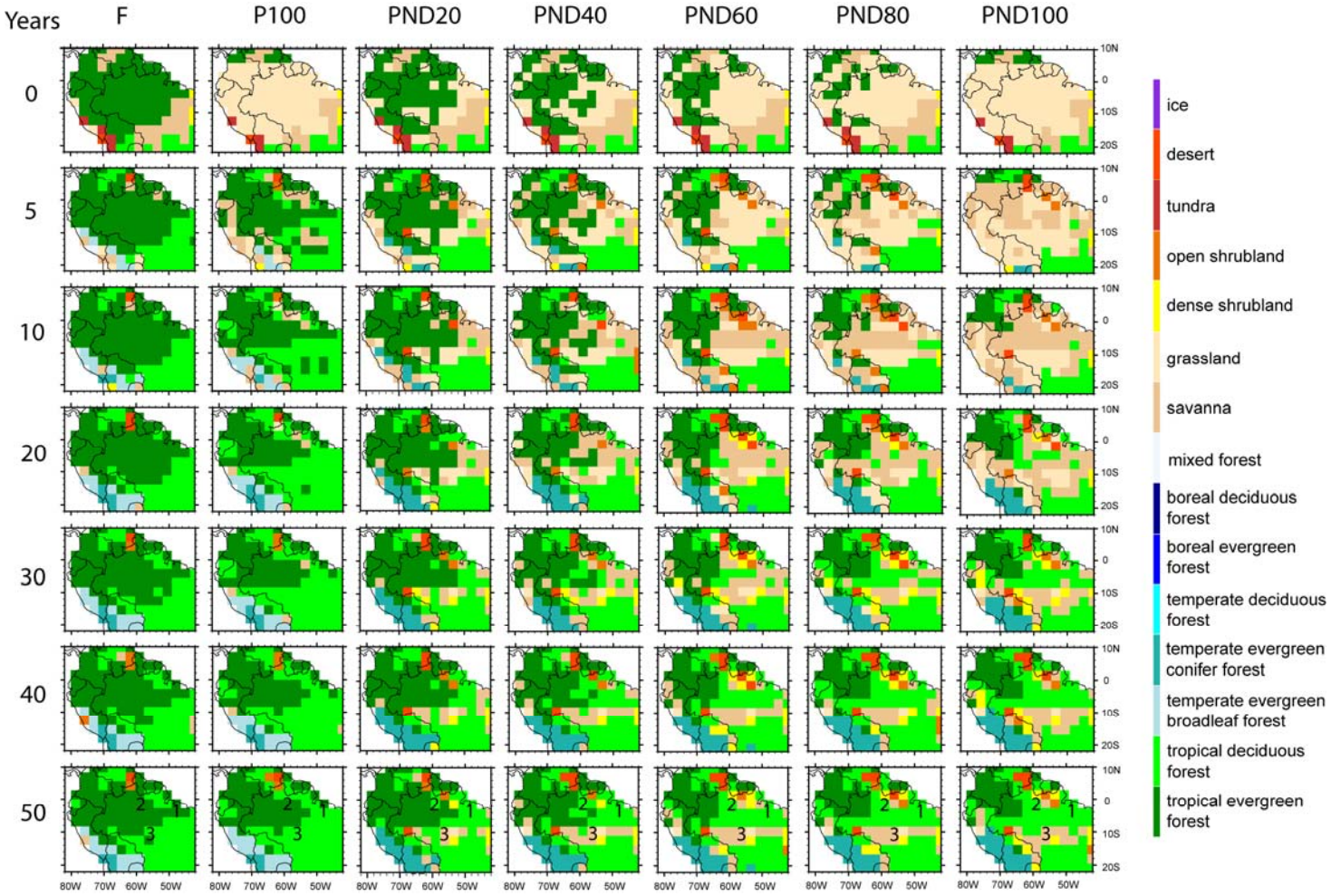

Figure 3.4. The initial land cover scenarios in the first line and the simulated land cover chronosequence of each simulation. The numbers 1, 2 and 3 are discussed in the text and represent eastern sites, Manaus site, and northern Mato Grosso, respectively.

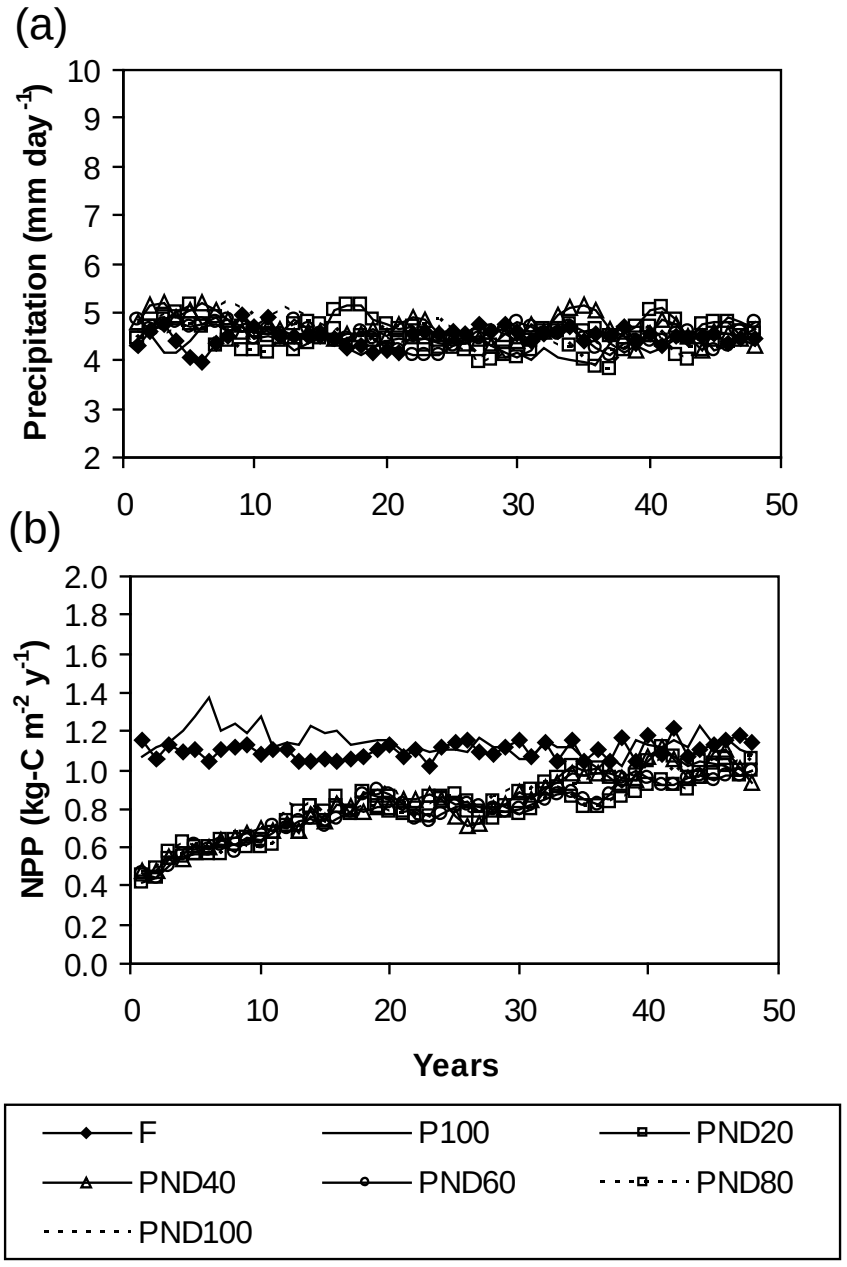

Figure 3.5. The simulated annual mean (a) precipitation and (b) net primary production for region 1 (eastern sites).

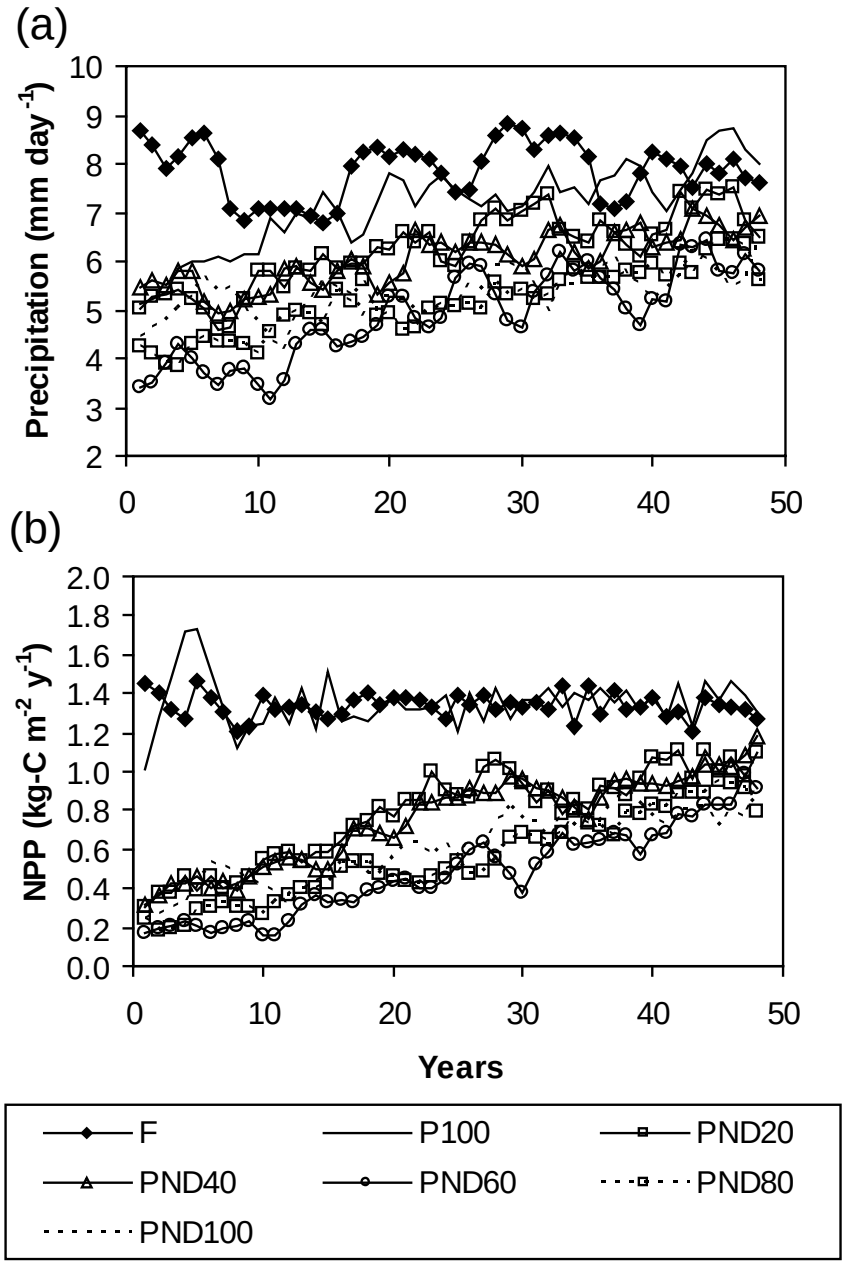

Figure 3.6. The simulated annual mean (a) precipitation and (b) net primary production for region 2 (Manaus site).

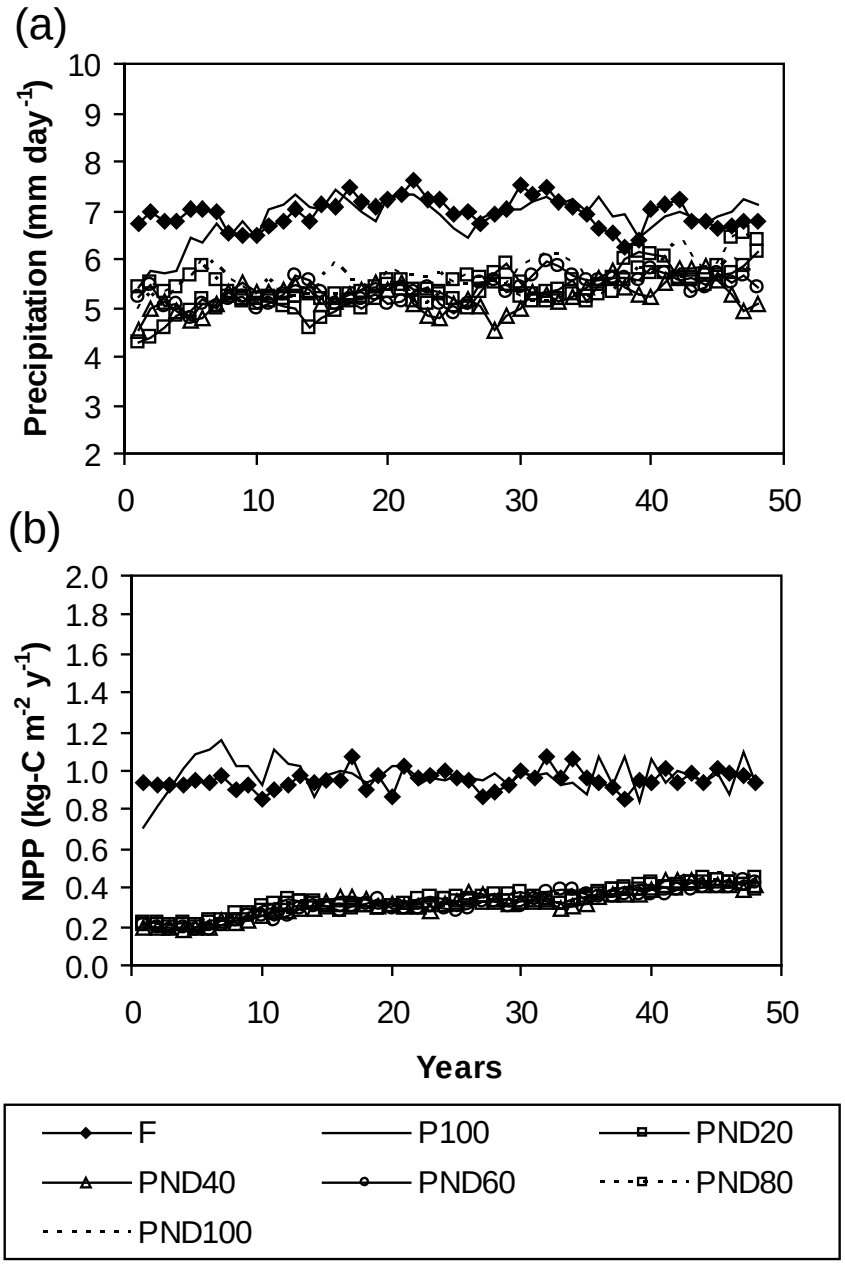

Figure 3.7. The simulated annual mean (a) precipitation and (b) net primary production for region 3 (northern Mato Grosso).

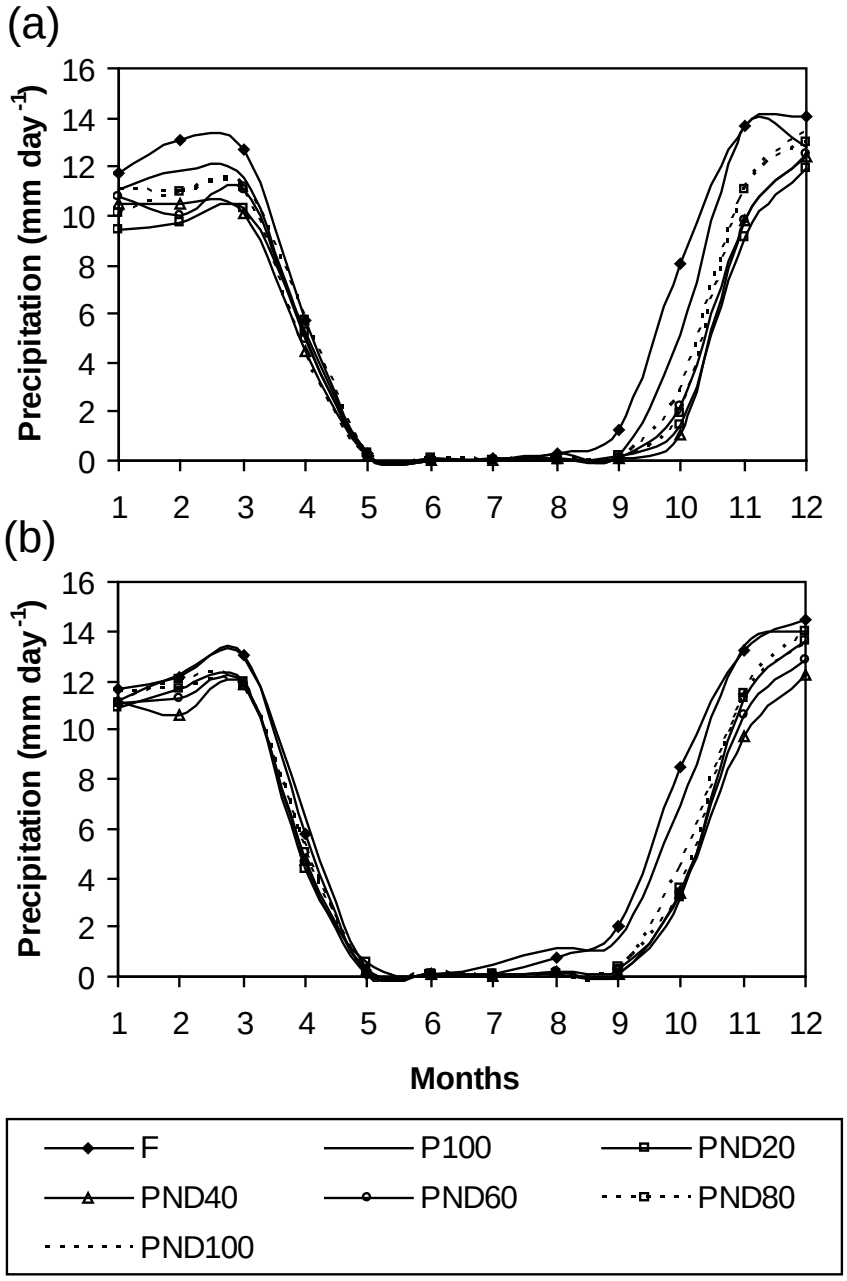

Figure 3.8. The simulated monthly mean precipitation for (a) the first ten years and (b) the last ten years over region 3 (northern Mato Grosso).

CHAPTER 4

GENERAL CONCLUSIONS

4.1. THESIS OVERVIEW

An understanding of the patterns of forest regrowth is a fundamental goal of research in tropical forests [*Baker et al.*, 2003]. Amazon tropical forests are being replaced by pasturelands and croplands, but they often revert to regrowth forest when abandoned after a period of agricultural use [*Fearnside*, 1996]. Secondary forest regrowth restores hydrological functions [*Sommer et al.*, 2002], provides plant and animal habitats [*Baar et al.*, 2004], re-establishes landscape connectivity [*Metzger*, 2003], and plays an important role in sequestering carbon at the regional scale [*Houghton et al.*, 2000]. Several studies suggest that this secondary regrowth may be limited by climate and nutrient availability [*Shukla et al.*, 1990; *Gehring et al.*, 1999; *Davidson et al.*, 2004; *Silva et al.*, 2006].

Using a fully coupled biosphere-atmosphere model, this thesis investigates how the climate feedback and the nutrient feedback interact to regulate the patterns in the regrowth of the Amazon tropical forest. To study this challenging subject, this thesis is divided in three chapters, and the conclusion of each chapter is summarized below.

Chapter 1 investigates how well the fully coupled biosphere-atmosphere model CCM3-IBIS can reproduce vegetation structure and dynamics in Amazonia. Most

variables are simulated within 10% of the estimates: average precipitation is within 5% and average incident solar radiation is within 7% of observations, average total NPP is within 5% and average aboveground NPP is within 2% of observations. Respiration rates and wood NPP are within 15% and 16% of the observations, respectively. Simulated aboveground biomass is within 12% of *Saatchi et al.* [2007] estimates. However, the correct simulation of seasonal and spatial patterns of climate, land cover and NPP does not warrant an accurate representation of the spatial patterns of vegetation structure and dynamics. The realistic representation of these spatial patterns still depends on the understanding of the spatial variation in carbon allocation and residence time parameters and their relationship to environmental factors.

Chapter 2 evaluates the effects of different initial land cover conditions (forest vs. pastureland), as well as different types of nutrient stress (continuous vs. dynamic) on the regrowth of the Amazon rainforest after a hypothetical full deforestation. Considering the continuous nutrient stress simulation PNF, the secondary forest is unable to regrow in most of the Amazon region. However, the results from the dynamic nutrient stress simulation PND, which is the most realistic scenario, suggest that the reduction of precipitation caused by large-scale deforestation is not sufficient to prevent secondary forest regrowth, but this decrease in precipitation combined with nutrient limitation prevents forest regrowth in southern Amazonia (northern Mato Grosso state).

Chapter 3 describes the climate and soil nutrient feedbacks involved in the Amazon rainforest regrowth after different deforestation scenarios, looking for a threshold of deforestation that could cause dangerous interference on the Amazon recovery. Although the simulated mean Amazon precipitation decreases with the increase of deforestation, the precipitation reduction alone is not sufficient to prevent the rainforest regrowth, but this precipitation reduction associated with a soil nutrient

stress does indeed prevent forest regrowth in northern Mato Grosso, no matter how much is deforested. Although, at timescales significantly longer than 50 years, the rainforest might recover if the region is fully protected from human land use and fire, and if the climate remains close to the simulated.

4.2. CONCLUSIONS

To improve understanding of vegetation-climate-soil nutrient feedbacks, the study of environmental change has adopted an integrated approach, in which Dynamic Global Vegetation Models (DGVMs) have been coupled to Global Climate Models (GCMs) [*Foley et al.*, 1998, 2000; *Delire et al.*, 2002, 2003]. Fully coupled climate-biosphere models, like CCM3-IBIS used in this work, are abstractions of a complex system. Many ecological processes are represented in detail, but some formulations are simplified. Validations across varied spatial and temporal scales are needed to refine and improve model performance. The validation conducted in chapter 1 shows the importance of implementing a new way to consider the carbon allocation and residence time (CART) parameters in the model. Research suggests that these parameters may vary spatially [*Malhi et al.*, 2004; *Phillips et al.*, 2004], and CCM3-IBIS considers them fixed and constant, leading to incorrect simulation of spatial patterns of vegetation structure. This will be a challenging work as the relation between these parameters and the environmental variables needs to be clarified. In addition, more field experiments are needed to allow estimation of partitioning coefficients and how this partitioning might vary with forest age and resource

availability [*Litton et al.*, 2007]. Even though we consider this spatial variation of CART parameters, nature may surprise us with adaptative mechanisms under climate change. Results of chapter 1 may stimulate the emergence of new insights toward improving model simulations of vegetation structure and dynamics in Amazonia.

The analysis of the results found in chapters 2 and 3 indicates that pursuing the interaction between reduced rainfall and nutrient depletion is a very productive pathway. The idea that some rainforests may not have the ability to recover after deforestation continues to be worthy of exploration. The major contribution from this thesis is the finding that, low soil nutrient combined with decreases in precipitation may deter forest regrowth. This approach thus may be a valuable tool for prioritizing forest conservation and for informing management in the Amazon region.

The most realistic simulated scenario of climate and nutrient interactions, which considers the secondary forest ability to rebuild nutrient stocks as it matures [*Davidson et al.*, 2007], shows that the rainforest regrows in great part of the Amazon, except over northern Mato Grosso, after a hypothetical full deforestation. But a question remained: is there a threshold of deforestation in which the rainforest over Mato Grosso could regrow?

To address this question, business-as-usual scenarios from *Soares-Filho et al.* [2006] and *Sampaio et al.* [2007] were used in the simulations. Again, the secondary forest regrows in great part of Amazonia, except over northern Mato Grosso, where the land cover becomes a savanna, no matter the extent of the deforested area. Previous research suggests that changes in climate, nutrient loading, habitat fragmentation, or biotic exploitation might result in a loss of resilience and a switch to an alternative state [*Scheffer et al.*, 2001; *Oyama and Nobre*, 2003]. This alternative state, however, may be

unstable. So, strategies for sustainable management of such regions should focus on maintaining resilience.

Another result from the simulations with several deforestation scenarios is that the reduction in precipitation is proportional to the amount of deforestation. This reduction is more drastic when the deforested area is higher than 40% of the original forest extent. This conclusion is consistent with previous studies that also considered partial deforestation scenarios [*Costa et al.*, 2007; *Sampaio et al.*, 2007].

Furthermore, an overview of the secondary forest aboveground biomass compiled by *Zarin et al.* [2005] demonstrates that some sites fit the nutrient-limited growth pattern, while others do not. The nutrient-limited simulations were calibrated against secondary forest regrowth data from Paragominas [*Davidson et al.*, 2004]. Then, the model behavior was extrapolated to the entire Amazonia. Although this is not the ideal procedure, it is the only feasible one, considering the available data. More studies focusing on soil fertility and biomass accumulation in secondary forests are needed, especially over central Amazonia and northern Mato Grosso, to perform reliable projections of potential ecological disruption.

Secondary forest regrowth in different areas of the Amazon may be differently controlled by climate and nutrient availability, and may require varied conservation efforts. The results presented here are concerning because large-scale mechanized agriculture, mostly for soybeans, is rapidly becoming a major force behind forest loss in northern Mato Grosso [*Morton et al.*, 2006]. What people do with the land – whether they leave it bare, plant crops, or convert it to pasture – influences the climate in different ways. Leaving the ground bare has the most significant influence, croplands have the second most significant impact, followed by pastures [*Costa et al.*, 2007;

Sampaio et al., 2007]. The low resilience of northern Mato Grosso forests presented here suggests that this region should be a major target for conservation initiatives.

Finally, it is important to remember that these simulations do not consider forest impoverishment through logging and fire [*Nepstad et al.*, 1999; 2001], rainfall inhibition due to a higher concentrations of aerosol particles [*Andreae et al.*, 2004] or due to sea surface temperature anomalies [*Marengo et al.*, 2008], and the potential for forest substitution by savanna due to global warming [*Cox et al.*, 2000; 2004]. The regrowth capacity of the rainforest might be significantly reduced considering the synergistic influence of several vicious feedbacks that exist within and among the ecosystems and climate of the Amazon region.

4.3. RECOMMENDATIONS FOR FUTURE RESEARCH

The results presented in this thesis elucidated some points, but also provoked many new questions. I recommend that future work should investigate these themes:

- Further simulations inputting the available spatial carbon allocation and residence time data [*Malhi et al.*, 2004; *Phillips et al.*, 2004] into the model. This would certainly improve the spatial performance in Amazonia, but may not be representative of a future climate.
- Parameterization of the carbon allocation and residence time considering the environmental variables, and the best candidate is soil fertility according to *Phillips et al.* [2004]. Again restricting to Amazonia, because there are no global maps of soil fertility.
- Field measurements of all components to allow carbon partitioning coefficients and their response to stand age, competition, and resource availability. A better understanding of carbon allocation would improve the capacity to model forest ecosystem metabolism and predict the effects of global change on carbon cycling.

- Compilation of high-quality validation data (atmospheric, ecological, tower measurements, remote sensing) to permit further model calibrations and sensitivity analysis. The validation would include annual means, seasonal cycles, interannual variability, and extreme events (e.g. droughts) patterns.
- Field measurements to obtain parameters for several land surface types, such as regrowth forests, degraded forests, crops, and savannas. Soil physical and chemical properties, plant nutrient concentration, and biomass accumulation rates would improve considerably the scope of these modeling exercises. The region of northern Mato Grosso should be a major area for field experiments.
- Development of a fire disturbance module including fire probability and intensity. Thus, CCM3-IBIS would integrate the major drivers of savannization in Amazonia.
- Development of a complete nutrient cycling module that directly affects the gross photosynthesis rate, hence affecting the simulated dominant vegetation type.
- Further simulations considering only the effects of nutrient limitation on forest regrowth. This can be done using the off-line IBIS version, to test whether nutrient effects alone are strong enough to limit the forest regrowth.
- Further simulations considering the atmospheric CO_2 concentration representative of different IPCC scenarios. This would provide a valuable assessment of vegetation-climate-soil nutrient feedbacks in a scenario of global climate change.
- Further simulations considering sea surface temperatures representatives of future climate and from several different models. This would investigate

whether the modulation of the Amazon climate system by the oceans affect the climatic sensitivity to deforestation under nutrient stress.

GENERAL REFERENCES

Alencar, A., D. Nepstad, and M. C. V. Diaz (2006), Forest understory fire in the Brazilian Amazon in ENSO and non-ENSO years: area burned and committed carbon emissions, *Earth Interactions*, *10*(6), 1-17.

Andreae, M., D. Rosenfeld, P. Artaxo, A. A. Costa, G. P. Frank, K. M. Longo, and M. A. F. Silva-Dias (2004), Smoking rain clouds over the Amazon, *Science*, *303*, 1337-1342.

Baar, R., M. R. Cordeiro, M. Denich, and H. Fölster (2004), Floristic inventory of secondary vegetation in agricultural systems of East-Amazonia, *Biodiversity and Conservation*, *13*(3), 501-528.

Baker, T. R., M. D. Swaine, M.D., and D. F. R. P. Burslem (2003), Variation in tropical forest growth rates: combined effects of functional group composition and resource availability, *Perspectives in Plant Ecology, Evolution and Systematics*, *6*, 21-36.

Bala, G., K. Caldeira, M. Wickett, T. J. Phillips, D. B. Lobell, C. Delire, and A. Mirin (2007), Combined climate and carbon-cycle effects of large-scale deforestation, *Proceedings of the National Academy of Sciences of the United States of America*, *104*, 6550-6555.

Betts, R. A., P. M. Cox, S. E. Lee, and F. I. Woodward (1997), Contrasting physiological and structural vegetation feedbacks in climate change simulations, *Nature*, *387*, 796-799.

Betts, R., M. Sanderson, and S. Woodward (2008), Effects of large-scale Amazon forest degradation on climate and air quality through fluxes of carbon dioxide, water, energy, mineral dust and isoprene, *Philosophical Transactions of The Royal Society of London Series B-Biological Sciences*, *363*, doi:10.1098/rstb.2007.0027.

Bonan, G. (Ed.) (2002), *Ecological Climatology: Concepts and Applications*, 678 pp., Cambridge University Press, Cambridge.

Bonan, G. B., S. Levis, S. Sitch, M. Vertenstein, and K. W. Oleson (2003), A dynamic global vegetation model for use with climate models: concepts and description of simulated vegetation dynamics, *Global Change Biology*, *9*, 1543-1566.

Botta, A., and J. A. Foley (2002), Effects of climate variability and disturbances on the Amazonian terrestrial ecosystems dynamics, *Global Biogeochemical Cycles*, *16*, 1070, doi:10.1029/2000GB001338.

Brookman-Amissah, J., J. B. Hall, M. D. Swaine, and J. Y. Attakorah (1980), A re-assessment of a fire protection experiment in North-eastern Ghana savanna, *Journal of Applied Ecology*, *17*, 85-99.

Brovkin, V., A. Ganopolski, M. Claussen, C. Kubatzki, and V. Petoukhov (1999), Modelling climate response to historical land cover change, *Global Ecology and Biogeography*, *8*, 509-517.

Carvalho, G. O., D. Nepstad, D. McGrath, M. del C. Vera Diaz, M. Santilli, and A. C. Barros (2002), Frontier expansion in the Amazon, *Environment*, *44*(3), 34- 45.

Ceballos, J. C., M. J. Bottino, and J. M. Souza (2004), A simplified physical model for assessing solar radiation over Brazil using GOES 8 visible imagery, *Journal of Geophysical Research*, *109*, D02211, doi:10.1029/2003JD003531.

Clark, D. A., S. C. Piper, C. D. Keeling, and D. B. Clark (2003), Tropical rain forest tree growth and atmospheric carbon dynamics linked to interannual temperature variation during 1984–2000, *Proceedings of the National Academy of Sciences of the United States of America*, *100*, 5852-5857.

Clark, D. A. (2004), Sources or sinks? The responses of tropical forests to current and future climate and atmospheric composition, *Philosophical Transactions of The Royal Society of London Series B*, *359*, 477-491.

Cochrane, M. A., A. Alencar, M. D. Schulze, C. M. Souza, D. C. Nepstad, P. Lefebvre, and E. A. Davidson (1999), Positive feedbacks in the fire dynamic of closed canopy tropical forests, *Science*, *284*(5421), 1832-1835.

Cochrane, M. A. (2003), Fire science for rainforests, *Nature*, *421*, 913-919.

Costa, M. H., and J. A. Foley (1998), A comparison of precipitation datasets for the Amazon basin, *Geophysical Research Letters*, *25*, 155-158.

Costa, M. H., and J. A. Foley (2000), Combined effects of deforestation and doubled atmospheric CO_2 concentrations on the climate of Amazonia, *Journal of Climate*, *13*(1), 18-34.

Costa, M. H., S. N. M. Yanagi, P. J. O. P. Souza, A. Ribeiro, and E. J. P. Rocha (2007), Climate change in Amazonia caused by soybean cropland expansion, as compared to caused by pastureland expansion, *Geophysical Research Letters*, *34*, L07706, doi:10.1029/2007GL029271.

Coutinho, L. M. (1982), Ecological effects of fire in Brazilian Cerrado, in: *Ecology of Tropical Savannas*, edited by B. J. Huntley and B. H. Walker, pp.273-291, Springer-Verlag, Berlim.

Coutinho, L. M. (1990), Fire in the ecology of the Brazilian Cerrado, in: *Fire in the Tropical Biota: Ecosystem Processes and Global Challenges*, edited by J. G. Goldammer, pp. 82-105, Springer-Verlag, Berlim.

Cox, P. M., R. A. Betts, C. D. Jones, S. A. Spall, and I. J. Totterdell (2000), Acceleration of global warming due to carbon-cycle feedbacks in a coupled climate model, *Nature*, *408*, 184-187.

Cox, P. M., R. A. Betts, M. Collins, P. P. Harris, C. Huntingford, and C. D. Jones (2004), Amazonian forest dieback under climate-carbon cycle projections for the 21st century, *Theoretical and Applied Climatology*, *78*, 137-156.

Davidson, E. A., C. J. R. Carvalho, I. C. G. Viera, R. O. Figueiredo, P. Moutinho, F. Y. Ishida, M. T. P. Santos, J. B. Guerrero, K. Kalif, and R. T. Sabá (2004), Nitrogen and phosphorus limitation of biomass growth in a tropical secondary forest, *Ecological Applications*, *14*, 150-163.

Davidson, E. A., C. J. R. de Carvalho, A. M. Figueira, F. Y. Ishida, J. P. H. B. Ometto, G. B. Nardoto, R. T. Sabá, S. N. Hayashi, E. C. Leal, I. C. G. Vieira, and L. A. Martinelli (2007), Recuperation of nitrogen cycling in Amazonian forests following agricultural abandonment, *Nature*, *447*, 995-998.

Delire, C., S. L. Levis, G. Bonan, J. A. Foley, M. T. Coe, and S. Vavrus (2002), Comparison of the climate simulated by the CCM3 coupled to two different land-surface models, *Climate Dynamics*, *19*(8), 657-669.

Delire, C., J. A. Foley, and S. Thompson (2003), Evaluating the carbon cycle of a coupled atmosphere-biosphere model, *Global Biogeochemical Cycles*, *17*, 1012, doi:10.1029/2002GB001870.

Denman, K. L., G. Brasseur, A. Chidthaisong, P. Ciais, P. M. Cox, R. E. Dickinson, D. Hauglustaine, C. Heinze, E. Holland, D. Jacob, U. Lohmann, S. Ramachandran, P. L. da Silva Dias, S. C. Wofsy, and X. Zhang (2007), Couplings between changes in the climate system and biogeochemistry, in: *Climate Change 2007: The Physical Science Basis. Contribution of Working Group I to the Fourth Assessment Report of the Intergovernmental Panel on Climate Change*, edited by S. Solomon, D. Qin, M. Manning, Z. Chen, M. Marquis, K. B. Averyt, M. Tignor, and H. L. Miller, pp. 499-587, Cambridge University Press, Cambridge.

Dirzo, R., and P. H. Raven (2003), Global state of biodiversity and loss, *Annual Review of Environment and Resources, 28*, 137-167.

Eltahir, E. A. B. (1996), Role of vegetation in sustaining large-scale atmospheric circulations in the tropics, *Journal of Geophysical Research*, *101*, 4255-4268.

Fearnside, P. M. (1996), Amazonian deforestation and global warming: carbon stocks in vegetation replacing Brazil's Amazon forest, *Forest Ecology and Management*, *80*, 21-34.

Figueira, M. A., H. Rocha, M. L. Goulden, S. D. Miller, M. Menton, C. Doughty, H. Freitas, C. A. Sousa, and A. Maia (2002), Litterfall and leaf area index before and after selective logging in Tapajós National Forest, *Eos Trans. AGU*, *83*, Fall Meet. Suppl., Abstract B22C-0771.

Foley, J. A., I. C. Prentice, N. Ramankutty, S. Levis, D. Pollard, S. Sitch, and A. Haxeltine (1996), An integrated biosphere model of land surface processes,

terrestrial carbon balance, and vegetation dynamics, *Global Biogeochemical Cycles*, *10*, 603-628.

Foley, J. A., S. Levis, I. C. Prentice, D. Pollard, and S. L. Thompson (1998), Coupling dynamic models of climate and vegetation, *Global Change Biology, 4***,** 561-579.

Foley, J. A., S. Levis, M. H. Costa, W. Cramer, and D. Pollard (2000), Incorporating dynamic vegetation cover within global climate models, *Ecological Applications*, *10*, 1620-1632.

Foley, J. A., M. H. Costa, C. Delire, N. Ramankutty, and P. Snyder (2003), Green surprise? How terrestrial ecosystems could affect earth's climate, *Frontiers in Ecology and the Environment*, *1*, 38-44.

Foley, J. A., G. P. Asner, M. H. Costa, M. T. Coe, R. DeFries, H. K. Gibbs, E. A. Howard, S. Olson, J. Patz, N. Ramankutty, and P. Snyder (2007), Amazonian revealed: forest degradation and loss of ecosystem goods and services in the Amazon Basin, *Frontiers in Ecology and Environment*, *5*(1), 25-32.

Friedlingstein, P., L. Bopp, P. Ciais, J. -L. Dufresne, L. Fairhead, H. LeTreut, P. Monfray, and J. Orr (2001), Positive feedback between future climate change and the carbon cycle, *Geophysical Research Letters*, *28*, 1543-1546.

Friedlingstein, P., P. Cox, R. Betts, L. Bopp, W. von Bloh, V. Brovkin, P. Cadule, S. Doney, M. Eby, I. Fung, G. Bala, J. John, C. Jones, F. Joos, T. Kato, M. Kawamiya, W. Knorr, K. Lindsay, H. D. Matthews, T. Raddatz, P. Rayner, C. Reick, E. Roeckner, K. -G. Schnitzler, R. Schnur, K. Strassmann, A. J. Weaver, C. Yoshikawa, and N. Zeng (2006), Climate–carbon cycle feedback analysis: results from the C^4MIP model intercomparison, *Journal of Climate*, *19*, 3337-3353.

Gehring, C., M. Kanashiro, M. Denich, and P. L. G. Vlek (1999), Response of secondary vegetation in eastern Amazonia to relaxed nutrient availability constraints, *Biogeochemistry*, *45*, 223-241.

Gill, A. M., R. H. Groves, and I. R. Noble (Ed.) (1981), *Fire and the Australian Biota*, 169 pp., Australian Academy of Science, Canberra.

Godoy, J. R., G. Petts, and J. Salo (1999), Riparian flooded forests of the Orinoco and Amazon basins: a comparative review, *Biodiversity and Conservation*, *8*(4), 551-586.

Hahmann, A. N., and R. E. Dickinson (1997), RCCM2-BATS model over tropical South America: applications to tropical deforestation, *Journal of Climate*, *10*(8), 1944-1964.

Henriques, R. P. B., and J. D. Hay (2002), Patterns and dynamics of plant populations, in: *The Cerrados of Brazil: Ecology and Natural History of a Neotropical Savanna*, edited by P. S. Oliveira and R. J. Marquis, pp. 140-158, Columbia University Press, Columbia.

Hoffmann, W. A. (1996), The effects of fire and cover on seedling establishment in a neotropical savanna, *Journal of Ecology*, *84*, 383-393.

Houghton, R. A., D. L. Skole, C. A. Nobre, J. L. Hackler, K. T. Lawrence, and W. H. Chomentowski (2000), Annual fluxes of carbon from deforestation and regrowth in the Brazilian Amazon, *Nature*, *403*, 301-304.

Huffman, G. J., R. F. Adler, P. Arkin, A. Chang, R. Ferraro, A. Gruber, J. Janowiak, A. McNab, B. Rudolf, and U. Schneider (1997), The global precipitation climatology project (GPCP) combined precipitation dataset, *Bulletin of the American Meteorological Society*, *78*, 5-20.

Hutyra, L. R., J. W. Munger, C. A. Nobre, S. R. Saleska, S. A. Vieira, and S. C. Wofsy (2005), Climatic variability and vegetation vulnerability in Amazonia, *Geophysical Research Letters*, *32*, L24712, doi:10.1029/2005GL024981.

Imbuzeiro, H. M. A. (2005), Calibration of the IBIS model in the Amazonian forest using multiple sites, M.S. thesis (in Portuguese with abstract in English), 67 pp., Federal University of Viçosa, Viçosa, 12 July.

INPE (Brazilian Space Research Institute) (2007), Legal Amazon deforestation 1988-2007, Prodes Project, Available from http://www.obt.inpe.br/prodes/.

Kalnay, E., M. Kanamitsu, R. Kistler, W. Collins, D. Deaven, L. Gandin, M. Iredell, S. Saha, G. White, J. Woollen, Y. Zhu, A. Leetmaa, B. Reynolds, M. Chelliah, W. Ebisuzaki, W. Higgins, J. Janowiak, K. C. Mo, C. Ropelewski, J. Wang, R. Jenne, and D. Joseph (1996), The NCEP/NCAR 40-year reanalysis project, *Bulletin of the American Meteorological Society*, *77*, 437-471.

Kauffman, J. B., C. Uhl, and D. L. Cummings (1988), Fire in the Venezuelan Amazon 1: Fuel biomass and fire chemistry in the evergreen rainforest of Venezuela, *Oikos*, *53*, 167-175.

Kauffman, J. B., R. L. Sanford Jr., D. L. Cummings, I. H. Salcedo, and E. V. S. B. Sampaio (1993), Biomass and nutrient dynamics associated with slash fires in neotropical dry forests, *Ecology*, *74*, 140-151.

Kauffman, J. B., D. L. Cummings, D. E. Ward, and R. Babbitt (1995), Fires in the Brazilian Amazon: biomass, nutrient pools, and losses in slashed primary forests, *Oecologia*, *104*, 397-408.

Kiehl, J. T., J. J. Hack, G. B. Bonan, B. A. Boville, D. L. Williamson, and P. J. Rasch (1998), The national center for atmospheric research community climate model: CCM3, *Journal of Climate, 11***,** 1131-1149.

Krinner, G., N. Viovy, N. de Noblet-Ducoudré, J. Ogée, J. Polcher, P. Friedlingstein, P. Ciais, S. Sitch, and I. C. Prentice (2005), A dynamic global vegetation model for studies of the coupled atmosphere-biosphere system, *Global Biogeochemical Cycles*, *19*, GB1015, doi:10.1029/2003GB002199.

Kucharik, C. J., J. A. Foley, C. Delire, V. A. Fisher, M. T. Coe, J. D. Lenters, C. Young-Molling, N. Ramankutty, J. M. Norman, and S. T. Gower (2000), Testing the performance of a dynamic global ecosystem model: water balance, carbon balance, and vegetation structure, *Global Biogeochemical Cycles*, *14*(3), 795-825.

Kummerow, C., W. Barnes, T. Kozu, J. Shiue, and J. Simpson (1998), The tropical rainfall measuring mission (TRMM) sensor package, *Journal of Atmospheric and Oceanic Technology*, *15*, 809-817.

Lacey, C. J., J. Walker, and I. R. Noble (1982), Fire in Australian tropical savannas, in: *Ecology of Tropical Savannas*, edited by B. J. Huntley and B. H. Walker, pp.246-272, Springer-Verlag, Berlim.

Lapola, D. M. (2007), Consequences of global climatic changes on South American biomes: a potential vegetation model including the carbon cycle, M.S. thesis (in Portuguese with abstract in English), 183 pp., Brazilian Space Research Institute, São José dos Campos, 26 March.

Laurance, W. F., S. G. Laurance, L. V. Ferreira, J. M. Rankin-de Merona, C. Gascon, and T. E. Lovejoy (1997), Biomass collapse in Amazonian forest fragments, *Science*, *278*(5340), 1117-1118.

Laurance, W. F., P. M. Fearnside, S. G. Laurance, P. Delamonica, T. E. Lovejoy, J. M. Rankin-de Merona, J. Q. Chambers, and C. Gascon (1999), Relationship between soils and Amazon forest biomass: a landscape-scale study, *Forest Ecology and Management*, *118*, 127-138.

Laurance, W. F., M. A. Cochrane, S. Bergen, P. M. Fearnside, P. Delamonica, C. Barber, S. D'Angelo, and T. Fernandes (2001), Environment: the future of the Brazilian Amazon, *Science*, *291*(5503), 438-439.

Lean, J., and P. R. Rowntree (1997), Understanding the sensitivity of a GCM simulation of Amazonian deforestation to the specification of vegetation and soil characteristics, *Journal of Climate*, *10*(6), 1216-1235.

Leemans, R., and W. P. Cramer (1990), The IIASA database for mean monthly values of temperature, precipitation and cloudiness on a global terrestrial grid, *IIASA Working Papers*, WP-90-41, Laxenburg, Austria.

Legates, D. R., and C. J. Willmott (1990), Mean seasonal and spatial variability in gauge-corrected, global precipitation, *International Journal of Climatology*, *10*, 111-127.

Levis, S., J. A. Foley, and D. Pollard (2000), Large scale vegetation feedbacks on a doubled CO_2 climate, *Journal of Climate*, *13*(7), 1313-1325.

Litton, C. M., J. W. Raich, and M. G. Ryan (2007), Carbon allocation in forest ecosystems, *Global Change Biology, 13***,** 2089-2109.

Liu, Z., M. Notaro, J. Kutzbach, and N. Liu (2006), Assessing global vegetation-climate feedbacks from observations, *Journal of Climate*, *19*, 787-814.

Lund, P. W. (1843), Blik paa Brasilien dryeverden, *Selsk Skrifter*, *11*, 1-82.

Mackensen, J., D. Hölscher, R. Klinge, and H. Fölster (1996), Nutrient transfer to the atmosphere by burning of debris in eastern Amazonia, *Forest Ecology and Management*, *86*, 121-128.

Magrin, G., C. G. García, D. C. Choque, J. C. Giménez, A. R. Moreno, G. J. Nagy, C. Nobre, and A. Villamizar (2007), Latin America, in: *Climate Change 2007: Impacts, Adaptation and Vulnerability. Contribution of Working Group II to the*

Fourth Assessment Report of the Intergovernmental Panel on Climate Change, edited by M. L. Parry, O. F. Canziani, J. P. Palutikof, P. J. van der Linden, and C. E. Hanson, pp. 581-615, Cambridge University Press, Cambridge.

Malhi, Y., T. R. Baker, O. L. Phillips, S. Almeida, E. Alvarez, L. Arroyo, J. Chave, C. I. Czimczik, A. Di Fiore, N. Higuchi, T. J. Killeen, S. G. Laurance, W. F. Laurance, S. L. Lewis, L. M. M. Montoya, A. Monteagudo, D. A. Neill, P. N. Vargas, S. Patiño, N. C. A. Pitman, C. A. Quesada, J. N. M. Silva, A. T. Lezama, R. V. Martinez, J. Terborgh, B. Vinceti, and J. Lloyd (2004), The above-ground coarse wood productivity of 104 neotropical forest plots, *Global Change Biology*, *10*, 563-591.

Malhi, Y., D. Wood, T. R. Baker, J. Wright, O. L. Phillips, T. Cochrane, P. Meir, J. Chave, S. Almeida, L. Arroyo, N. Higuchi, T. J. Killeen, S. G. Laurance, W. F. Laurance, S. L. Lewis, A. Monteagudo, D. A. Neill, P. N. Vargas, N. C. A. Pitman, C. A. Quesada, R. Salomão, J. N. M. Silva, A. T. Lezama, J. Terborgh, R. V. Martínez, and B. Vinceti (2006), The regional variation of aboveground live biomass in old-growth Amazonian forests, *Global Change Biology*, *12*, 1107-1138.

Malhi, Y., J. T. Roberts, R. A. Betts, T. J. Killeen, W. Li, and C. A. Nobre (2008), Climate change, deforestation, and the fate of the Amazon, *Science*, *319*(5860), 169-172, doi:10.1126/science.1146961.

Malhi, Y., L. E. O. C. Aragão, D. B. Metcalfe, S. Patiño, C. A. Quesada, S. Almeida, L. Anderson, P. Brando, J. Q. Chambers, A. L. Costa, L. Ferreira, L. R. Hutyra, P. Oliveira, E. H. Pyle, and A. L. Robertson, Comprehensive assessment of carbon productivity, allocation and storage in three Amazonian forests, *Global Change Biology*, submitted.

Marengo, J. A., C. A. Nobre, J. Tomasella, M. D. Oyama, G. S. Oliveira, R. Oliveira, H. Camargo, L. M. Alves, and I. F. Brown (2008), The drought of Amazonia in 2005, *Journal of Climate*, *21*, 495-516.

Mesquita, R. C. G., P. Delamonica, and W. F. Laurance (1999), Effect of surrounding vegetation on edge-related tree mortality in Amazonian forest fragments, *Biological Conservation*, *91*(2-3), 129-134.

Metzger, J. P. (2003), Effects of slash-and-burn fallow periods on landscape structure, *Environmental Conservation*, *30*, 325-333.

Miranda, H. S.,M. M. C. Bustamante, and A. C. Miranda (2002), The fire factor, in: *The Cerrados of Brazil: Ecology and Natural History of a Neotropical Savanna*, edited by P. S. Oliveira and R. J. Marquis, pp. 51-68, Columbia University Press, Columbia.

Moorcroft, P. R. (2003), Recent advances in ecosystem-atmosphere interactions: an ecological perspective, *Proceedings of The Royal Society of London Series B-Biological Sciences*, *270*, 1215-1227.

Morton, D. C., R. S. DeFries, Y. E. Shimabukuro, L. O. Anderson, E. Arai, F. del Bon Espirito-Santo, R. Freitas, and J. Morisette (2006), Cropland expansion changes deforestation dynamics in the southern Brazilian Amazon, *Proceedings of the National Academy of Sciences of the United States of America*, *103*, 14637-14641, doi:10.1073/pnas.0606377103.

Nemani, R. R., C. D. Keeling, H. Hashimoto, W. M. Jolly, S. C. Piper, C. J. Tucker, R. B. Myneni, and S. W. Running (2003), Climate-driven increases in global terrestrial net primary production from 1982 to 1999, *Science*, *300*, 1560-1563.

Nepstad, D. C., A. Verissimo, A. Alencar, C. Nobre, E. Lima, P. Lefebvre, P. Schlesinger, C. Potter, P. Moutinho, E. Mendoza, M. Cochrane, and V. Brooks

(1999), Large-scale impoverishment of Amazonian forests by logging and fire, *Nature*, *398*(6727), 505-508.

Nepstad, D., G. Carvalho, A. C. Barros, A. Alencar, J. P. Capobianco, J. Bishop, P. Moutinho, P. Lefebvre, U. L. Silva-Jr., and E. Prins (2001), Road paving, fire regime feedbacks, and the future of Amazon forests, *Forest Ecology and Management*, *154*, 395-407.

Nepstad, D. C., C. M. Stickler, and O. T. Almeida (2006), Globalization of the Amazon soy and beef industries: opportunities for conservation, *Conservation Biology*, *20*(6), 1595-1603.

New, M., M. Hulme, and P. Jones (1999), Representing twentieth-century space-time climate variability. Part I: development of a 1961-90 mean monthly terrestrial climatology, *Journal of Climate*, *12*, 829-856.

Nobre, C. A., P. J. Sellers, and J. Shukla (1991), Amazonian deforestation and regional climate change, *Journal of Climate*, *4*(10), 957-988.

Notaro, M., S. Vavrus, and Z. Liu (2007), Global vegetation and climate change due to future increases in CO_2 as projected by a fully coupled model with dynamic vegetation, *Journal of Climate*, *20*, 70-90.

Oyama, M. D., and C. A. Nobre (2003), A new climate-vegetation equilibrium state for Tropical South America, *Geophysical Research Letters*, *30*(23), 2199, doi:10.1029/2003GL018600.

Phillips, O. L., T. R. Baker, L. Arroyo, N. Higuchi, T. J. Killeen, W. F. Laurance, S. L. Lewis, J. Lloyd, Y. Malhi, A. Monteagudo, D. A. Neill, P. N. Vargas, J. N. M. Silva, J. Terborgh, R. V. Martínez, M. Alexiades, S. Almeida, S. Brown, J. Chave, J. A. Comiskey, C. I. Czimczik, A. Di Fiore, T. Erwin, C. Kuebler, S. G. Laurance, H. E. M. Nascimento, J. Olivier, W. Palacios, S. Patiño, N. C. A. Pitman, C. A.

Quesada, M. Saldias, A. T. Lezama, and B. Vinceti (2004), Pattern and process in Amazon tree turnover, 1976-2001, *Philosophical Transactions of The Royal Society of London Series B-Biological Sciences*, *359*, 381-407.

Pielke, R., R. Avissar, M. Raupach, A. J. Dolman, X. Zhen, and A. S. Denning (1998), Interactions between the atmosphere and terrestrial ecosystems: Influence on weather and climate, *Global Change Biology*, *4*, 461-475.

Pinto, L. I. C. (2007), Comparison of precipitation and incident solar radiation products for South America: observed data and reanalysis, M.S. thesis (in Portuguese with abstract in English), 75 pp., Federal University of Viçosa, Viçosa, 18 June.

Prance, G. T., H. Beentje, J. Dransfield, and R. Johns (2000), The tropical flora remains undercollected, *Annals of the Missouri Botanical Garden*, *87*(1), 67-71.

Prentice, I. C. (2001), Interactions of climate change and the terrestrial biosphere, in: *Geosphere-Biosphere Interactions and Climate*, edited by L. O. Bengtsson and C. U. Hammer, pp. 176-195, Cambridge University Press, Cambridge.

Ramankutty, N., and J. A. Foley (1999), Estimating historical changes in global land cover: croplands from 1700 to 1992, *Global Biogeochemical Cycles*, *13*, 997-1027.

Rizzini, C. T. (Ed.) (1979), *Tratado de Fitogeografia do Brasil: Aspectos Sociológicos e Florísticos*, 325 pp., Hucitec Ltda, São Paulo.

Roberts, J. M., O. M. R. Cabral, J. P. Costa, A. L. C. McWillian, and T. D. A. Sá (1996), An overview of the leaf area index and physiological measurements during ABRACOS, in: *Amazonian Deforestation and Climate*, edited by J. H. C. Gash, C. A. Nobre, J. M. Roberts, and R. L. Victoria, pp. 287-306, John Wiley & Sons, Chichester.

Saatchi, S. S., R. A. Houghton, R. C. S. Alvalá, J. V. Soares, and Y. Yu (2007), Distribution of aboveground live biomass in the Amazon basin, *Global Change Biology*, *13*, 816-837.

Sampaio, F. A. R., L. E. F. Fontes, L. M. Costa, and I. Jucksch (2003), Nutrient and phytomass dynamics in a yellow Argissol under Amazonian tropical forest after burning and rice cultivation (in Portuguese with abstract in English), *Revista Brasileira de Ciência do Solo*, *27*(6), 1161-1170.

Sampaio, G., C. Nobre, M. H. Costa, P. Satyamurty, B. S. Soares-Filho, and M. Cardoso (2007), Regional climate change over eastern Amazonia caused by pasture and soybean cropland expansion, *Geophysical Research Letters*, *34*, L17709, doi:10.1029/2007GL030612.

Sampaio, G. (2008), Climatic consequences of gradual conversion of Amazonian tropical forests into degraded pasture or soybean cropland: a GCM simulation study, Sc.D. thesis (in Portuguese with abstract in English), 352 pp., Brazilian Space Research Institute, São José dos Campos, 28 March.

San José, J. J., and M. R. Fariñas (1991), Temporal changes in the structure of a Trachypogon savanna protected for 25 years, *Acta Oecologica*, *12*, 237-247.

Scheffer, M., S. Carpenter, J. A. Foley, C. Folke, and B. Walker (2001), Catastrophic shifts in ecosystems, *Nature*, *413*, 591-596.

Scheffer, M., M. Holmgren, V. Brovkin, and M. Claussen (2005), Synergy between small- and large-scale feedbacks of vegetation on the water cycle, *Global Change Biology*, *11*, 1003-1012.

Shukla, J., C. A. Nobre, and P. J. Sellers (1990), Amazon deforestation and climate change, *Science*, *247*(4948), 1322-1325.

Silva, C. E. M., J. F. C. Gonçalves, T. R. Feldpausch, F. J. Luizão, R. R. Morais, and G. O. Ribeiro (2006), Nutrient use efficiency for pioneer species grown on abandoned pastures in central Amazonia (in Portuguese with abstract in English), *Acta Amazonica*, *36*(4), 503-512.

Silva Dias, M. A. F., S. Rutledge, P. Kabat, P. L. Silva Dias, C. Nobre, G. Fisch, A. J. Dolman, E. Zipser, M. Garstang, A. O. Manzi, J. D. Fuentes, H. R. Rocha, J. Marengo, A. Plana-Fattori, L. D. A. Sá, R .C. S. Alvalá, M. O. Andreae, P. Artaxo, R. Gielow, and L. Gatti (2002), Cloud and rain processes in a biosphere-atmosphere interaction context in the Amazon region, *Journal of Geophysical Research*, *107*(8072), doi:10.1029/2001JD000335.

Skole, D., and C. Tucker (1993), Tropical deforestation and habitat fragmentation in the Amazon - satellite data from 1978 to 1988, *Science*, *260*(5116), 1905-1910.

Soares-Filho, B. S., D. C. Nepstad, L. M. Curran, G. C. Cerqueira, R. A. Garcia, C. A. Ramos, E. Voll, A. McDonald, P. Lefebvre, and P. Schlesinger (2006), Modelling conservation in the Amazon basin, *Nature*, *440*, 520-523, doi: :10.1038/nature04389.

Sommer, R., T. D. A. Sá, K. Vielhauer, A. C. Araújo, H. Fölster, and P. L. G. Vlek (2002), Transpiration and canopy conductance of secondary vegetation in the eastern Amazon, *Agricultural and Forest Meteorology*, *112*, 103-121.

Trollope, W. S. W. (1982), Ecological effects of fire in South African savannas, in: *Ecology of Tropical Savannas*, edited by B. J. Huntley and B. H. Walker, pp.292-306, Springer-Verlag, Berlim.

Uppala, S. M., P. W. Kållberg, A. J. Simmons, U. Andrae, V. C. Bechtold, M. Fiorino, J. K. Gibson, J. Haseler, A. Hernandez, G. A. Kelly, X. Li, K. Onogi, S. Saarinen, N. Sokka, R. P. Allan, E. Andersson, K. Arpe, M. A. Balmaseda, A. C. M. Beljaars,

L. van de Berg, J. Bidlot, N. Bormann, S. Caires, F. Chevallier, A. Dethof, M. Dragosavac, M. Fisher, M. Fuentes, S. Hagemann, E. Hólm, B. J. Hoskins, L. Isaksen, P. A. E. M. Janssen, R. Jenne, A. P. McNally, J. F. Mahfouf, J. J. Morcrette, N. A. Rayner, R. W. Saunders, P. Simon, A. Sterl, K. E. Trenberth, A. Untch, D. Vasiljevic, P. Viterbo, and J. Woollen (2005), The ERA-40 re-analysis, *Quarterly Journal of the Royal Meteorological Society*, *131*, 2961-3012, doi:10.1256/qj.04.176.

Vieira, I. C. G., A. S. Almeida, E. A. Davidson, T. A. Stone, C. J. R. Carvalho, and J. B. Guerrero (2003), Classifying successional forests using Landsat spectral properties and ecological characteristics in eastern Amazônia, *Remote Sensing of Environment*, *87*, 470-481.

Xie, P., and P. A. Arkin (1997), Global precipitation: a 17-year monthly analysis based on gauge observations, satellite estimates, and numerical model outputs, *Bulletin of the American Meteorological Society*, *78*, 2539-2558.

Yanagi, S. N. M. (2006), Albedo of an Amazon tropical rainforest: field measurements, remote sensing, modeling, and its influence on the regional climate, Sc.D. thesis, 128 pp., Federal University of Viçosa, Viçosa, 31 October.

Zaks, D. P. M., N. Ramankutty, C. C. Barford, and J. A. Foley (2007), From Miami to Madison: Investigating the relationship between climate and terrestrial net primary production, *Global Biogeochemical Cycles*, *21*, GB3004, doi:10.1029/2006GB002705.

Zarin, D. J., M. J. Ducey, J. M. Tucker, and W. A. Salas (2001), Potential biomass accumulation in Amazonian regrowth forests, *Ecosystems*, *4*, 658-668.

Zarin, D. J., E. A. Davidson, E. Brondizio, I. C. G. Vieira, T. Sá, T. Feldpausch, E. A. G. Schuur, R. Mesquita, E. Moran, P. Delamonica, M. J. Ducey, G. C. Hurtt, C.

Salimon, and M. Denich (2005), Legacy of fire slows carbon accumulation in Amazonian forest regrowth, *Frontiers in Ecology and the Environment*, *3*(7), 365-369.

Zeng, N., and J. D. Neelin (1999), A land-atmosphere interaction theory for the tropical deforestation problem, *Journal of Climate*, *12*(3), 857-872.